TEMPORAL DATA FUSION APPROACHES TO REMOTE SENSING-BASED WETLAND CLASSIFICATION

JOSHUA S. M. MONTGOMERY
Bachelor of Science, University of Lethbridge, 2011

A Thesis
Submitted to the School of Graduate Studies
of the University of Lethbridge
in Partial Fulfillment of the
Requirements for the Degree

MASTER OF SCIENCE

Department of Geography
University of Lethbridge
LETHBRIDGE, ALBERTA, CANADA

TEMPORAL DATA FUSION APPROACHES TO REMOTE SENSING-BASED
WETLAND CLASSIFICATION

JOSHUA S. M. MONTGOMERY

Date of Defence: August 18, 2017

Dr. Christopher Hopkinson	Professor	Ph.D.
Supervisor		
Dr. Stewart Rood	Professor	Ph.D.
Thesis Examination Committee Member		
Dr. Laura Chasmer	Assistant Professor	Ph.D.
Thesis Examination Committee Member		
Dr. Stefan Kienzle	Professor	Ph.D
Chair, Thesis Examination Committee		

ACKNOWLEDGEMENTS

ABSTRACT

This thesis investigates the ecology of wetlands and associated classification in prairie and boreal environments of Alberta, Canada, using remote sensing technology to enhance classification of wetlands in the province. Objectives of the thesis are divided into two case studies, 1) examining how satellite borne Synthetic Aperture Radar (SAR), optical (RapidEye & SPOT) can be used to evaluate surface water trends in a prairie pothole environment (Shepard Slough); and 2) investigating a data fusion methodology combining SAR, optical and Lidar data to characterize wetland vegetation and surface water attributes in a boreal environment (Utikuma Regional Study Area (URSA)). Surface water extent and hydroperiod products were derived from SAR data, and validated using optical imagery with high accuracies (76-97% overall) for both case studies. High resolution Lidar Digital Elevation Models (DEM), Digital Surface Models (DSM), and Canopy Height Model (CHM) products provided the means for data fusion to extract riparian vegetation communities and surface water; producing model accuracies of (R^2 0.90) for URSA, and RMSE of 0.2m to 0.7m at Shepard Slough when compared to field and optical validation data. Integration of Alberta and Canadian wetland classifications systems used to classify and determine economic value of wetlands into the methodology produced thematic maps relevant for policy and decision makers for potential wetland monitoring and policy development.

TABLE OF CONTENTS

LIST OF TABLES

LIST OF FIGURES

LIST OF SYMBOLS & ABBREVIATIONS

GIS	Geographic information system
GoA	Government of Alberta
IMU	Inertial Measurement Unit
Km	Kilometre (s)
Lidar	Light Detection and Ranging
M	Metre (s)
N	Sample size
NIR	Near-infrared
Nm	Nanometre (s)
NRCan	Natural Resources Canada
PCI	PCI Geomatics
RADAR	Radio Detection and Ranging
RE	RapidEye
RMSE	Root mean square error
SAR	Synthetic Aperture Radar
SWIR	Short-wave infrared

1.0 Overview of Wetlands and Wetland Regulation

1.1 Introduction

Wetlands are areas of land that hold water, either temporarily or permanently, and contain waterlogged and altered soils with water tolerant (hydrophytic) vegetation adapted for life in saturated soil conditions (Government of Alberta 2013). These areas play a crucial role in replenishing and storing groundwater, functioning as natural water reservoirs that prevent flooding and reduce erosion, as well as filtering and purifying water. Wetlands, especially in boreal regions, also store substantial amounts of carbon and methane, and have exceptional biodiversity that provides habitat for roughly 1/3 of Canada's species at risk (Stewart & Kantrud 1971; Warner & Rubec 1997, DUC 2011, Government of Alberta 2013). Therefore, wetland ecosystems provide many ecosystem services and have marked environmental, social, and economic impacts.

Wetlands have become one of the world's most threatened ecosystems and continue to decline in quantity and health due to the effects of climate change, anthropogenic activities, and land cover change (Mitsch & Gosselink 2000, Daily 1997). The global extent of wetlands, or the Wetland Extent Trends (WET) index estimates wetland have declined between 64-71% in the 20th century, (30% between 1970-2008), and continue to rapidly degrade and decline in area (Dixon et al. 2016). Therefore, directly affecting wet area extents, riparian extent, hydrological regimes, biodiversity, and the functioning of wetland ecosystems (DUC 2011, Russi et al. 2013). Costanza et al. (2014) analyzed the global monetary loss associated with degrading wetland ecosystem services and area from 1997-2011. Over this time, monetary losses due to changes in swamps and floodplains were estimated to be US$ 2.7 trillion in ecosystem services per year, while changes in marshes and mangroves were estimated at US$7.2 trillion per year.

Even in water rich countries such as Canada, which has 1.2 million square kilometers of wetlands (25% of the world's total) (de Groot et al. 2013), decline and degradation of these ecosystems has become a grave concern. In the province of Alberta, approximately 70% of wetlands found in the settled areas of the province no longer exist, mainly due to agricultural drainage and rapid urban development (Government of Alberta 2013, de Groot et al. 2013). In less populated boreal regions, warmer temperatures and reduced precipitation trends are causing drying of wetland surface and groundwater, resulting in changes to hydrology and vegetation (e.g., Roulet 2000; Stow et al. 2004; Klein et al. 2005; Riordan et al. 2006; Smith et al. 2014). While policy makers have sufficient scientific information to understand the need to take steps toward conservation, the global extent of wetlands is immense. One of the technologies that can provide cost and time effective solutions to mitigate these problems is remote sensing. Remote sensing can be defined as the collection of data about an object from a distance (Jensen 2007). This includes mechanical devices such as cameras and laser sensors attached to aircraft and satellites.

Satellite and airborne remote sensing of surface water allows for large scale monitoring of wetland environments, especially isolated Northern wetland environments, by detecting and measuring spatial variations in inundation areas to estimate stage or discharge (eg. Smith et al. 1996, Pietroniro et al. 1999, Zhang et al. 2004, Brackenridge et al. 2005, Brackenridge et al. 2007).

1.2 Wetlands in Alberta

Wetlands come in many sizes and forms, generally developing where the water table is at or near the surface allowing water to settle on the land surface promoting development of soil conditions for hydrophytic vegetation (National Wetlands Working Group 1998). Canada has over 150 million hectares of wetlands, occupying approximately 14% of the land area of Canada, which is estimated to be 24% of the wetlands in the world (Government of Canada 1991, Pole Star Geomatics Inc. 1996, Environment Canada 2016). Most Canada's wetlands are found in the boreal regions, where rates of boreal forest disturbance in 2008 were found to be approximately 78%, and among the highest in the world (Komers and Stanojevic 2013). Boreal wetlands are which are predominantly comprised of shallow ponds, treed fens and bogs on poorly drained organic soils. With increasing disturbance and changing hydrological patterns, accurate, high resolution classification of these boreal wetlands is required for understanding rates of boreal wetland change, many of which have yet to be accurately identified or mapped, therefore there is a need to characterize baseline wetland areas for the boreal region. Many wetlands, especially in boreal regions, evapotranspiration may exceed precipitation, are sensitive to warming and drying trends that affect the hydrology of a wetland and subsequently the vegetation successive cycles and diversity (Devito et al. 2005, Petrone et al. 2007). Drying trends in many northern regions of Canada and the USA have been observed over the past 30 years, where changes in ground and surface water hydrology have been observed, thereby increasing vegetation succession (Kettridge et al. 2013) in some years and altering wetland growth patterns (Stow et al. 2004, Riordano et al. 2006, Petrone et al. 2007, Smith et al. 2014).

The prairie pothole region of West-Central North America encompasses an area approximately 715,000km^2 extending from Central Alberta, Canada south to the state of Iowa, USA. Prairie potholes are a result of glacial retreat during the last ice age, approximately 12,000 years ago (Winter, 1989). Wetlands within depressions created by the glacial retreat are highly variable in size and permanency, but are generally characterised as having less than 1m water depth at peak volume. The anthropogenic pressures of oil and gas industry, urban expansion, and to a greater degree, highly productive and diverse agriculture, all hydrologically affect the wetlands situated in the prairie pothole region of Alberta. Many of the wetlands in the prairie pothole region are often viewed as isolated (or closed) basins that only connect within a hydrological system during wet conditions, where the depression reaches bank-full conditions and begins to spill into adjacent depressions. This is described by Winter and Labaugh, (2003), as the "fill and spill" mechanism. Efficient monitoring of wetland hydrological mapping on large temporal and spatial scales using remote sensing techniques has proven to be challenging in the prairie pothole region, particularly seasonal and often ephemeral wetlands.

As a wetland basin fills with spring snowmelt or precipitation runoff, it promotes growth of dormant vegetation. Flora of a prairie wetland is a function of its water regime and salinity where water depth and duration determines distribution and composition of species (Kantrud et al. 1989). Wetlands which are only flooded briefly in the spring are dominated by grasses, sedges and forbs and characterised as seasonal or temporary wetlands. In wetland basins deep enough to have standing water throughout the entire year, and through drought conditions, the central zone will be dominated by mid to tall emergent species. Within a wetland zone, it may take a year or more to adjust to changing

environmental conditions or physical disturbance, which results in abnormal zonation patterns that are most evident after changes in water level (Kantrud et al. 1989). Many of the wetlands in the prairie pothole region of Alberta are ephemeral, meaning they last for only a short period of time, and are found in terrain affected by the water table near, at, or above the ground surface for a short period. As a result, ephemeral prairie ponds and wetlands can be difficult to properly classify compared to wetlands that are more permanent due to the dynamic vegetation cycles and soil conditions caused by frequent water stage changes.

A typical wetland environment can be divided into five vegetation zones based on the topography in and surrounding the wetland (Figure 1.1). These zones include upland, shrub-land, wet meadow, emergent, and submergent, each having distinct vegetation communities, which are a function of the ground water level. Therefore, vegetation zones and species composition in many wetland environments are subject to change seasonally and annually, which relates to the type (classification) of wetland.

Upland: Forested woody vegetation including cottonwood and birch trees

Shrub-land: Low, woody vegetation such as willows

Wet Meadow: Sedges, rushes and grasses

Emergent: Vegetation emerging from waters surface such as cattail and bulrush

Sub-mergent: Submerged and floating aquatic vegetation

Ground-Water Level
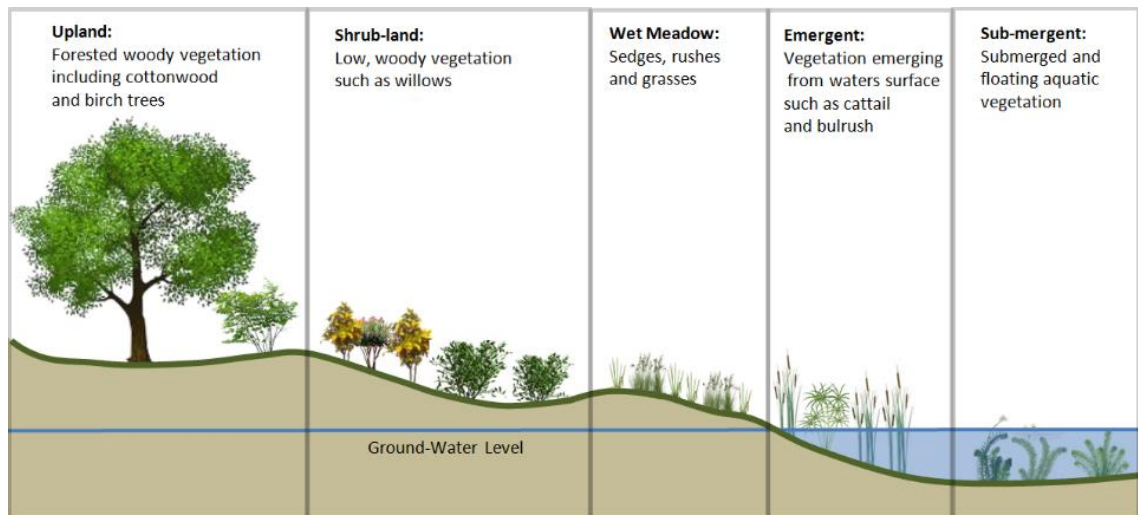
Figure 1.1. Typical vegetation zones of a wetland in Alberta showing the transition from upland woody vegetation to hydrophytic submergent vegetation based on Stewart and Kantrud (1971, 1989) wetland descriptions.

1.3 Wetlands and Classification in Alberta, Canada

The province of Alberta, located in Western Canada, has a population of over 4 million people and an area of approximately 661,000 square kilometers. Roughly 20 per cent of Alberta's surface area is covered by wetlands, more than 90 per cent of which are peatlands (Government of Alberta 2013, 2014). Natural regions in the province include: grassland, parkland, boreal forest, foothills, Rocky Mountain, and Canadian shield ecosystems. Each region has distinct types of wetlands that can be divided into five broad types: bogs, fens, marshes, swamps, and open-shallow water—most of which have unique biological characteristics and dynamic seasonal water extents (Stewart & Kantrud 1971, National Wetlands Working Group 1997, Government of Alberta 2015). Prior to June 2015, wetland classification and function was largely based on Stewart and Kantrud (1971), which describes in detail different types of prairie pothole wetlands, specifically vegetation, as indicators of wetland type and permanency. The Stewart and Kantrud classification system was used widely throughout Alberta in both 'green' (crown) and 'white' (private) lands to determine what appropriate action should be taken for wetland preservation when industrial and urban developments impact wetlands. Wetland policy and classification in Alberta was modified in June 2015 to incorporate additional literature. This new classification system considers wider varieties of wetland forms that includes the importance of vegetation structure, and water permanence on wetland biodiversity, hydrology, and biological processes. As a result, Stewart and Kantrud (1971), Ducks Unlimited (Smith et al. 1997), Alberta Wetland Inventory (AWI) (Halsey et al. 2004), the field ecosites guides to Alberta (Beckingham 1996; Beckingham and Archibald 1996), and the Canadian Wetland Classification System (CWCS, National

6

Wetlands Working Group 1997), have all been incorporated into the new Alberta

Wetland Classification System (AWCS 2015).

There are five broad classes of wetlands in the AWCS; marshes, swamps, bogs,

fens (bog and fen are forms of peatland), and shallow open waters (Figure 1.2). These

five different types (classes) are divided into form (vegetation), salinity, water

permanence (relating to classes described in Stewart and Kantrud 1971, not applicable to

Fen or Bog), and alkalinity (peatlands only) (Table 1.1).

Marsh Wetland

Swamp

Peatland (Bog & Fen)

Shallow Open-Water Wetland

Figure 1.2. Wetland classes found throughout Alberta in prairie, mixedwood, and boreal environments. a) depicting a typical marsh environment with flooded vegetation and open water; b) swamp with woody vegetation and distinct riparian zone transitions; c) peatland environment in northern Canada with numerous bogs; d) large, alkaline shallow-open water wetland with abrupt vegetation boundaries and dynamic water extent changes.

Table 1.1. The five types of wetlands found in Alberta with corresponding characteristics and associated Stewart and Kantrud (1971) permanency classification for Marsh, Shallow-Open Water, and Swamp wetlands.

Wetland Class	Vegetation Form	S&K (1971) Water Permanence	Salinity	Acidity-Alkalinity
Bog	1-Wooded, Coniferous 2-Shrubby 3-Graminoid.	-	Freshwater	Acidic
Fen	1-Wooded, coniferous 2-Shrubby 3-Graminoid	-	Freshwater to slightly brackish	1 -poor (pH < 5.5) 2-moderate rich (pH 5.5-7) 3-extreme rich (pH >7.0)
Marsh	Graminoid	Temporary (II) Seasonal (III) Semi-permanent (IV)	Freshwater to brackish	-
Swamp	1-wooded coniferous 2-wooded, mixedwood 3-wooded, deciduous 4-shrubby	Temporary (II) Seasonal (III)	1-Freshwater to slightly brackish 2-moderately brackish to sub-saline	-
Shallow Open Water	Submerged and/or floating aquatic vegetation, or bare	Seasonal (III) Semi-permanent (IV) Permanent (V) Intermittent (VI, Saline)	1-Freshwater to moderately brackish 2-combinations of sub-saline, freshwater and slightly brackish	-

In Alberta marshes are the dominant wetland type. The dominant plant community zone in marshes is determined by the plant community found in the deepest portion of a wetland (Stewart & Kantrud 1971). Therefore, marsh and shallow open water wetlands may not exhibit the wetland type every year due to varying weather or anthropogenic drainage conditions. As such, data from numerous months or years must be used in the classification of these wetland types (Government of Alberta 2015). Marshes are divided into seven different types based on vegetation zones (Figure 1.3). Each of these vegetation zones are subject to highly variable water levels and therefore vegetation

growth and succession. Fen zones are occasionally found along the margins of brackish, saline ponds and lakes on gently sloped terrain where ground water is on or near the ground surface, represented by a normal emergent vegetation phase and an open water phase that gradually merges with other vegetation zones (Stewart & Kantrud 1971). These alkali fen zones can also be found in conjunction with temporary and seasonal wetlands that experience frequent agricultural tilling or prolonged drought conditions. Rich fens are alkali, whereas poor fens are acidic and generally seen most commonly in boreal regions.
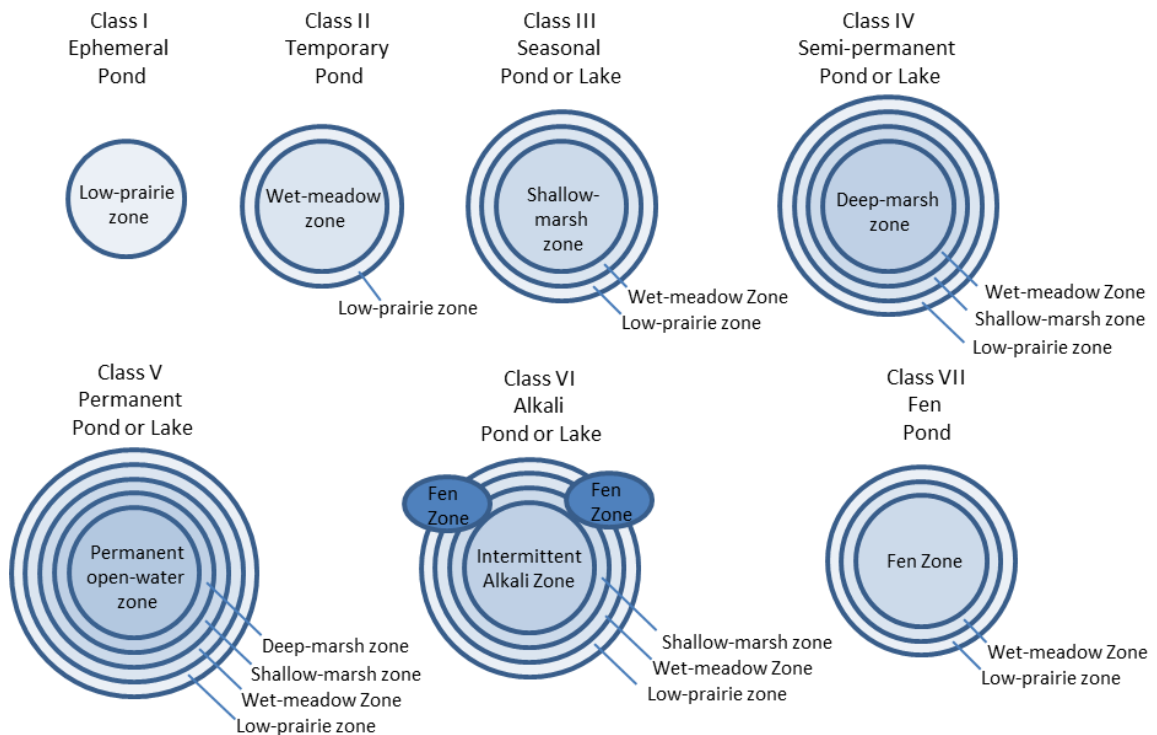
Figure 1.3. Marsh wetland classifications and spatial relation of associated wetland riparian zones of prairie pothole wetlands. Adapted from Stewart & Kantrud 1971.

While there are seven marsh wetland classes, the most common marsh environments in the prairie pothole region of Alberta are temporary, seasonal, semi-permanent and permanent (Table 1.2). Vegetation and soil characteristics are generally the best wetland class indicators, but the hydroperiod of these four marsh wetland types is

quite indicative of how permanent the wetland is both seasonally and annually, and

dictates vegetation vigor and biodiversity (Stewart & Kantrud 1971, 1989, Government of

Alberta 2015).

Table 1.2. Four commonly found marsh environments based on the Stewart and Kantrud (1971) wetland classification system, with corresponding hydroperiod and vegetation characteristics.

Wetland Type (S&K)	Hydroperiod	Plant Community Zone
Temporary (II)	Surface water present for short period of time after snowmelt or heavy rainfall	Wet meadow
Seasonal (III)	Surface water present throughout growing season, typically dry by end of summer	Shallow wetland
Semi-permanent (IV)	Surface water is present for most or all of the year, except in drought conditions	Deep wetland
Permanent (V)	Surface water present throughout the year	Open water

Climatic cycles affecting water level fluctuation are typically accompanied by

changes in vegetation (Galatowitsch et al. 1996). Basing wetland classification on a single

visit, or on information collected from a single year or time of year, provides only a single

climatic snapshot of a wetland, which fails to reflect its dynamic processes (Government

of Alberta 2015). Perhaps one of the most important aspects of wetland classification is

understanding and anticipating how wetlands change seasonally, especially in the

growing season, which reflects most of the vegetation growth and dynamic water level

rise. One of the more quantitative methods for understanding wetland change and the

impacts of changing climate and disturbance on wetlands is to monitor surface water

extents, where vegetation growth in each zone is related to surface water extent during the

growing season.

The length of growing season is measured in frost free days starting from the

estimated seeding date (10 days after the average daily temperature is above 5°C), until

fall frost (minimum daily temperature is 0°C) or until October 31st, whichever comes first. This provides a measure of the period during which plant growth can occur uninterrupted by frost and provides a way to compare growing conditions within the province (Chetner 2003).

Quantifying changes in wetland ecosystems can be difficult and logistically complex, but is necessary to monitor wetland change and make informed conservation decisions (Chasmer et al. 2016). Globally, changes in the surface-water extent over the past 15 to 30 years are highly variable among regions, including instances of shrinkage and expansion observed within a single watershed (Prigent et al. 2012, Pekel et al. 2016). Persistence of surface water is affected by both human and climatic factors (Vorosmarty et al. 2000), where most continental regions show a net gain in surface water attributed to reservoir construction, whereas net loss is more geographically concentrated to North America, the Middle East, and Central Asia. Long-term climate studies show frequency and severity of drought conditions, where climate change is implicated (Lutz et al. 2014), resulting in a net loss of surface water being observed in certain regions (MacDonald et al. 2010, Pekel et al. 2016).

Efficient environmental mapping and monitoring of wetlands and wetland hydrology on large temporal and spatial scales using remote sensing techniques has proven challenging in the prairie pothole region, particularly due to the dynamic wet area extent of the shallow and often ephemeral wetlands. Therefore, there is a need to develop remote sensing methods to quantify wetland physical and functional changes on broad temporal and spatial scales to appropriately identify wetland types (classify), and monitor open water and riparian changes to preserve wetland environments

1.4 Thesis Objectives

The main objectives of this research are to examine how Lidar, optical and radar data can be combined using data fusion techniques to assist in the production of high resolution wetland classification models and geospatial layers in Alberta, Canada. The work is divided along two case study objectives:

1) Examine use of C-band (HH) SAR intensity decibel thresholding for surface water extraction in a prairie pothole environment, to develop a time series for marsh and shallow-open water wetland hydroperiod classification. Surface water extent and permanence is evaluated in accordance with the current Alberta Wetland Classification System (2015).

2) Developing a decision-tree data fusion wetland classification methodology for boreal wetlands based on hydroperiod and associated riparian vegetation community attributes using multi-temporal, multi-mode data from Lidar (Optech Titan), Synthetic Aperture Radar (RADARSAT-2, single & quad polarisation), and optical (SPOT) sensors with similar acquisition dates. Wetland classification follows a combination of criteria according to the Alberta Wetland Classification System, and the Canadian Wetland Classification System.

1.5 Thesis Organisation

This thesis is divided into five chapters. Chapter two discusses technical details of Optical, Light Detection and Ranging (Lidar), and Synthetic Aperture Radar (SAR) remote sensing sensors relevant to research at both Shepard Slough and Utikuma Region Study Area (URSA) study sites. A review of literature including image filtering, classification and surface water extraction is also discussed. Chapter three presents threshold water extraction of prairie pothole marsh wetlands at Shepard Slough using SAR time series to examine surface water permanence and wetland hydroperiods. Chapter four presents decision-tree driven Lidar/SAR/optical data fusion for boreal wetland classification at URSA. Chapter five concludes the thesis, summarising the major findings and discussing the relevance of the research to current wetland policy in Alberta, providing potential directions for future research. The study examines two end member regions that represent a large portion of wetlands in Alberta.

2.0 Remote Sensing Technical Details and Wetland Applications

2.1 Remote Sensing of Wetlands

Remote sensing is defined as the acquisition of data about an object without touching it, using imaging sensors from a distance (Jensen 2005). Remote sensing is a valuable technology that can provide cost and time-effective solutions to mitigate the logistical, spatial and temporal difficulties associated with monitoring of large areas. Wetlands are among the most difficult ecosystems to characterize using remote sensing data due to their high spatial heterogeneity and temporal variability (Wickham et al. 2004, Wright & Gallant 2007, Bourgeau-Chavez et al. 2009, Klemas 2011). Sizes and shapes of wetlands are highly variable and depend on numerous environmental and climatic factors. Diversity of plant species, growth rates and physical structure (eg. open water, submerged, floating, emergent, woody shrubs, and forest) are also highly spatially variable.

Monitoring and inventory of wetland using satellite remote sensing has many advantages and is distinctly advantageous due to repeat coverage capabilities that can monitor wetlands seasonally or yearly. In addition, remote sensing is cheaper than field methods, covers very large areas and may (in the case of Landsat, Advanced Very High-Resolution Radiometer (AVHRR) and Moderate Resolution Imaging Spectroradiometer (MODIS), and air photos), have a long-term record for which changes and long-term trends in wetlands can. Remote sensing technologies can supply the following information: (1) extent of wetlands, (2) identify the wetland ecosystem type, (3) characterise the general wetland land cover type, (4) identify sub-mergent and emergent wetlands, and (5) hydrological regime details using multiple spectral analysis of remote sensor data.

The use of high spatial resolution digital image data in the classification of riparian structure as part of terrestrial ecosystem monitoring, should be actively pursued, with further research focused on advancing segmentation and object-oriented classification approaches to improve classification accuracies (Johansen et al. 2007, Moffet and Gorelick 2013). Wetland classification can be difficult because of confusion with other wetland classes in the same spatial area, as well as spectral confusion with other land cover classes among different types of wetlands. Multi-spectral data shows only marginally improved classification of wetland when defining broad classes of wetlands, treed wetlands and upland forests. However multi-temporal data improves the classification of wetlands in localised biodiversity as a spectral response, especially in combination with supplementary data such as soil data, ecological data, and elevation and topography data derived from ground validation Lidar data (Ozesmi and Bauer 2002; Chasmer et al. 2014).

Water levels and extents also fluctuate daily, seasonally, and annually, which confounds spectral classification. Furthermore, many wetland plant species are spectrally similar to one another, which makes separation of unique signatures difficult (Wright & Gallant 2007, Bourgeau-Chavez 2009). Larger scale, accurate monitoring and classification of wetland type is fundamental for understanding and quantifying the changing wetland environments in order to make informed political decisions regarding wetland management, preservation and inventory (Verpoorter et al. 2014, Chasmer et al. 2016). Satellites are therefore the most commonly used remote sensing platform to map large wetland ecosystems and (Ozesmi & Bauer 2002).

2.2 Remote Sensing for Water Mask Generation

Remote sensing provides methods to quantify changes to these areas over broad spatial areas within the last century, where changes can be tied to ecosystem function using *in situ* validation methods. Therefore, there is a need to develop remote sensing methods to quantify wetland physical and functional changes on broad temporal and spatial scales to appropriately identify wetland types (classify), and monitor open water and riparian changes to preserve wetland environments. Water resource assessments, flooding and wetlands benefit from accurate water mask mapping and monitoring got characterizing wetland condition. Accurate delineation and classification of open water wetland and watercourse riparian areas is an important aspect of remote sensing applications in hydrology (eg. Marsh et al. 2009, Brisco et al. 2011, Brisco 2015, Crasto et al. 2015,). Water resources monitoring, ecological studies, and infrastructure management are greatly enhanced by remote sensing applications with spatial and temporal data such as Lidar (Light detecting and ranging), SAR (Synthetic Aperture Radar), optical (SPOT, LANDSAT, RapidEye), all of which can be used for water masking (Ozesmi & Bauer 2002, Sawaya et al. 2003, Brisco et al. 2009, Ferguson et al. 2009, Maxa & Bolstad 2009, Crasto et al. 2015). Beyond wetlands, water masks are also important for understanding water resources, ecology, and risk/disaster management, all of which benefit from accurate, spatial and temporal water area surface maps.

Direct mapping of surface water elevation and area changes with radar and Lidar sensors have also been examined (eg. Alsdorf 2000, Alsdorf et al. 2003, Frappart et al. 2005, Frappart et al. 2006, White et al. 2014, Brisco et al. 2015, 2017), suggesting that both water extent, and vegetation associated with flooding, can be accurately described. Hodgson et al. (1987) also indicate that wetlands are best defined using remote sensing

imagery acquired in the spring, when the water table is high and shows the most contrast between land and water.

The best wavelength for discrimination of water from land is in the near-infrared and middle-infrared regions at wavelengths between 740-2500nm (Jensen 2007). Water bodies will appear dark because nearly all the incident radiant flux is absorbed by the water, in contrast to land, which appears bright due to reflection from vegetation and bare soil in these wavelengths (Jensen 2007). The automatic extraction of waterbodies from satellite images is well documented. One such method, for example, is the Normalized Difference Water Index (NDWI) used to extract water based on the ratio of the difference between the green and the NIR bands divided by the sum of those two bands (Mcfeeters, 1996).

Water masks are geographical layers that can be derived from many types of remote sensing data that indicate areas of water versus land. Different approaches are taken when extracting water masks, which is dependent on the type of sensor being used. Optical satellite-based open water classification is an established technique (Sawaya et al. 2003), and, under appropriate conditions, could provide an excellent comparative dataset for Lidar-based approaches by combining spectral, textural, and topographic information that has increased the classification accuracy for the majority vegetation structural classes (Johansen et al. 2007). Optical passive methods rely on reflectance over water, predominantly the absorption of multispectral wavelengths, whereas radar and Lidar rely on directional scattering that occurs away from the sensor, or from direct specular reflectance back to the sensor. Surface texture properties are also important when extracting water masks, as the surface properties interact directly with emitted energy of the sensors. Therefore, water can be identified by its spectral reflectance in optical data,

whereas the amount of reflectance from a body of water is used for Lidar or radar data

water mask extraction (Brisco et al. 2014, Chasmer et al. 2014, Crasto et al. 2015). While

both methods differ, and are reliant on sensor specific information, the combination of

water masks from the different sensors can be capitalised upon in data fusion (integration

of multiple types and sources of data), enhancing the accuracy of final products and

useful for validation purposes. Synthetic Aperture Radar (SAR) is recognised as an

important source of data for monitoring surface water, and is therefore used for many

wetland and flood applications. SAR is not subject to sunglint, can penetrate through

cloud and smoke cover, and can collect data at night, making it a reliable source of data

for monitoring water bodies (Brisco et al. 2008, 2009).

2.3 Optical Sensors

Aerial photography is one of the earliest and simplest remote sensing technologies

that developed significantly during the early 1900's with the advent of World War I

reconnaissance missions. Before airplanes, cameras were attached to balloons and

pigeons, or set up on high oblique angles from mountaintops. Aerial photographs are

generally either oblique (side-looking) or vertical (looking straight down) dependent on

the orientation of the camera relative to the ground (Jensen 2007). The camera systems

are passive optical sensors, commonly sensitive to light from 0.3µm to 0.9µm

wavelengths covering the visible, ultraviolet (UV) and near-infrared (NIR) that use lenses

to form an image in the focal plane. Panchromatic film is sensitive to UV and visible

portions of the spectrum, producing black and white images which are the most common

type of film used for aerial photography due to the high resolution of image and contrast

between objects within the image. Air photo interpretation (feature identification) and

photogrammetry (precise locations and height) are the two main interpretation methods of

aerial photography. The strength of aerial photography is the vast temporal record of high

quality images that are useful for change detection studies, such as wetland delineation

(Scarpace et al. 1981, Barrette et al. 2000), and historic imagery can be acquired often at

little or no cost. Where images in a flight line are taken sequentially with 50-60% overlap

between images, two images can be placed side by side and viewed stereoscopically in 3

dimensions, using a stereoscope. This practice is used to gain depth and terrain

information enhancing interpretation of the scene, enabling extraction of features such as

perched lakes or tree line in mountainous regions, and vegetation structural attributes.

These aerial photographs are often useful supplementary information for temporal studies

using more sophisticated sensors as a source of validation.

LANDSAT (USGS/NASA) and SPOT (*Centre national d'études spatiales*

(CNES)) are both optical sensors and the major satellite systems that was widely used for

wetland studies beginning in the 1980's and continue to provide the means for multi-

temporal water studies including: Haack and Messina (1997), Pietroniro et al. (1999),

Goward et al. (2006), Feyisa et al. (2014), Yamazaki et al. (2015), Mueller et al. (2016).

SPOT was first launched in 1986 and was the first satellite focused on earth resources to

have pointable optics, increasing the stereoscopic image capabilities more a wide range of

environmental applications such as water and land resource management. Early SPOT

studies include: Rutchey and Vilchek (1994 & 1999), Forgette and Shuey (1997). Landsat

TM band 5 is the most useful band for identifying wetlands due to its ability to

discriminate between vegetation and differences in surface soil moisture. Whereas bands

3, 4, when combined with band 5 provide the best combination of bands to detect

wetlands (Ozesmi & Bauer 2002). While Landsat is an older satellite (comprised of 8

satellites), and one of the first satellite systems used for wetland mapping, the wavelength of Landsat bands can be found similarly in other modern sensors such as SPOT and RapidEye (Planet Labs) (Table 2.1). The ranges of electromagnetic radiation vary to some degree between sensors, but also between Landsat series satellites. Optical remote sensing can range in spatial resolution, but typically higher pixel resolution is found on more recent systems as the technology has advanced.

Table 2.1. Typical spectral bands (blue, green, red, NIR), and some unique bands (Red Edge, SWIR) with associated wavelengths, of SPOT, LANDSAT, RapidEye and Worldview optical satellite systems, with respective pixel resolutions.

Sensor Wavelength (nm)				
Band	**SPOT 6-7**	**Landsat-7**	**RapidEye**	**Worldview 3-4**
Blue	455-525	450-520	440-510	450-510
Green	530-590	520-600	520-590	510-580
Red	625-695	630-690	630-685	655-690
Red Edge	-	-	690-730	705-745
NIR	760-890	770-900	760-850	780-920
SWIR	-	1550-1750	-	1195-2365
Resolution (m)	**6**	**30**	**5**	**0.30 to 1.24**

RapidEye (Planet Inc. (USA)) is a constellation of five multispectral earth observation satellites launched in 2008. These satellites have the capacity to provide large area images with frequent visit time, at relatively high spatial resolution (5-6.5m) that includes the Red Edge band (690-730nm) (Table 2.1), which is sensitive to changes in chlorophyll content (Tyc et al. 2005), and allows better estimation of the ground cover and vegetation (Haboudane et al. 2002, Vinal and Gitelson, 2005). While RapidEye data is primarily used for agricultural purposes, Tetteh et al. (2015) show RapidEye imagery is also suitable for water identification, accomplished by isolating certain bands, similar to

methods used with other optical sensors (green and NIR), with an overall accuracy of 95% and 0.889 kappa value.

Worldview 3 and 4 (DigitalGlobe Inc.) are constellation earth observation satellites launched in 2014 and 2016 respectively. Worldview has enhanced resolution (0.30m panchromatic, 1.24m MS) and a <1-day revisit time aimed to offer precise images for change detection, and detecting and monitoring disasters. Worldview 4 has 29 bands for enhanced mapping of snow, clouds and atmospheric penetration, as well as typical spectral bands (Table 2.1). New and enhanced applications for the high resolution and wide range of bands includes land classifications, bathymetry and feature extraction/change detection, with superior haze penetration reducing the amount of atmospheric interference (Lane et al. 2014). Lane et al. (2014) achieved an overall classification accuracy of 86.5% and 0.85 Kappa coefficient for 22 classes of aquatic and wetland habitats using a hybrid unsupervised approach. While the use of Worldview data is well documented, water and land classification studies (Chasmer et al. 2016) is less documented compared to other optical sensors.

Optical sensors have been utilised in many remote sensing studies investigating feature extraction and change detection in wide variety applications and landscapes. Wetland studies generally use a combination of sensors to increase accuracy of wetland classification, specifically optical data, where accuracies are increased in combined with other optical or active sensors (Lidar, Radar) in data fusion, and have over 40 years of continuous acquisitions. While optical data such as LANDAT and SPOT have been used widely to map wet areas and accurately delineate water body boundaries, atmospheric

effects such as haze, clouds and smoke which can be problematic when trying to construct long-term monitoring programs over large areas (White et al. 2015).

2.4 Light Detecting and Ranging (Lidar)

Lidar is an active satellite, airborne, or in-situ sensor that provides topographic and bathymetric (dependent on sensor) information that can be used to determine wetland basins and water level at a certain time. Discrete pulse, scanning airborne Lidar systems can attain a return spacing of less than 1m and is increasingly being collected and used for wetland studies due to the high resolution and wealth of topographic information that can be extracted, such as slope, aspect and elevation. Common Lidar systems used for topographic mapping, emit laser pulses in near-infrared at a wavelength of 1064nm due to ND YAG (neodymium-doped yttrium aluminium garnet) crystal availability, and ease of manufacture (Wehr and Lohr 1999, Boland et al. 2004). For bathymetric mapping blue-green lasers centered at approximately 532 nm (achieved through frequency doubling) are used due to increased water penetration capabilities (Mikhail et al. 2001).

Contemporary Differential Global Positioning System (DGPS) (Figure 2.1) technology uses (at least) two Global Navigation Satellite Systems (GNSS): GPS and GLONASS. The GNSS, a terrestrial static base station receiver, and a roving receiver located on an aircraft simultaneously record the position of the aircraft throughout data collection. GNSS data are post-processed with the known location of the base station to determine the exact location of the aircraft's antenna during flight to an accuracy of ~5 cm (Goulden and Hopkinson 2010). An Inertial measurement unit (IMU) measures the orientation of the Lidar antenna at the time a pulse is both transmitted and received by using three primary axes: x = in flight aircraft axis (roll axis); y = horizontally

perpendicular to x (pitch axis); z = vertical axis perpendicular to x (yaw or heading axis)

(Hopkinson 2006).
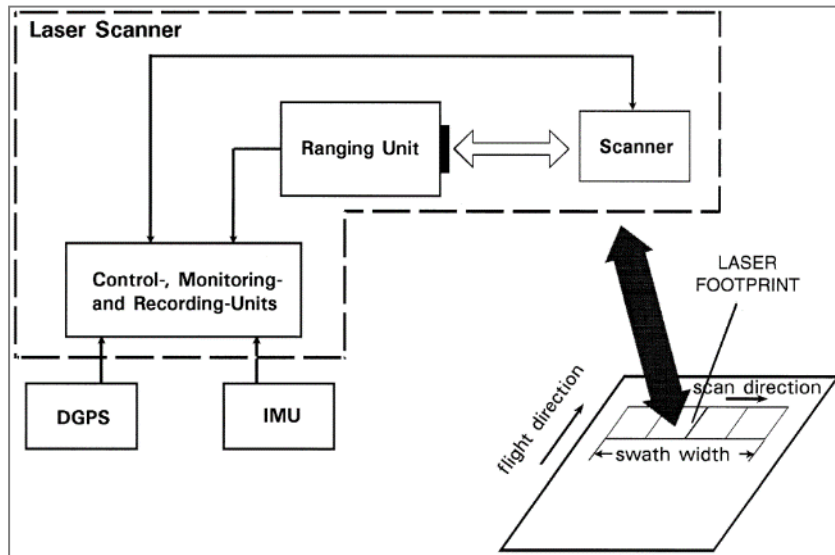
Figure 2.1. Typical components and instrument interaction in an ALS system (Wehr and Lohr 1999).

The aircraft IMU contains three gyroscopes, which measure movement of the aircraft

(orientation), as well as three accelerometers, which measure non-gravitational

acceleration and vibration. The result is an output file detailing the aircraft position

including latitude, longitude, and elevation relative to the ellipsoid, as well as sensor

orientation including roll, pitch, yaw and heading—all of which are indexed by GPS time

(Jensen 2007).

Lidar data provides measurements of the 3D canopy, understory, and ground

surface topography, which are important for understanding if any morphological changes

have occurred in elevation (provided temporal data is available), derivation of vegetation

structural characteristics, spectral characteristics, and for extracting water levels of

standing water (Toyra et al. 2003, Chasmer et al. 2014, Crasto et al. 2014 and 2015, Irwin

et al. 2017.). The morphology of the ground surface and vegetation structural

characteristics are important for hydrology, productivity, photosynthesis, greenhouse gas fluxes, and can be mapped using a digital elevation model (DEM) derived from Lidar data. There is a need to further explore automated Lidar-based and multi-temporal boundary delineation and water classification, especially as high-resolution, large area coverage data becomes increasingly available (Crasto et al 2015). The merit of using Lidar for hydrological research is the ability to map surface morphology at a high resolution, and under a wide range of land surface conditions (Hopkinson and Pietroniro 2008; Hopkinson et al. 2011). The utility of Lidar for topographic and vegetation canopy representation is well established but more work is needed to evaluate the utility of Lidar over channel, lake, and wetland surfaces (Hopkinson et al. 2005; Hopkinson et al. 2011; Crasto et al. 2015).

Contemporary Lidar systems emit pulses, referred to as the *pulse repetition frequenc*y (PRF) (Jensen 2007), at rates up to 1MHz. PRF has increased from <1KHz during the early 1990's, to current systems that have a PRF ranging from 200 to 1000 KHz; approximately three orders of magnitude in increased speed and data capture in 20 years. Range measurements can be determined by the equation r=t/2 x c, where 'r' is the distance between the target and Lidar sensor, 't' is round trip travel time of the pulse from emission to reflection to reception, and 'c' is the speed of light in air ($\sim 3 \times 10^8$ m s^{-1}) (Boland et. al., 2004). Scanning units can be subdivided into the following key components described by Wehr and Lohr (1999): laser ranging unit, opto-mechanical scanner, control, and processing unit. Scans can either be uni- or bidirectional depending on the scanning mechanisms, allowing for an array of calibration options and scanning patterns. The scanning mirror unit is an integrated mechanism that measures the scan angle of the mirror controlled by a galvanometer controlling the amount of angular

motion of the mirror (Goulden and Hopkinson 2010). Mirrors inside the laser transmitter typically rotate in a sweeping motion perpendicular to the flight direction in order to blanket the surface of the Earth with a swath width field of view of up to 75° (Brovelli et al. 2004).

Typical scanning mechanisms used for airborne Lidar survey include oscillating mirrors (bidirectional scan) producing parallel lines or arcs, nutating (swaying) mirrors (Palmer scan) producing an elliptical pattern, rotating polygon scanners producing parallel lines (unidirectional scan), and fiber scanners producing a parallel line scan (Figure 2.2.) (Wehr and Lohr 1999).
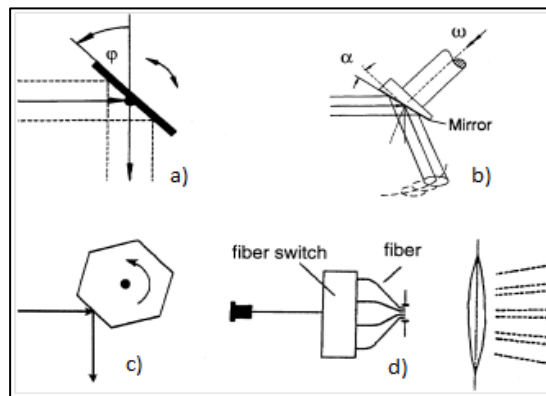
Figure 2.2. Scanning Mechanisms. a) oscillating mirror b) Palmer scan c) fiber scanner d) rotating polygon. Adapted from Wehr and Lohr (1999).

As the off-nadir scan angle (Θ) increases, so does the amount of vegetation foliage that must be penetrated in order for a pulse to be sent to and received from the ground, often resulting in multiple returns (Jensen 2007). Single return Lidar involves a single pulse that generally returns from the first near-ground object it encounters. This can be useful for deriving a bare-earth or a canopy height model, but doesn't allow for derivation of 3-dimensional canopy structure information (Jensen 2007). Multiple returns are generated when the laser pulse encounters ground and above ground features, such as

vegetation, then scatters back to the receiver. Such occurrences are described as the 1st

return from the incident laser pulse, intermediate returns from below the 1st return, and

the last return, which is often from the ground (Figure 2.3).
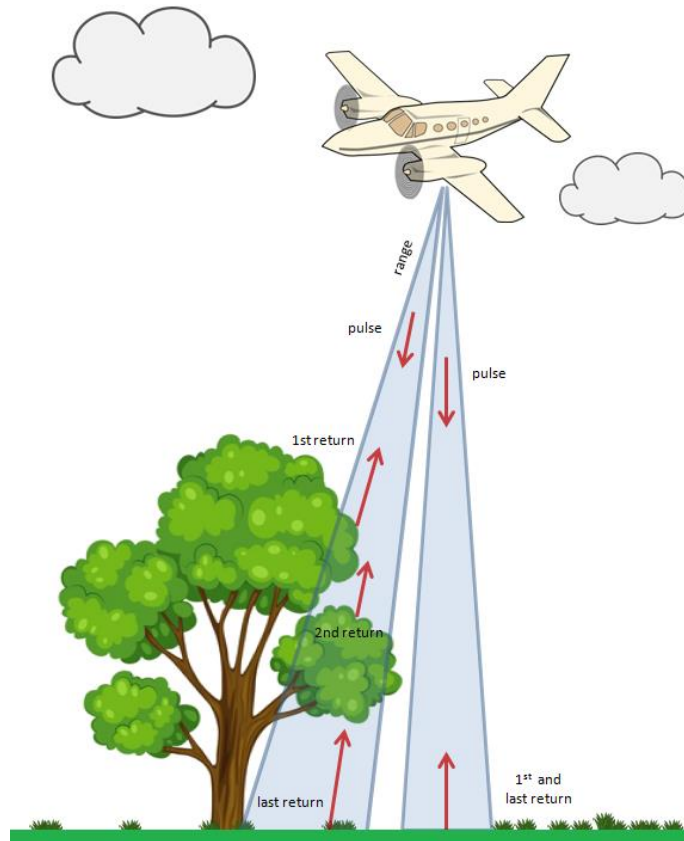
Figure 2.3. Illustration of 1st, 2nd, and last returns from airborne Lidar laser pulses
interacting with a forested and grassy environment (adapted from Hopkinson 2006).

Systematic errors and uncertainties occur in all data collection equipment, causing

imprecise and inaccurate measurements. Therefore, determination of uncertainty in data

collection is important to understanding the value and application of results. In order to

estimate final observation uncertainty, individual sources of error from GNSS, IMU, laser

scanner, and ranging components of the overall mapping system must be combined in an

error propagation model (Goulden and Hopkinson 2010). This is achieved by

transforming the laser range observation to a coordinate system by transferring the range

observation between three co-ordinate systems through time:

1) *Scanning Mirror Frame* which has an axis to the mirror's surface and parallel to

    the flight direction where the reference frame rotates with the scanning mirror

    corresponding to the observed range in the Z axis;

2) *Platform or Body Frame* is a transformation of the one-dimensional range

    observation created by the scanning mirror frame where it has a Z axis in the

    direction of normal gravity, X axis in the aircraft heading direction, and Y axis to

    complete the system, therefore, is unaffected by roll, pitch and yaw of the aircraft;

3) *Topocentric Mapping Frame* represents the coordinates of the point location on

    the ground. The height origin is set to the ellipsoid or geoid and the planimetric

    origin is set at the centre of a UTM zone and the equator. Transformation of a

    vector uses GPS data from the scanning mirror for comparison to other data sets

    (Schwarz et al. 1993).

This framework, development for testing uncertainty in Lidar observations, is

useful because it can be employed to predict uncertainty prior to acquisition, and accounts

for unavoidable and predicted error that can be corrected or expected in the dataset before

extensive geo-processing (Goulden and Hopkinson 2010).

 A Digital Elevation model (DEM) represents the shape of a surface using a

continuous mathematical model. Generally, two types of DEM can distinguish elevation

as a function of latitude and longitude: digital surface model (DSM) expressing the

Earth's surface, and digital terrain model (DTM) expressing the ground surface with

removed terrain cover such as canopy cover and vegetation. Mass points used in DEM

creation can be viewed individually, which is useful for identifying data voids, multiple

flight lines, and effectively portraying last return data (Jensen 2007).

Traditional wetland delineation requires resource-intensive on-site investigations

of soils, vegetation, and hydrology. Lidar provides spatially distributed ground elevations

that have a density appropriate for creating fine-scale topographic maps suitable for

delineation applications (Jensen 2007). These maps can enhance the visualization of

depressions and associated wetlands if the data are modeled. To be useful in hydrologic

modelling, elevation data is typically interpolated into an even grid, or a DEM (Toyra et

al. 2003). Wetland visualization is greatly enhanced in smoother models within one to

three meters resolution, with the triangular irregular network providing the most accurate

border. Mapping of depressions has many implications to both surface and subsurface

hydrology. Closed depressions are landforms with no outlet point, whereby water either

infiltrates into the soil or pools and becomes a wetland (Hayashi et al, 2003). These

closed depressions are often viewed as errors, and are removed to eliminate barriers to

hydrological connectivity, largely justified based on the assumption that the depressions

are artifacts, therefore sources of error in a DEM (Jensen 2007). Lindsey and Creed

(2004, 2005) suggest removing all closed depressions from a DEM is inappropriate

because a DEM surface represents a combination of both artifact and actual depressions,

that when removed may remove actual depressions that are important environmental

features. Lindsey and Creed (2004) developed a method that identifies actual closed

depressions using a stochastic based simulation, to estimate the likelihood of a real versus

digital depression based on an iterative model where sources of error were randomly

added to a DEM before filling depressions. This method enables the likelihood that a

depression is a real feature by assuming the degree of error in topography of a normally

distributed and spatially autocorrelated DEM. The stochastic simulation based approach to depression identification requires little additional data and is applicable to all landscapes, accounting for uncertainty in the DEM data, and is able to identify if depressions contain water. Traditional triangular irregular network (TIN)-based processing yields a DEM that can be used to accurately detect the edge of a depressional wetland within 1-3 meters (Maxa and Bolstad 2009), but with high resolution (<1m resolution) and bathymetric datasets (water surface and bottom topography), this accuracy can likely be improved upon.

2.5 Synthetic Aperture Radar (SAR) Technical Details

Radio detection and ranging (Radar) operates in the microwave portion of the EM spectrum, beyond the visible and thermal infrared regions. Operating in the microwave region of the spectrum improves signal penetration (decreases attenuation) especially in the atmosphere, providing many benefits for temporal studies. Radar is different from optical sensors in that it is an active, self-illuminating sensor that operates on the microwave spectrum, with the distinct advantage for remote sensing for two reasons: (1) radar systems can collect any time of day or night and under poor weather or atmospheric conditions; (2) backscatter (radar reflections) provide different information than optical sensors. Unlike optical, radar is sensitive to surface texture, particularly in studies discriminating the contrast or brightness between objects such as land and water (Hess et al. 1990, Rio and Lozano-García 2000; Alsdorf et al. 2001, Bourgeau-Chavez et al. 2001, Ozesmi & Bauer 2002, Brisco et al. 2013, White et al. 2015).

Most Radar systems operate between wavelengths of 2 and 100cm dependent on the purpose of the radar system (Table 2.2). Some bands have specific wavelengths that

are suited for a certain type of application or terrain, such as X-band which is commonly used for snow and ice monitoring, or L-band, commonly used in geologic applications (Jensen 2005).

Table 2.2. Typical radar bands and wavelengths with associated common applications.

Band	Wavelength	Common Applications
X-Band	2.4 - 3.75cm (12.5 - 8ghz)	Military terrain survey. Ice survey.
C-Band	3.75 - 7.5cm (8 - 4ghz)	Good medium for all applications.
S-Band	7.5 - 15cm (5 - 2ghz)	Land classification.
L-Band	15 - 30cm (2 -1ghz)	Geologic survey.
P-Band	30 - 100cm (1 - 0.3ghz)	Foliage extraction.

Shorter wavelength X-band signals generally interact with the upper sections of vegetation, while the intermediate C-band penetrates further into the entire canopy, also interacting with the ground surface. The L-band is capable of penetrating throughout the vegetation and interacts with the surface beneath the vegetation (Hong et al. 2009). Since C-band interacts with both the vegetation and ground surface, it is widely utilised in flooded vegetation and wetland studies (Adam et al. 1998, Touzi et al. 2007, Brisco et al. 2008, 2009, White et al. 2014, 2015). Radar polarisation is dependent on the direction the SAR signal is transmitted and received to the satellite's antenna. Early SAR satellite systems in the 1990's operated on single polarisation mode such as HH (horizontal transmitted and horizontal received) or VV (vertical transmitted and vertical received). More recent systems launched in the 2000's are equipped with quadruple mode, also called 'quad pol', which is capable or acquiring data in four channels (HH, HV, VH, VV) for enhanced terrain and vegetation studies (Hong et al. 2009).

TerraSAR-X (*German Aerospace Center* (DLR)) is a space-born X-band SAR system, launched in 2007 with an 11 day repeat orbit. The high spatial resolution (0.25m – 40m), combined with the repeat orbit has been found suitable for monitoring water-level changes over wetlands (Hong et al. 2009, Schmitt et al. 2012). TerraSar-X can generate coherent interferograms in wetland areas and has been used in multi-temporal mapping of the distribution of vegetation formations for determining flood duration (Schmitt 2012). Another recent satellite is Sentinel-1A and Sentinel 1B (European Space Agency (ESA)), which is a C-band, two SAR satellite constellation mission part of a larger mission (Copernicus), launched in 2014 and 2016 respectively with a 6 day repeat cycle (Potin et al. 2015). One of the benefits of the mission is the relatively open access data, which has been made available to public for research applications. Specific water resource studies with Sentinel-1 include Amitrano et al. (2014) and Ardhuin et al. (2017) focused on calibration of the data and mapping of large water bodies at high resolution. The demand for sentinel data has been steadily growing as the Copernicus mission progresses and develops. As additional satellites become active (Sentinel 1 to Sentinel 6), with a wide variety of active and passive imaging sensors, there will be added capabilities for more comprehensive ocean, land and atmospheric monitoring through data fusion.

RADARSAT-2 (RS2) is a Canadian Space Agency (CSA) satellite launched in 2007 at an altitude of approximately 798km and orbits Earth 14.3 times per day, with a repeat cycle of 24 days. It carries a C-band (5.405 GHz) synthetic aperture radar, which is a good wavelength for earth observation applications over land and water, offering a wide range of beam modes well suited for wetland monitoring (Livingstone et al. 2005, White el a. 2015). Since RS2 data is used to conduct the wetland classification and hydroperiod analyses in Chapters 3 and 4, additional radar principles and technical details of the

satellite will be discussed as it relates to RS2, but these principles also apply to other radar satellite systems. The position of the satellite is derived from an on-board GPS that is also used to determine the position of the acquired data on the Earth's surface. The antenna and sensor electronics (SE) comprise the two major systems of the satellite. These systems execute all radar functions and are controlled by the spacecraft management unit (SMU) that is linked to the antenna SE that interacts with transceivers that form the link to ground receiving facilities (Livingstone et al. 2005). Radar acquisitions are scheduled by an internal clock that is synchronised to GPS time provided by the satellite GPS receivers, allowing for the unique ability to direct and image the satellite to the desired area of interest. RADARSAT-2 can transmit and receive fully polarimetric radar waves in both horizontal and vertical polarisation planes (HH, VV, HV, VH); maintaining the phase information and allowing for enhanced mapping of the difference between low and high backscatter values (White et al. 2015). Phase relates to the location and shape of the wave pattern allowing for the measurement of the time it takes for the radar signal sent from the satellite to interact with the target in the ground and return to the satellite (Brisco et al. 2013). RADARSAT-1, the predecessor to the RADARSAT-2, was launched in 1995, but only had the capability to transmit and receive waves horizontally to the ground target, limiting the ability to detect and calculate phase information. The upcoming RADARSAT Constellation Mission (RCM), which is anticipated to launch in 2018, will also offer a wide range of beam modes well suited to water monitoring applications similar to RADARSAT-2. RCM will be composed of 3 satellites that will have an average daily coverage for 95% of the world. RCM will also have a much shorter revisit time (four days) compared to RADARSAT-2 (24 days), due

to the larger swath-width and nature of the constellation, which will greatly enhance temporal monitoring applications.

The spatial resolution of SAR is determined by built in range and processor constraints and depends on beam mode used at the time of data acquisition, which dictates scene size and the nominal resolution. Range resolution is dependent on the length of the processed beam pulse, where shorter pulses result in higher resolution found in ultra-fine or spotlight modes. SAR data can be acquired in a variety of modes (Table 2.3). Higher resolution modes are best suited for applications requiring high spatial resolution over small spatial areas, such as change detection, whereas broad area coverage modes are intended for applications requiring wide area coverage where coarser resolution is not a limiting factor.

Table 2.3. High resolution SAR modes of Radarsat-2 with associated nominal resolution, scene size and incident angle.

Mode	Scene Size *(km)*	Nominal Resolution *(m)*	Nominal Incident Angle(°)
Fine	50 x 50	8	30 to 50
Multi-Look Fine	50 x 50	8	30 to 50
Extra-Fine	125 x 125	5	22 to 49
Ultra-Fine	20 x 20	3	20 to 54
Spotlight	18 x 18	1	20 to 54

2.5.1 SAR Interaction with Wetland Surfaces

The utility, limitations, and accuracy of radar derived data in water extent mapping, flooded vegetation delineation, and water mask generation and has been well investigated (Hess et al. 1995, Kasischke & Bourgeau-Chavez 1997, Brisco et al. 2014; Santoro and Wegmuller 2014). Synthetic Aperture Radar (SAR) can effectively map and monitor changes in surface water, on annual and seasonal scales in near real-time (Irwin et al. 2017). Most surface water features are detectable on radar imagery because of the

contrast in return between smooth water surface and the rough land surface. Therefore, Synthetic Aperture Radar (SAR) can effectively map and monitor changes in surface water (Brisco et al. 2008, Brisco et al. 2009), on annual and seasonal scales in near real-time (Hess et al. 1990, Touzi et al. 2007, White et al. 2014). Moisture content of a material can change electrical properties, thus affecting how material appears in the radar image. Increased moisture increases a material's complex dielectric constant (i.e. ability to store electric charge), influencing the ability of a material to absorb, reflect and transmit energy which factors into both water and vegetation feature extraction, whereby reflectivity and image brightness of most natural vegetation and surfaces is increased with increasing moisture content (Toyra et al. 2002). Radar data are good for detecting open surface water because the dielectric constant of water is high compared to soil and vegetation, and have been shown to be important for wetland water extent characterization (Toyra et al. 2001, Brisco 2015, Irwin et al. 2017). Since water has a high dialectic constant, it acts as a specular reflector under calm weather conditions (no rain or wind). Therefore, due to the off-NADIR emission and view angle, very little backscatter is returned to the satellite sensor, which makes water appear as a dark feature in radar images compared to land features which are brighter due to increased texture and backscattering responses (Di Baldassarre et al. 2011, White et al. 2015).

Rain and wind poses one of the biggest challenges for surface water mapping using SAR. As wind increases it causes rough surface back-scattering rather than specular scattering which is typical in calm conditions. As the water roughness increases, the scattering pattern of the incident wave changes and more energy is backscattered (Figure 2.4). As a result, the contrast is lowered between water and land making surface water mapping more problematic (Brisco 2015).
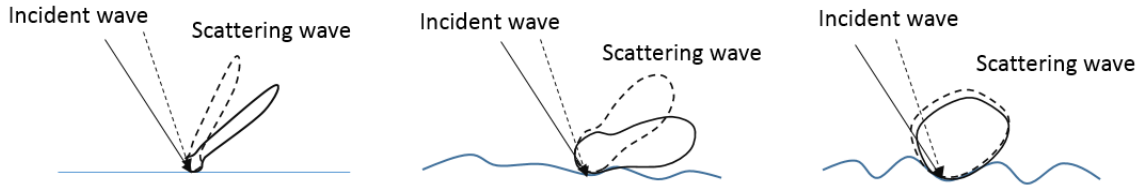
Figure 2.4. Schematic drawing illustrating specular scattering and the increase in backscatter due to increased surface roughness over a waterbody (adapted from Brisco 2015).

Radar signals are often reduced in wetlands dominated by herbaceous vegetation with low biomass, largely due to the specular reflectance (Smith et al. 2007). While surface wave action has a large influence on the scattering response, different types of vegetation also produce variable types of scattering, which are dependent on vegetation density and height (Figure 2.5). Wetlands present four different types of backscattering-under different polarisations and acquisition conditions in SAR data (Brisco et al 2011). Scattering is predominantly influenced by wave effects and varying emergent phases of vegetation (Figure 2.5).

The four common types of scattering in wetland environments are as follows:

1) **Specular Scattering: weak or** no return to the satellite. Occurs from smoother surfaces such calm water and bare soil.

2) **Rough Scattering**: single bounce return to the SAR from surfaces such as rough water or low emergent vegetation.

3) **Double-Bounce Scattering**: two smooth surfaces create a right angle that deflects the incoming radar signal off both surfaces such that most of the energy is returned to the sensor.

4) **Volume Scattering**: signal is backscattered in multiple directions from features such as vegetation or canopies
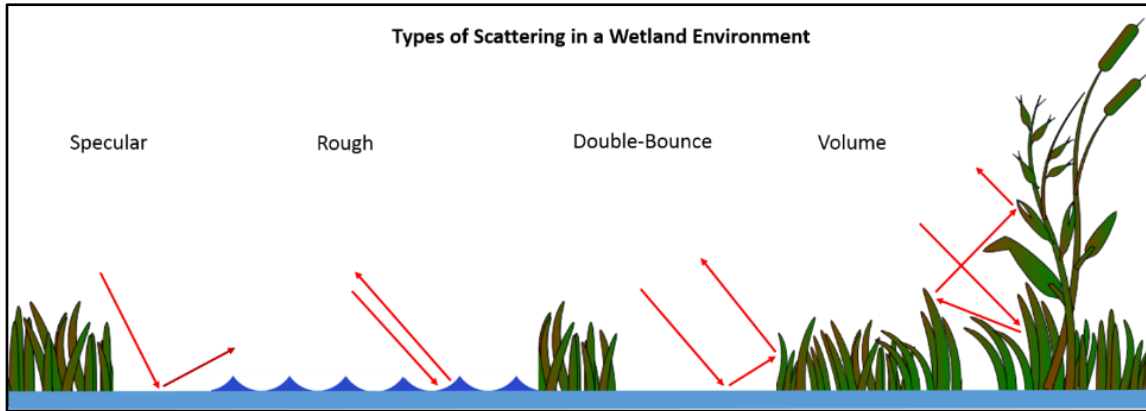
Figure 2.5. Schematic illustrating four types of Radar scattering that occurs in wetland environments as a function of surface roughness and vegetation (adapted from Brisco et al. 2015).

As mentioned, RADARSAT-2 can transmit and receive fully polarimetric radar waves in both horizontal and vertical planes (HH, VV, HV, VH). HH Polarisation generally yields a higher contrast between upland and open water (Brisco et al. 2008, 2009). Therefore, differences in backscatter response between land and water are the greatest in the HH polarization. HH polarization is better able to separate land from water under calm water conditions because open water results in less scattering, resulting in higher contrast between land and water compared to the HV or VV polarization (Brisco et al. 2008, 2009). Therefore, differences in backscatter responses between land and water are the greatest in the HH polarization (Adam et al. 1998). While HH is best utilised under calm conditions, the HV polarization is better suited for surface water mask processing when there are waves or high wind because backscatter is more independent of surface roughness, and largely independent of incidence angle and wind direction (Toyra et al. 2001). When waves are present in water there is often an increase in backscatter that causes water features to appear as vegetation. Therefore, HH/HV dual polarisation images are better suited to ensure accurate delineation of open water in variable conditions (White et al. 2015). Data for mapping wetlands are best acquired in

36

the spring, summer, and fall to avoid any ice-on imagery (Van der Sanden et. al. 2012). For example, rough surface water can produce a backscatter response similar to ice, thus making it difficult to distinguish between the two land covers (Van der Sanden et. al. 2012).

2.5.2 SAR Intensity Thresholding for Surface Water extraction

Areas of known surface water can be sampled to determine the range of intensity thresholds (dB) that represent surface water in a SAR image, in order to create a surface water extent mask. When mapping using an intensity threshold, the user must consider beam mode, and polarization ancillary sources of data for post-editing to obtain an accurate result. Intensity thresholding is a commonly used approach where all pixels in an intensity image are mapped as water when their backscatter co-efficient is lower than a specific threshold based on intensity ranges sampled in areas of known water (White et al. 2014). The intensity threshold decibel (dB) of water in SAR images is largely influenced by weather, polarization, and incidence angle. Lower incidence angles tend to be more sensitive to waves on water, therefore a combination of high and low incidence angle images is sometimes required to accurately map surface water features (Toyra et al. 2001). A smaller incidence angle is better able to penetrate vegetation, therefore offering better detection of flooded vegetation, especially noted in delta or floodplain areas with dynamic seasonal inundation (Crevier et al. 1996, Adam et al. 1998). Generating water masks using intensity thresholds is described in Chapter 3 of the thesis as the primary objective of the chapter, whereas Chapter 4 focuses more on extracting flooded vegetation characteristics using SAR.

2.6 Image Orthorectification

While ortho-rectification of optical imagery is well documented (Leprince et al. 2007, Marsetic et al. 2015), ortho-rectification of SAR data has proven to be more difficult due to its unique and complicated geometry, predominantly caused by the interaction of side-looking imaging geometry of the sensor (Leberl 1990, Schreier 1993, Leberl 1998). Any geometric distortion of the mosaics limits the use of these data for scientific applications, especially when integrated with data from other sources, and can't be compared temporally. The interpretive and mosaicking problems of side-looking radar images are well known, and described by Lewis et al. (1970) and Curlander et al. (1984). One such issue is known as radar fore-shortening, which occurs when imaged terrain surfaces slope toward the radar sensor creating the appearance that they are shortened relative to those sloping away from the sensor. Another common issue called 'radar layover' is an extreme case of foreshortening that occurs when the slope of the terrain is greater than the angle of the incident signal (Sheng et al. 2003). Both issues create geometric complications when attempting to ortho-rectify SAR images, specifically without control data found in the meta-data from acquisition. DEM data are required to correct topographic distortion in SAR imagery and image simulation due to the dependence of SAR echoes to terrain topography. An indirect strategy uses the technique of SAR image simulation from DEM data (Guindon 1993, Sheng et al. 2003). The direct strategy determines the ground coordinates of a SAR image pixel through an iterative process using the SAR Doppler equation, SAR range equation, and Earth surface model (Kwok et al. 1987). These equations are commonly used in SAR spatial processing in modern software that directly uses meta-data of the sensor. The direct method requires as input the precise sensor position and imaging parameters. Since these data do not function

when creating SAR mosaics due to differing meta-data unique to each image, the direct strategy is not applicable to SAR mosaic rectification.

Typical SAR ortho-rectification procedures are as follows: 1) simulating a SAR image from the DEM according to the imaging geometry of the real SAR image; 2) manually selecting or automatically deriving reliable tie-points that appear in both real and the simulated SAR images; 3) warping the real SAR image to the simulated image using a polynomial function fitted from the tie-points; and 4) projecting the warped real SAR image back to the map coordinate system using a DEM (Sheng et al. 2003). As previously stated, the procedures only work well in rectifying individual scenes of SAR imagery (Kwok et al. 1987, Sheng et al. 2003). With a proper DEM for topographic correction and proper meta-data for layover and foreshortening distortion correction, the radar images can be projected to regular map coordinate systems, at which point they are denoted as orthorectified or orthographic SAR images (Kropastch 1990). The result of the whole process is an orthorectified SAR image in the DEM map coordinate system.

2.7 Common SAR Image Enhancement Methods

2.7.1 Filters

Image filtering is a common procedure in SAR data due to the noise characteristics present in each image. Filters are used for a variety of reasons to perform adjustments to an image to reduce speckle (noise) while also preserving edge effects of pixels (White et al. 2014). Image variance is known as speckle, which is a function of the radar system not the scene. The difference between scene texture and image texture is explained by speckle in a SAR image. The presence of speckle makes SAR imagery very different from most optical imagery because speckle causes SAR imagery to have broad

spatial bandwidth, meaning that the spectral width for SAR data approaches the upper

limit set by the sampling rate. Speckle variance in an image reduces with increased

effective number of looks (ENL), but by increasing the ENL and averaging the

reflectivity in an image, the area of each speckle increases which can also reduce the

resolution of an image (Brisco et al. 2013, White et al. 2014). Filtering allows the user to

mitigate or correct distortion caused by the imaging sensor or environmental effects such

as windy or rainy weather. While there are many filters available to adjust imagery,

almost all filters perform averaging on clusters of pixels, based on the pixels value

compared to adjacent pixels. In order to reduce the amount of speckle in an image, a

moving weighted function filter with varying filter window sizes can be applied to the

image pixels to reduce the amount of speckle (Lee at al. 1994). Common filters used for

SAR processing can be found in Geomatica (PCI Geomatics) software developed for geo-

spatial analysis and remote sensing applications, which includes the following three

processing filters:

1) 'FAV' (Averaging Filter)

FAV is a filter that performs spatial average filtering on individual pixels in an

image using the gray-level values in a square or rectangular window that surrounds each

pixel (Figure 2.6). Dimensions of the filter size must be odd numbers, and can be between

1x3 or 3x1 to 1001x1001. The filter size cannot exceed the size of the image. Common

resample pixel sizes are 3, 5 or 7. Values higher than 7 will result in significantly altered

and dissolved data which is not indicative of the SAR response in most cases.

```
Image before filtering              Image after filtering

8 8   8 9 9 9 7 6 6 6   6 6
8 8   8 9 9 9 7 6 6 6   6 6
      +---------------+             +---------------+
8 8  |8 9 9 9 7 6 6 6 | 6 6        |8 8 8 8 7 7 6 6 |
8 8  |8 9 9 7 6 6 6 6 | 6 6        |8 8 8 7 7 6 6 6 |
9 9  |9 8 8 6 6 6 6 6 | 6 6        |8 8 8 7 7 6 6 6 |
9 9  |9 8 7 7 6 5 6 6 | 6 6        |8 7 7 7 6 6 6 6 |
7 7  |7 7 7 6 6 6 6 6 | 6 6        |7 7 7 6 6 6 6 6 |
6 6  |6 6 6 6 6 6 6 6 | 6 6        |7 7 6 6 6 6 6 6 |
6 6  |6 6 6 6 6 6 5 | 5 5         |6 6 6 6 6 6 6 6 |
6 6  |6 6 6 6 6 6 6 6 | 6 6        |6 6 6 6 6 6 6 6 |
      +---------------+             +---------------+
6 6   6 6 6 6 6 6 6 6   6 6
6 6   6 6 6 6 6 6 6 6   6 6
```
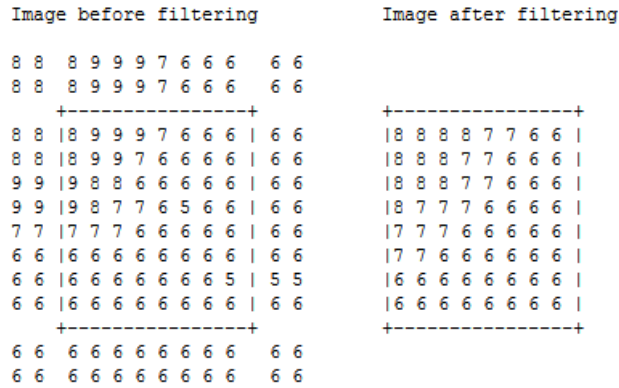
Figure 2.6. FAV averaging filter example using a 5x5 filter on an 8x8 pixel image
(Geomatica 2015).

Pixels with values within the minimum and maximum background range are excluded

from the calculations. If one value is specified, the image contains one background value.

If a parameter is not specified, the image will contain no background value.

2) 'FGAMMA' (Gamma Filter)

FGAMMA performs gamma map filtering on image data that removes high

frequency noise (speckle), while preserving high frequency features (edges). When a

scene reflectivity is assumed to have a Gaussian distribution, it assumes a negative

reflectivity (Lopes et al. 1990; Lopes et. al. 1993). The filter performs spatial filtering on

each individual pixel in an image using the gray-level values in a window surrounding

each pixel. Horizontal and vertical filter size selected by the user specifies the size of the

filter in pixel units between 1 and 33. The dimensions of the filter must be an odd number

that can range from 3x3 to 11x11 pixels. To retain higher resolution and visual detail, 3,

5, or 7 are the most commonly used pixel sizes. Pixels near the edge of the image are

replicated to provide sufficient data for the filter.

3) 'FMO' (Mode Filter)

The FMO mode filter computes the modal gray-level values (the most frequently occurring gray-level value) in the square or rectangular filter window that surrounds each pixel. FMO mode filtering is best for cleaning thematic maps for presentation purposes because it replaces small 'island' effects with larger surrounding pixel clusters (Figure 2.7).

```
      Image before filtering          Image after filtering

88   899976666   66
88   899976666   66
     +---------------+                +---------------+
88  |899976666| 66                   |899666666|
88  |899766666| 66                   |899666666|
99  |988666666| 66                   |977666666|
99  |987765666| 66                   |976666666|
77  |777666666| 66                   |666666666|
66  |666666666| 66                   |666666666|
66  |666666665| 55                   |666666666|
66  |666666666| 66                   |666666666|
     +---------------+                +---------------+
66   666666666   66
66   666666666   66
```
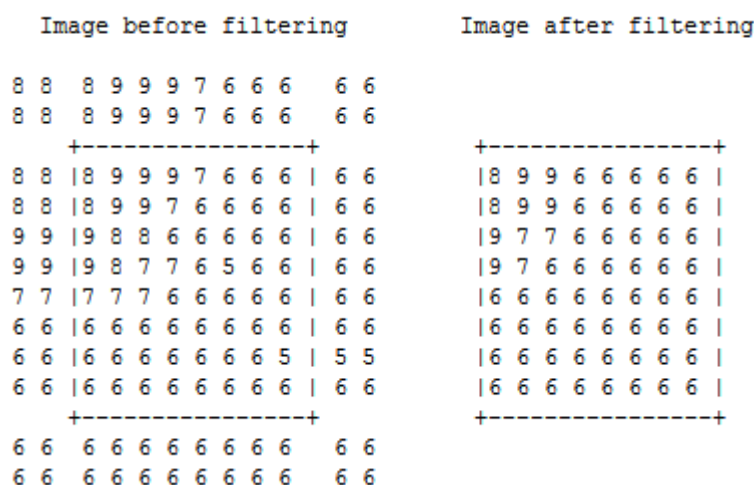
Figure 2.7. Mode filter (5x5) applied to an 8x8 database image that cleans thematic maps (PCI Geomatica, 2015).

While filtering allows the user to mitigate or correct distortion caused by the imaging sensor or environmental effects, it may also distort or degrade the image to the degree that the resolution changes markedly, resulting in loss of valuable spatial information on a per-pixel basis.

2.7.2 SAR Polarimetric Decompositions for Flooded Vegetation

Vegetation canopy penetration of the microwaves in a SAR system allows for mapping and classification of flooded vegetation due to enhanced backscatter from a double-bounce scattering mechanism (Brisco 2015). This results in enhanced HH backscattering with less increase seen in VV, therefore dual (HH/VV) or quad (HH, HV,

VH, VV) polarised data sets can be used to identify flooded vegetation using polarimetric decomposition techniques (Brisco et al. 2011, Brisco 2015). Decompositions are physically based models that can be decompressed from several channels in quad polarised SAR data, into a single intensity channel that estimates the amount of different types of scattering contributing to the total backscatter from each pixel (Freeman & Durden 1998, White et al. 2015). The phase information in the SAR data allows for the SAR decomposition to discriminate between different scattering mechanisms, and in particular between areas of double bounce scattering which is indicative of flooded vegetation (Brisco 2015). Well documented decomposition techniques include: Van Zyl (Van Zyl, 1989), Cloude-Pottier (Cloude and Pottier 1997), Freeman- Durden (Freeman and Durden 1998), and Touzi (Touzi et al. 2007). The most suitable decomposition for extracting flooded vegetation has been found to be the Freeman-Durden decomposition, which produces three bands identifying volume scattering (taller vegetation and forest), double-bounce scattering (flooded vegetation) and surface scattering (water or rough surface), (Freeman and Durden 1998, Brisco et al. 2013, White et al. 2014, 2015). Decomposition techniques are widely accepted and validated, and have been developed and implemented in remote sensing software for SAR processing.

2.8 Data Fusion

Data fusion is a technique that seeks to enhance the detection of features in an image by creating composite data from a variety of sensors or geospatial data sources. Remote sensing fusion decreases classification error and increases interpretation robustness, something that is generally only accomplished through integration of data collected from more than one sensor (Wald 2001, Wald 2002, Ramsey et al. 1998). The

utility of adding more than one sensor data type can be assessed by whether the fused classification product is more accurate compared to the results without fusion (Wald 2001, Irwin et al. 2017). Ideally, processes manipulating spatial data that fuse data from multiple sensors create quality products that provide improved accuracy and aid in interpretation of spatial data, which could not be otherwise achieved without data fusion. Fusion can be integrated in a wide variety of applications that have very different sensor characteristics, but can be modified to meet specific objectives that require rigorous quality control to meet research or consumer needs (Wald 2001, Wald 2002, Chasmer et al. 2014, Brisco et al. 2015).

Sometimes it can be difficult to map flooded vegetation with only SAR data because there are other targets in a scene that can have the same brightness as the flooded vegetation (White et al. 2014). While the use of multi-polarisation or multi-frequency data can improve accuracies, errors of omission and co-mission are still observed (Brisco 2015). As a result, many approaches use optical and terrain data to improve delineation of water features, identifying additional topographic high and lows, which greatly aid in delineation of surface water and flooded vegetation (Townsend and Walsh 1998, Pierdicca et al. 2008, Hostache et al. 2009). This is also true for detailed mapping of ephemeral water bodies for monitoring seasonal and annual changes in flooded vegetation due to changing climate factors (Brisco 2015). Therefore, the need for enhanced data fusion methods has been identified, and studies are increasingly using more than one type of sensor due to the different interactions with the ground surface, and feature extraction capabilities of the sensors. For example, Radar records the backscatter attributes of various polarisations, whereas optical sensors record the sum of radiance reflected. As a result, passive optical products are far more directly interpretable due to being analogous

to what we see with our eyes compared to radar, which is considered more difficult to visually interpret and is less intuitive. But, radar and optical remote sensing have similar attributes defined by reflectance, transmittance, backscatter and absorption, even though they operate on different regions of the electromagnetic spectrum (Jensen 2007). Optical is recording the passive reflectance from solar illumination, whereas radar sensors provide their own illumination, therefore, reflectance characteristics differ markedly. These two types of images are therefore not comparable in information content, which ultimately affects interpretation of the image. Therefore, data fusion (combination of different sensors) is valuable to derive similar products, such as canopy reflectance or land cover type (Hong et al. 2009). While there is limited literature on combining Lidar and optical derived water masks to evaluate temporal change, temporal Lidar products integrated with temporal multispectral products and hydrometric data provide a basis for monitoring surface volume changes in wetlands and support development of monitoring frameworks over large areas (Zhang et al. 2014).

2.9 Image Classification

Landscape classification is often tedious due to the size of most spatial datasets. Classification methods can also create discrete classes and overlapping units, inaccurately grouping features from interpreted landscapes. Clustering algorithms with many variants called K-means, is often used for land classification of spatial data. Methods of K-means classification have been successfully used to overcome problems of class overlap and to create increasingly spatially accurate land class maps, especially when combined with a high-resolution DEM (Burrough et al. 2000). K-means cluster classification aims to partition observations into clusters in which each observation belongs to the cluster with

the nearest mean, serving as a prototype of the cluster (Kanungo et al. 2002). The aim of the K-means algorithm divides points into clusters so that the within cluster sum of squares is minimised. The Euclidean distance is then calculated repeatedly between points and clusters by moving points from one cluster to another (Hartigan & Wong 1979). This process results in partitioning of the data into separate cells described in Figure 2.8. Hamerly et al. (2002) suggest by pre-processing data to exclude detected noise data, the accuracy of the clustering algorithm used in K-means classification is significantly improved.

1) k initial "means" (in this case $k=3$) are randomly generated within the data domain (shown in color).

2) k clusters are created by associating every observation with the nearest mean. The partitions here represent the Voronoi diagram generated by the means.

3) The centroid of each of the k clusters becomes the new mean.

4) Steps 2 and 3 are repeated until convergence has been reached.

Figure 2.8. Demonstration of the K-means standard algorithm generating clusters (Hamerly et al. 2002).

Other widely used classification methods in geography are decision tree (DT) hierarchical models based on decisions (decision tree) and rules that can be applied to predict land cover by determining the highest probability of prediction with input data and manually delineated areas, such as wet areas. Decision-tree hierarchical classification is more accurate than manual delineation from aerial photography, and can also be used with many types of spatial data to classify land cover types through supervised and unsupervised clustering techniques (Strahler 1980, Goodale et al. 2007; Chasmer et al. 2014). Decision tree fusion can be used to quantify the highest probability of prediction in

a set of input data and sample sites distributed throughout a watershed (Chasmer et al.

2014), which is specifically useful for wetland delineation and classification in forested

wetlands such as bogs and fens. In addition to generating water masks, a decision tree

water mask and/or level approach can be extended into use in water storage calculations

by using data-fusion for classification, or integrated with channel and bank delineation

routines to characterize flood hydrology in wetland environments (Crasto et al 2012;

Chasmer et al. 2014). This is accomplished by determining the highest probability of

prediction with input data and manually delineated wet areas distributed throughout a

watershed; specifically, for wetland delineation and land classification in forested wetland

environments (Chasmer et al. 2014), effectively identifying different types of wetlands in

spatially large, logistically challenging areas.

3.0 Prairie Pothole Region Wetland Hydroperiod Classification Using Multi-Temporal Sar in Alberta, Canada

*Joshua Montgomery[1], Christopher Hopkinson[1], Brian Brisco[2], Shane Patterson[3] Stewart Rood[4]

[1]*Department of Geography, University of Lethbridge, 4401 University Drive, Lethbridge, Alberta T1K3M4, Canada*

[2]*Canada Centre for Mapping and Earth Observation, 588 Booth St., Ottawa, Ontario, K1A 0Y7, Canada*

[3]*Alberta Environment and Parks, 9920 108 Street, Edmonton, Alberta, T5K 2M4, Canada*

[4]*Department of Environmental Science, University of Lethbridge, 4401 University Drive, Lethbridge, Alberta T1K3M4, Canada*

*Corresponding Author: joshua.montgomery@uleth.ca
Author contributions are as follows: **Joshua Montgomery** – principal author and writer, performed all field data collection, developed methodology, conducted analysis and interpretation of results. **Christopher Hopkinson** – supervised development of work, helped in data interpretation and evaluation, and manuscript editing. **Brian Brisco** – data provider of SAR data, and helped evaluate the manuscript. **Shane Patterson** – data provider of optical and Lidar data, and helped to evaluate and edit manuscript. **Stewart Rood** – assisted with vegetation interpretation and manuscript editing.

ABSTRACT

The Shepard Slough wetlands area is an urban fringe, suburban, agri-human modified prairie pothole environment in the Foothills Fescue Natural Subregion, located east of Calgary, Alberta, Canada. Due to low precipitation, development. and dry conditions with high evaporation, only approximately 1% of the natural subregion is continuously occupied by water, with natural wetlands confined to depressions in undulating terrain, making it challenging to monitor these wetland ecosystems.

This study examines how high resolution, single polarisation (HH) RADARSAT-2, Synthetic Aperture Radar (SAR), can be utilized in spatial-temporal studies to classify wetlands by associating surface water hydroperiod to wetland permanence and classification. The innovative hydroperiod analysis and methodology presented provides a

baseline for long-term, high resolution water resource monitoring describing more than just water extent of wetlands, allowing for enhanced characterization and classification of wetlands that can be applied to any wetland or floodplain environment. An intensity (dB) threshold routine is used to extract open surface water extent of marsh wetlands in the growing season over three years (2013, 2014, 2015). Wetland hydroperiod is examined using a pixel frequency analysis and classified in accordance with the current Alberta Wetland Classification System (2015).

The results of this three-year study indicate that SAR derived multi-temporal open-water masks provide an index of wetland permanence class, with overall accuracies of 88.7 to 95.2% compared to optical validation data, and RMSE between 0.2m and 0.7m between model and field validation data. Hydroperiod variation and surface water extent was found to be heavily influenced by short-term rainfall events in both wet and dry years (rainfall events of ~30+mm corresponded with a marked increase in temporary surface water). Persistent and staggered rainfall yielded the largest water surface area. Seasonal hydroperiod in wetlands was found to be highly variable if there was a decrease in temporary or semi-permanent hydroperiod classes. In years with extreme rain events, the more temporary hydroperiod classes were observed in higher total area percentages compared to seasonal and semi-permanent/permanent classes (ie. 84% in 2015 which has significant rainfall events, compared to 42% which did not have a significant rainfall event). Flooding controls, water diversion, and highly variable precipitation may also be affecting the hydrological regimes of these prairie pothole wetlands, contributing to changes to wetland riparian vegetation, and therefore how these wetlands are classified and what class they fall in to under the Alberta Wetland Classification System (2015).

Keywords: SAR, wetlands, hydroperiod, time series, frequency analysis

3.1 Introduction

3.1.1 Wetland Resources

Wetlands are defined as areas of land that hold water, either temporarily or permanently, and contain waterlogged and altered soils with water tolerant (hydrophytic) vegetation adapted for life in saturated soil conditions (Government of Alberta 2013). Wetlands are vital for replenishing and storing groundwater, preventing flooding, reducing erosion, filtering and purifying water, and storing substantial amounts of carbon (Stewart & Kantrud 1971; Warner & Rubec 1997, Government of Alberta 2013). Therefore, wetland areas have environmental, social, and economic impacts given the role wetland ecosystems have in local ecology. Wetlands are one of the world's most threatened ecosystem types, estimated to have diminished between 64-71% in extent in the 20th century, and continue to decline in quantity and function due to the effects of climate change, anthropogenic activities, and land cover change (Daily et al. 1997, Dahl et al, 2007, Costanza 2014). Wetlands found at high latitude or in semi-arid regions have been found to be vulnerable to climate changes due to their poor capability to adapt to changing temperature and precipitation regimes (Lane et al. 2014).

Even in water rich countries such as Canada, decline and degradation of these wetland ecosystems has become concerning (Komers and Stanojevic 2013, Smith et al. 2014). Agricultural drainage and urban expansion in the settled areas (known as the 'White Zone') in the province of Alberta, has resulted in the disappearance of approximately 2/3 of wetlands in the region (Government of Alberta 2013, de Groot et al. 2013). In addition, warmer temperatures and reduced precipitation trends are causing drying of wetland surface and groundwater, resulting in changes to hydrology and vegetation (Roulet 2000; Stow et al. 2004; Klein et al. 2005; Riordan et al. 2006; Smith et

al. 2014). Wetland water-levels and extent can fluctuate daily, seasonally and unpredictably following prolonged periods of rainfall, affecting the ecological characteristics of a wetland controlled by the presence and duration of open water, referred to as the *'hydroperiod'* (Ewel 1990). Surface water frequency and hydroperiod characterizes wetland type, directly relating to the perceived value of a wetland in time series investigations (eg. Foster 2007, Mitsch and Gosselink 2007). Therefore, if a wetland has a high proportion of more permanent water (semi-permanent) determined in hydroperiod analysis, and has dynamic hydroperiod changes (temporary hydroperiod), it is likely of more value ecologically and economically based on the services it provides.

As these valuable freshwater resources become increasingly scarce, there is a need for improved wetland monitoring and management through mapping and inventory (Ozesmi and Bauer 2002). While policy makers have sufficient scientific information to understand the need to take steps toward conservation, the global extent and spatial scale of wetlands is immense. Therefore, governing entities increasingly rely on developing remote sensing techniques to quantify wetland physical and functional changes for water monitoring and management where changes can be tied to ecosystem function using *in situ* validation methods. This enables temporal studies to be conducted over large areas to preserve and better understand the dynamics of wetland environments.

3.1.2 Remote Sensing for Water Mask Generation

Accurately mapping the hydrology in the prairie pothole region using remote sensing techniques can be challenging on a large temporal and spatial scales, particularly the dynamic wet area extent of the shallow and often ephemeral wetlands. While optical data such as SPOT or RapidEye has been used widely to map wet areas and accurately

delineate water body boundaries it is not able to capture the extent of the water surface

following significant precipitation events, and atmospheric effects such as haze and

clouds are problematic when trying to construct long-term monitoring programs over

large areas (White et al. 2015).

Traditional mapping requires significant amounts of in- situ data collection, which

can be logistically challenging, costly and may miss or underestimate the extents of many

smaller seasonal or annual wetlands (eg. Halsey et al. 2004, Frey & Smith 2007). Remote

sensing applications have been found to greatly enhance water resources monitoring,

ecological studies, and infrastructure management with spatial and temporal data (Ozesmi

& Bauer 2002; Toyra et al. 2002, Brisco et al. 2009; Maxa & Bolstad 2009, White et al.

2014, Brisco et al. 2017). Water masks are spatial data layers that can be derived from

many types of remote sensing data, providing a snap-shot of water versus land at a

specific time (White et al. 2014, 2015). Application domains include flood extent

delineation, water resource monitoring, habitat mapping and wetland assessments

(Goodale et al. 2007, Chasmer et al. 2014, Brisco et al. 2015, Crasto et al. 2015).

Synthetic Aperture Radar (SAR) backscattering signals obtained using radar satellites

have been commonly used for surface water extraction (White et al. 2014, Brisco et al.

2015, Schlaffer et al. 2016), and flooded vegetation monitoring in a variety of ecosystems

(Kasischke & Bourgeau-Chavez 1997, Brisco et al. 2008; Touzi et al. 2007, Brisco et al.

2009, Brisco et al. 2017).

Radar is different to optical sensors in that it is an active, self-illuminating sensor

technology that operates in the microwave spectrum, with two distinct benefits for earth

observation applications: (1) radar systems can collect any time of day or night and under

poor weather or atmospheric conditions; (2) backscatter (radar reflections) provide

different information to optical sensors. Unlike optical, radar is sensitive to surface texture, particularly in studies discriminating the contrast or brightness between objects such as land and water (Hess et al. 1990, Rio & Lozano-García, 2000; Bourgeau-Chavez et al. 2001; Alsdorf et al. 2001; Ozesmi & Bauer 2002, Brisco et al. 2013, White et al. 2015). Higher spatial resolution modes from RADARSAT-2 have been used to monitor smaller wetlands and enhance discrimination between land, flooded vegetation and water surrounding or beneath vegetation, allowing for better characterization and classification of wetland types (Touzi et al. 2007, Brisco et al. 2011, Schmitt et al. 2012, White et al. 2014). Open water areas have a high dielectric constant and act as a specular reflector under calm conditions causing very little backscatter to the sensor, therefore water appears dark (Di Baldassarre et al. 2011). Based on this, several water boundary extraction algorithms have been developed using pixel, object based or threshold classification approaches (Martinis et al. 2015, Bolanas et al. 2015, Brisco 2015).

3.1.3 Wetland Classification System

While the combination of several wetland classification systems (regionally variable), enhances and clarifies wetland classification, Stewart and Kantrud (1971) is still the foundation for assessments of marsh wetlands found in the prairie pothole region of North America (USA and Canada).

Prairie potholes are depressions formed after glacial retreat in the last ice age (~12,000 years ago), promoting wetland formation in these depressions following melting of land ice (Winter, 1989). Prairie pothole wetlands are highly variable in size and permanency, but are generally characterized as having less than 1m water depth at peak volume (Stewart and Kantrud 1971). Winter and Labaugh, (2003) describe how prairie

pothole wetlands change dynamically, making wetland function and classification

difficult to consistently assess through the growing season and between years. Stewart

and Kantrud (1971) describe prairie pothole marsh wetlands in detail, specifically

vegetation and surface water cover as indicators of wetland type and permanency.

Marshes are divided into seven different types based on open water and vegetation zones

(Figure 3.1). Each of these zones is subject to highly variable water levels and vegetation

succession depending on snowpack melt and rainfall.
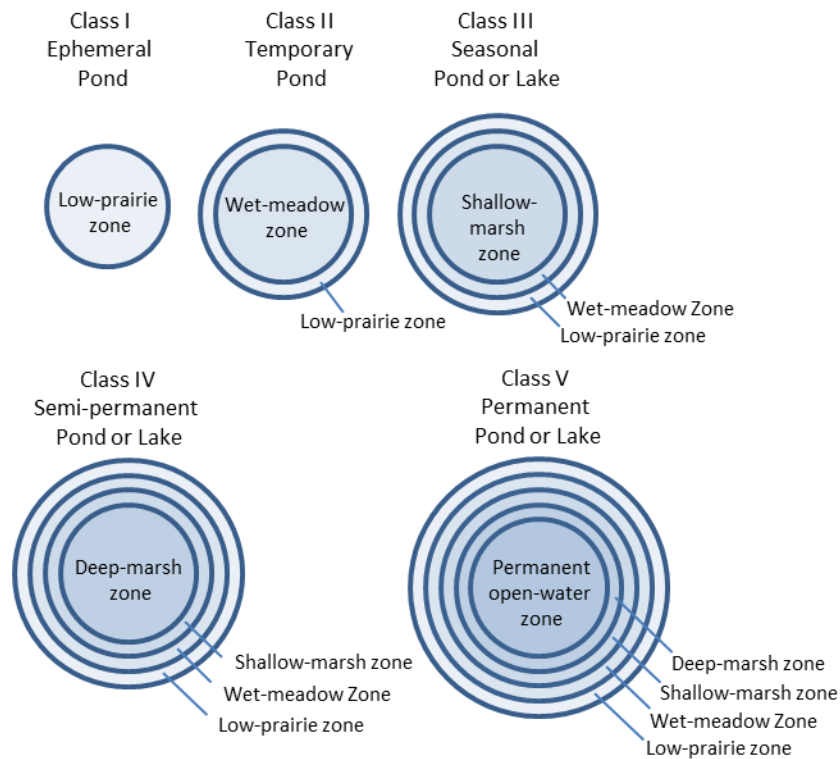
Figure 3.1. Marsh wetland classifications based on water permanence and spatial relation
of associated wetland riparian zones. *Adapted from Stewart & Kantrud (1971).*

The most common marsh environments in the prairie pothole region of Alberta are

temporary (class II), seasonal (class III), semi-permanent (class IV) and permanent (class

V) (Table 3.1). Wetland classes from Stewart and Kantrud (1971) have been narrowed

from seven to five, removing fen and alkali wetlands, better representing the common

marsh environments. Semi-permanent and permanent wetland types have been merged

into one class as a result of the limited three-year data series (permanent (V) requires a

longer timeframe (at least ~five consecutive years of data) to be classified as permanent).

Vegetation and soil characteristics are generally the best wetland class indicators, but the

hydroperiod of these four marsh wetland types is indicative of how permanent the

wetland is both seasonally and annually (Stewart & Kantrud 1971, Kantrud 1989,

Government of Alberta 2015, Ameli et al. 2017).

Table 3.1. Four commonly found marsh environments based on the Stewart and Kantrud (1971) wetland classification system, with corresponding hydroperiod and vegetation characteristics.

Wetland Type (S&K)	Hydroperiod	Vegetation Zone
Temporary (II)	Surface water present for short period of time after snowmelt or heavy rainfall.	Wet meadow
Seasonal (III)	Surface water present throughout growing season, typically dry by end of summer.	Shallow wetland
Semi-permanent (IV)	Surface water is present for most or all the year, except in drought conditions.	Deep wetland
Permanent (V)	Surface water present throughout the year	Open water

3.1.4 Study Objective

This study examines how high resolution, C-HH SAR data can be utilized to

classify dynamic marsh and shallow-open water wetlands by associating surface water

extent and permanence in accordance with the current Alberta Wetland Classification

System (2015). Objectives of the study were to: (1) present and evaluate an effective

approach to derive water masks from SAR imagery and compare them to water masks

derived from temporally similar optical imagery, and (2) classify open water wetland

hydroperiod and permanency using frequency analysis over a three-year time-period.

3.2 Data & Methods

3.2.1 SAR Data

RADARSAT-2 SAR data were collected at each repeat cycle (24 days) in 2013 to 2015. A total of 18 (6 each year, (Table 3.2)) Ultra-Fine (U77) single look complex (SLC) 20 x 20km swath images in ascending orbit are used to derive surface water masks, which have a nominal resolution of 2.8 x 2.8m. While the nominal resolution of the U77 mode is 2.8 x 2.8m, the SAR dataset was re-sampled using cubic convolution to 5 x 5m to match the optical datasets used for validation purposes.

Table 3.2. Ultra-Fine (U77) beam-mode SAR acquisition dates at Shepard Slough for 2013 to 2015 (2016)

2013	2014	2015
April 19	April 14	April 9
May 13	May 8	May 3
June 6	June 1	June 7 (2016)
June 30	June 25	-
July 24	July 19	July 14
August 17	August 12	August 31
-	-	September 24

To maintain consistent frequency values (discussed in results section) the sample size n=6 was used for each year. For 2013 and 2014 high quality acquisitions were available for April to August. Unfortunately, data quality limitations prohibited temporally similar analysis in 2015, specifically in June. To maintain temporal continuity for all years, an acquisition from June 7, 2016 was substituted based on similar environmental conditions. A missing acquisition issue was also encountered for September 2014; therefore, to be temporally consistent to 2014, September 2013 was also not included in the series. September 2015 is included in the analysis as it provides six

high quality images for the 2015 series and showcases the effects of substantial late growing season precipitation (results section).

3.2.2 Optical Data

RapidEye (Planet Labs) optical image data from May 8, 2014, and SPOT (*Centre national d'études spatiales*) from July 15, 2015, and September 20, 2015 sampled at 5 x 5m resolution were acquired on near-coincident or coincident days as some of the SAR data for validation purposes. Images contain atmospheric effects such as clouds or haze which required atmospheric correction using PCI Geomatica Focus atmospheric correction tools. While primarily used for agricultural purposes, RapidEye imagery is also suitable for water identification (Tapsall et al. 2010, Giardino et al. 2014). Surface water was classified using K-means unsupervised classification in PCI Geomatica Focus 2015 (Burrough et al. 2000, 2001, Lane et al. 2014).

3.2.3 Airborne Lidar Data

Airborne Lidar data was collected by Airborne Imaging (Calgary, Canada) in 2008 over the Shepard Slough area. Processing of a bare earth 1m x 1m digital elevation model (DEM) was carried out using TerraScan (Terrasolid, Finland) and Surfer (Golden Software, Colorado) following methods of Hopkinson et al. (2005). The Lidar DEM was primarily used for orthorectification of the SAR and optical data, but also provided topographic validation for water surfaces within wetland basins while illustrating the surface hydrologic flow pathways for the study area.

3.2.4 Ground Validation Data Collection

Wetlands were chosen for the study from a series of optical images based on observed riparian disturbance, wetland size, pre-existing stilling wells (GoA), and

logistical feasibility (Figure 2b-2e). Of the four chosen study locations, two were visited

in the last week of July 2015 to determine surface water extent and riparian habitat

boundaries within cm accuracy using a Global Navigation Satellite System kinematic

'stop and go' survey techniques, where rover positions were corrected to a nearby static

base station location. The topographic transition between wetlands and surrounding

upland is gradual but the transition between wetland vegetation communities and upland

vegetation communities is abrupt due to agricultural activities near or within the wetland

riparian area. Cross-sectional transects were performed extending away and upwards

from the wetlands to reflect vegetation zones and apparent changes in vegetation

community composition, which includes identification of predominant plant species, with

abundance ranking by foliar cover. Naming, taxonomic treatment, and life history

characteristics are in accordance with 'USDA-Plants' of the United States Department of

Agriculture, Natural Resources Conservation Service (https://plants.usda.gov/java/), with

some wetland characteristics from Washington State Department of Transportation lists

(wsdot.wa.gov).

3.2.5 Study Area

The Shepard Slough study site is a 278km^2 polygon east of the City of Calgary,

Alberta, Canada in the Municipal District of Rockyview (M.D. #44) (Figure 3.2a).

Shepard Slough is characterized as an urban fringe, suburban, agri-human, modified

prairie pothole environment in the grassland natural region, Foothills Fescue Natural

Subregion, with gently rolling plains dominated by moderately calcareous glacial tills at

an average elevation of 1030m (Natural Regions Committee 2006). Only approximately

1% of the natural subregion is continuously occupied by water due to low precipitation

and high evaporation, with wetlands confined to prairie pothole depressions. The Shepard Slough region has lost much of its natural prairie pothole character due to extensive modification, and is therefore distinct to true prairie pothole regions. Cultivation, irrigation networks, and urbanization has greatly impacted the local ecology and hydrology of the natural subregion, in some areas reversing the drainage pattern to the north through reservoirs and irrigation canals.

Marsh wetlands were selected to best reflect the overall wetland population in the study polygon. Four study sites were selected in the Shepard Slough Study Area based on accessibility and previously established field data collection activities. The wetlands do not have official names, therefore are identified by defining features or proximity to infrastructure. 'West Chestermere' (Figure 3.2b) and 'Pumpjack' (Figure 3.2c) are individual wetlands in agricultural fields in well-defined depressions (determined from a Lidar DEM), chosen to represent wetlands known to be more permanent features on the landscape. Their overall permanence derives from surface hydrological connectivity at a low point in the landscape (West Chestermere) or by partial obstruction of surface drainage by surrounding road development (Pumpjack). 'Algae' (Figure 3.2d) and 'Pothole' (Figure 3.2e) are larger spatial scale areas containing many individual hydrologically variable wetland components in dynamic prairie pothole landscapes. These latter two wetland areas are more disconnected from surface hydrological inflows either by virtue of upstream anthropogenic flow diversion (Algae) or their shallow and disconnected catch basins on the land surface (pothole). The differences in hydrological drainage characteristics and spatial coverage between the wetland focus areas was chosen to evaluate the utility and effectiveness of the presented hydroperiod analysis over a range of scales and wetland types.

59
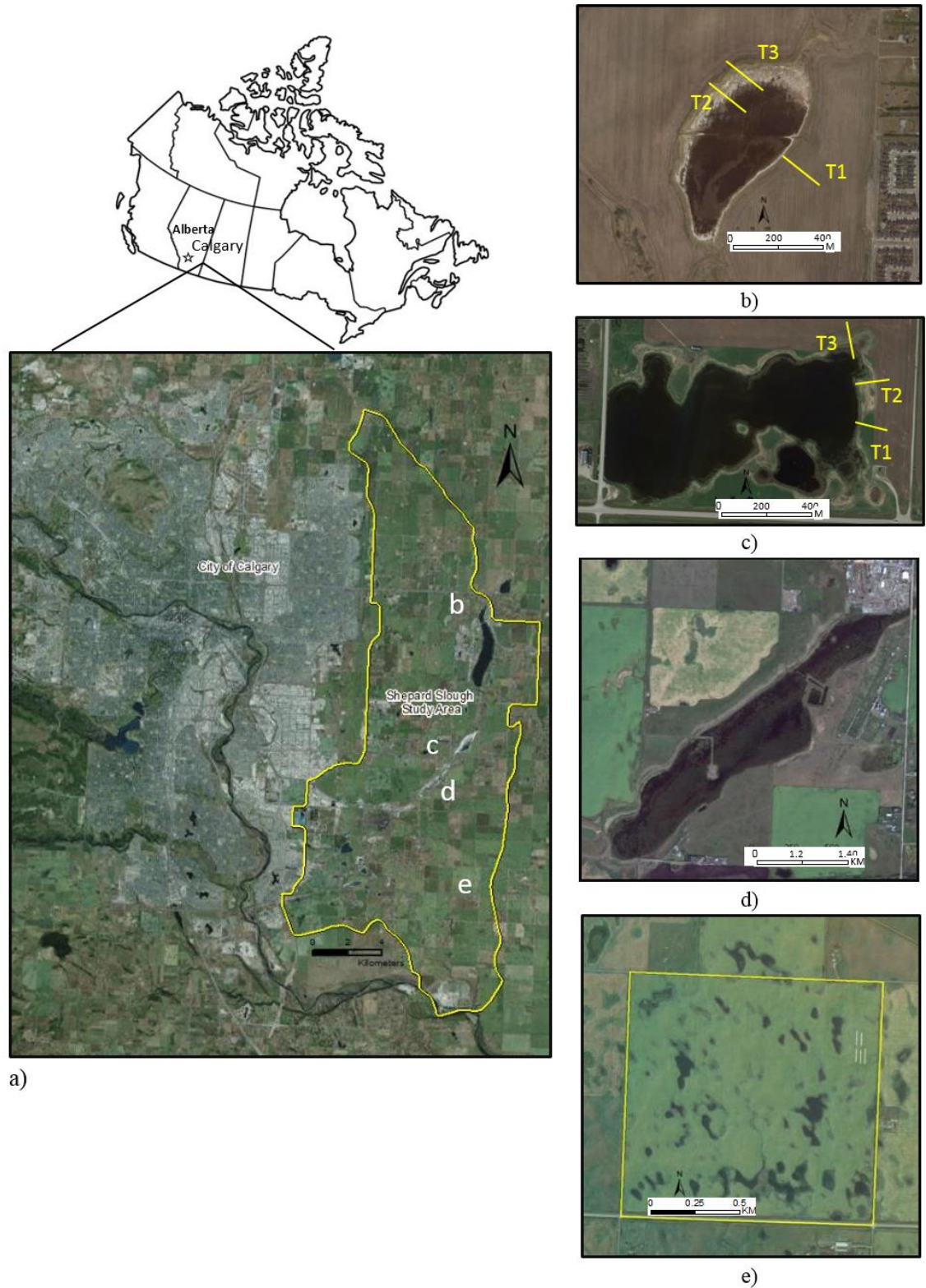
Figure 3.2a-e. Shepard Slough case study area ~10x30km in Canada, a) adjacent to the City of Calgary, and location of the four chosen wetlands focus areas used in the hydroperiod classification analysis b) West Chestermere, c) Pumpjack, d) Algae, and e) Pothole. Vegetation transects surveyed in 2015 are shown as yellow in (b) and (c).

3.2.6 Surface Water Extraction

Geomatica 2015 (PCI Geomatics) was used for filtering and surface water extraction procedures using the SAR data. A model developed by White et al. 2014 using Geomatica v10.3.2 was updated to current module versions to extract surface water using input threshold intensity/decibel (dB) range values (Appendix A). The first steps convert from linear to decibel then reduce the amount of speckle before applying a threshold value to the image, reducing speckle noise while maintaining spatial resolution and edges (White et al. 2014). Speckle reduction methods are used to remove unwanted 'noise' while preserving edge features in an image using moving weighted filters and resampling algorithms (e.g. Lee et al. 1994, Schmitt et al. 2013, White et al. 2014). The FGAMMA adaptive filter is used to preserve edges, which is important for surface water extent analysis (Toutin 2011, Zhang et al. 2012). The FAV filter is used to reduce speckle and noise, and the FMO filter is used to further reduce noise and has been found to help with the ortho-rectification (White et al. 2014, 2015). FGAMMA and FAV filters are applied independently in parallel, to avoid the possibility of compounded loss of water edge detail, then combined later in the routine (White et al. 2014). Figure 3.3 presents a flow diagram of the image processing, threshold range and surface water extraction workflow.
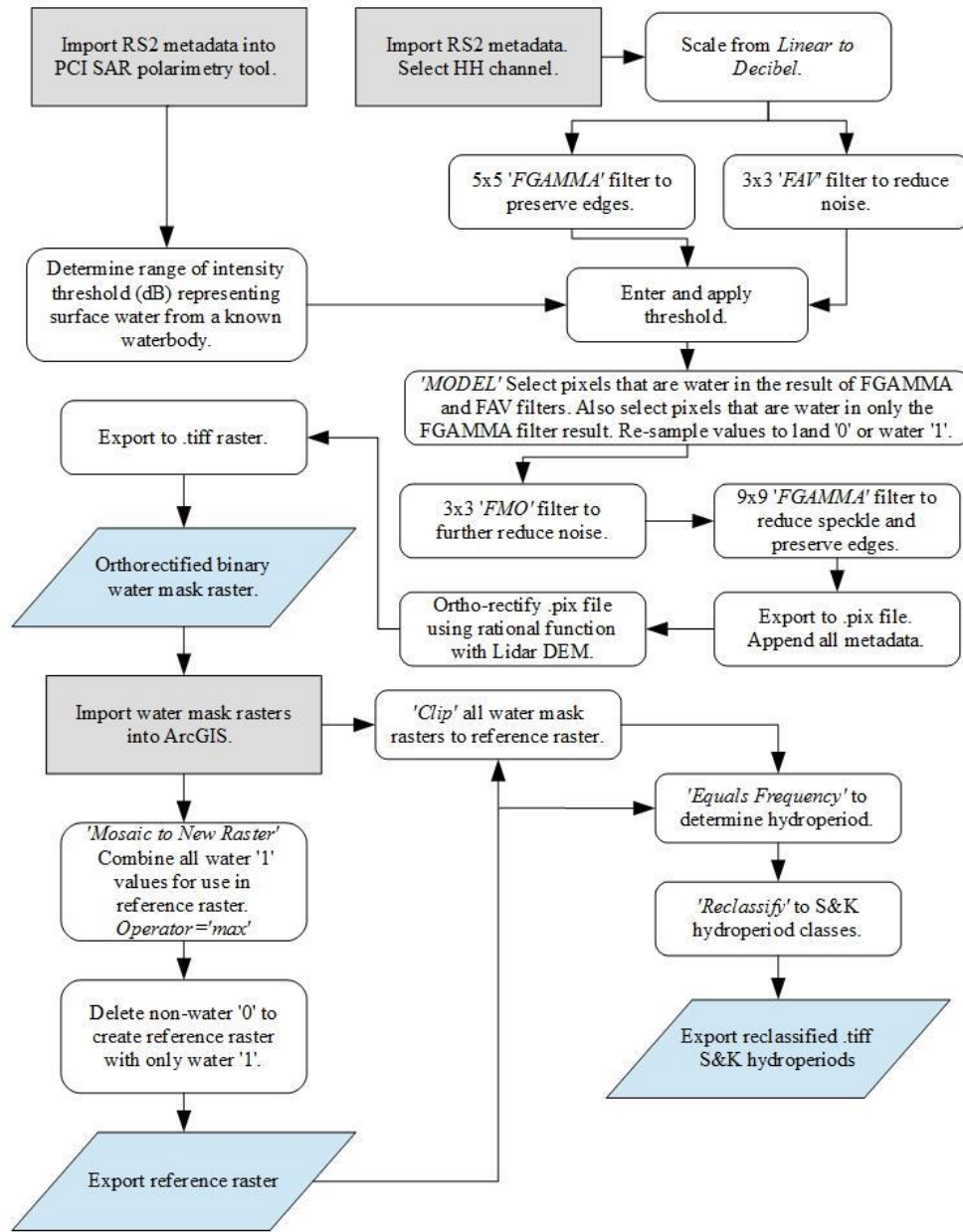
Figure 3.3. Flow diagram of intensity (dB) threshold routine in PCI Modeller and Ortho-Engine to create binary water masks, and hydroperiod classification conducted in ESRI ArcGIS. Grey rectangles indicate inputs, white icons with rounded corners are intermediate processes, and blue parallelograms represent final outputs. Functions within software are italicized.

Extraction of the threshold decibel (dB) ranges that represent surface water was conducted through the PCI SAR Polarimetry Tool in the PCI Geomatica suite using a consistent area polygon ~70 hectares in area over Chestermere Lake, which is a known

and controlled body of water with persistent water permanency and water extent (Figure

3.4a). This threshold (dB) sampling routine is presented as a manual process in this study

and the values are scene specific due to weather effects on the backscattering, but can be

automated based on training data from known geographic locations or other surface water

inventories (Peiman et al. submitted). Outlier pixels with values contributing five or less

percent of the dB sample polygon area were excluded from the threshold input range

(Figure 3.4b).
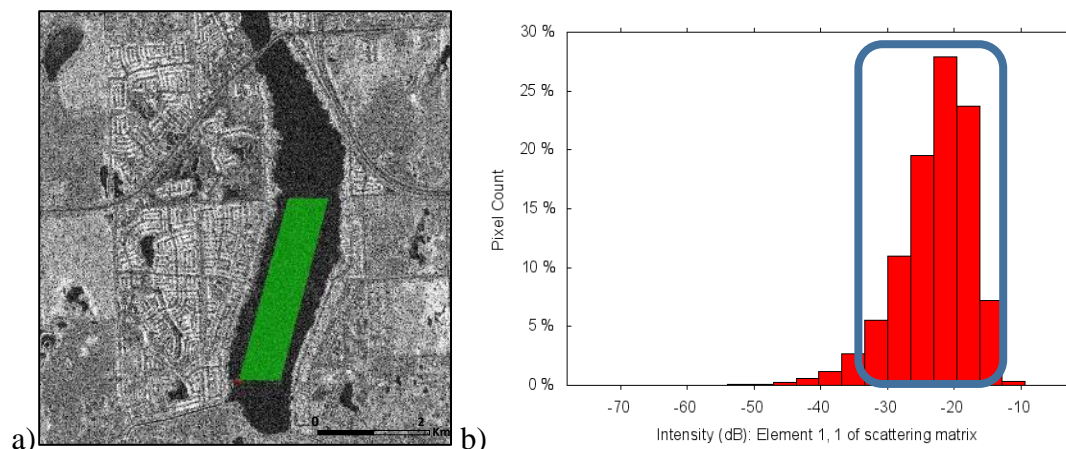
Figure 3.4a and b. a) consistent sample polygon used to derive the intensity (dB) range
for each image over Chestermere Lake. b) histogram output from August 12, 2014 of the
intensity (dB) ranges from the sample polygon (-14 to -32, 90% of total pixels) showing
values over 5% total pixel count (blue outline).

After the threshold range is input into the model, pixels that were only water in

FGAMMA and not FAV are assigned to the water class so that the water edge is

preserved. Pixels not selected as surface water after the FAV filter and not in FGAMMA

are then not included as open water to again preserve edges (White et al. 2014). Ortho

rectification to the high resolution 2008 Lidar DEM was performed in Geomatica 2016

Ortho-engine using rational function and metadata ground control points.

3.2.7 Hydroperiod Analysis

The wetland surface water hydroperiod classification was performed using an *'equals frequency'* routine in ESRI ArcMap 10.3, executed on six binary surface water raster images for each year. The *equals frequency* routine calculated the number of times a pixel was identified as water in the same geographic location in each of the rasters, providing a measure of water permanence throughout the growing season (Figure 3.5). Hydroperiod frequency analysis criteria is illustrated in Figure 3. Reference rasters were created that contain a numerical pixel value that corresponds to the pixel values in the input rasters. Input rasters are binary and contain only '0' (land) and '1' (water) values, therefore all the pixel values in the reference raster are all '1' (water) (Figure 3.5). Reference rasters were created by mosaicing all input water mask rasters into a new mask with only '1' (water) values of the maximum extent of all input water mask rasters. Land values '0' were reclassified or deleted in the reference raster to avoid commission of land in the frequency results.
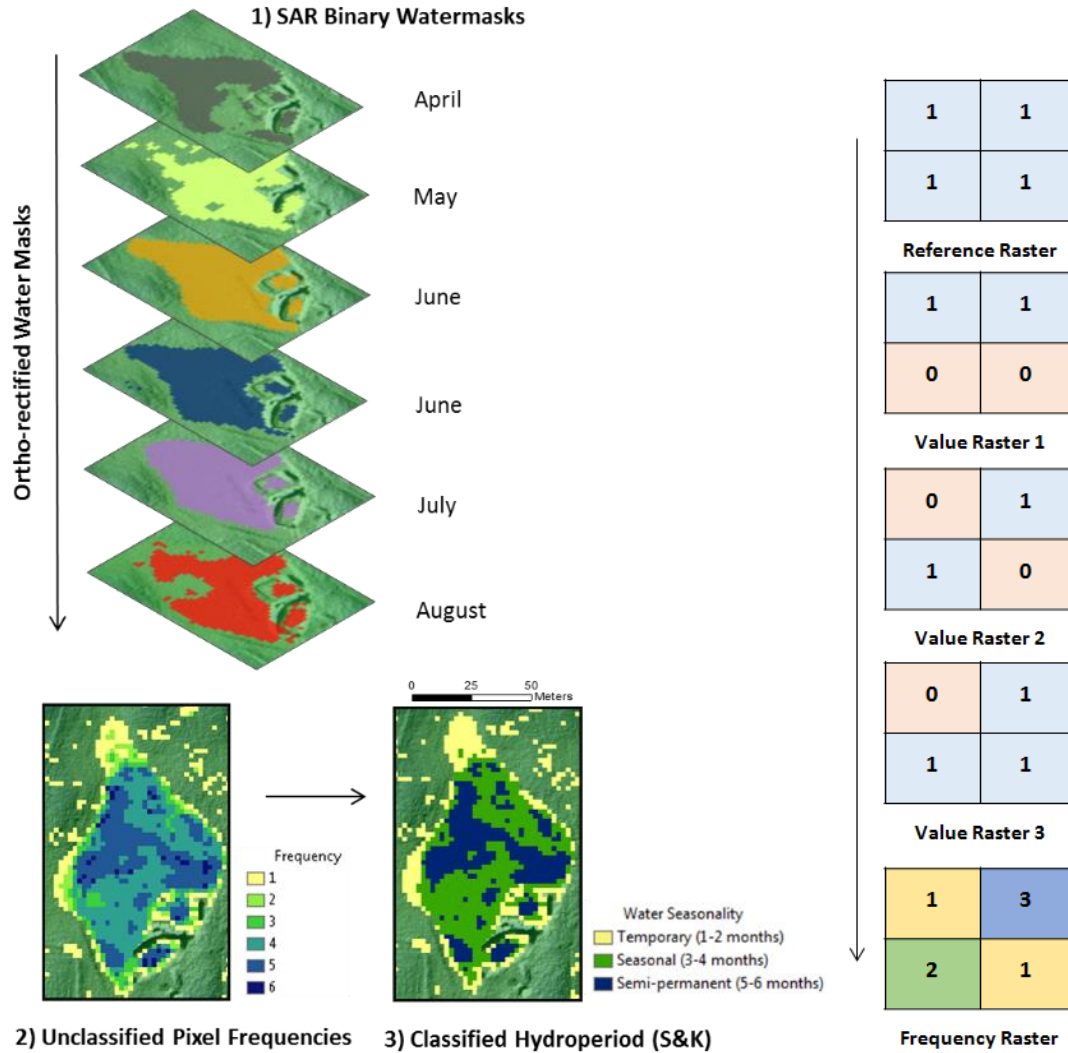
Figure 3.5. Visual flow diagrams of the binary water mask frequency processing and hydroperiod classification. The binary water masks and hydroperiod rasters overlay the Lidar DEM for texture and visualization purposes.

Before executing the 'equals frequency' routine, all binary water masks were clipped to the reference raster (combined area of all water values in all rasters) to avoid commission of land. The output pixel frequency (Figure 3.5) corresponds to the number of months (n=6) used in each year, which was reclassified from frequency values (1 to 6) to water hydroperiod values (temporary, seasonal, and semi-permanent) based upon the Stewart and Kantrud (1971) marsh wetland classification criteria (Table 3.1). The six-month time series coincides with the growing/rainy months at Shepard Slough (April to

August/September) where frequency values of 1-2 months are reclassified to represent

'temporary' (S&K class II), 3-4 months to 'seasonal' (S&K class III), and 5-6 months to

'semi-permanent' (S&K class IV). 'Permanent' (S&K class V) wetlands that exist year-

round even in drought years were not differentiated from 'semi-permanent' in this study

because SAR cannot directly detect water under winter snow and ice conditions, and

certainty of permanent wetland classification requires a period longer than 3 years

(Government of Alberta 2015). Consequently, class V (permanent water bodies)

constitute a sub-set of class IV wetlands in this study.

3.3 Results

3.3.1 SAR Binary Water Mask Extraction

Results of this study show that the intensity thresholding technique developed by

White et al. 2014 is an effective method for extracting surface water of large and small

wetlands in a dynamic prairie pothole marsh environment (Figure 3.6). The average upper

SAR dB threshold limit was found to be -14dB, and the lower limit -31dB, with dB

ranges varying with weather and ground conditions (variable dependent on weather

conditions) (Table 3.3 and Figure 3.7).

Table 3.3. Calgary, Alberta International Airport weather station data. SAR acquisition dates and intensity decibel (dB) ranges for surface water in each image, with associated percentage of pixels contributing to the overall number of pixels sampled within the sample area polygon. Wind (km/hr) and daily precipitation (mm) information is also provided.

Acquisition Date (yyyy-mm-dd)	Upper Limit (dB)	Lower Limit (dB)	dB range percentage (%) of pixels used from sample area	Wind/Gust Speed (km/hr)	Daily Precipitation (mm)
2013-04-19	-16	-30	89	21/NoData	1 cm snow
2013-05-13	-18	-32	89	28/67	Trace rain
2013-06-06	-17	-30	90	23/43	Trace rain
2013-06-30	-15	-28	85	15/35	0
2013-07-24	-13	-30	85	14/31	0.8
2013-08-17	-18	-32	90	14/50	0.6
2014-04-14	-9	-25	89	20/37	0
2014-05-08	-15	-30	85	34/44	0
2014-06-01	-8	-28	94	13/46	5.4
2014-06-25	-14	-30	86	14/57	2.1
2014-07-19	-15	-32	90	17/31	NoData
2014-08-12	-14	-32	90	27/48	0
2015-04-09	-15	-33	85	13/31	0
2015-05-03	-15	-32	92	5/35	Trace Rain
2016-06-07	-15	-30	88	34/44	0
2015-07-14	-8	-31	90	19/52	0.4
2015-08-31	-10	-30	88	12/57	0
2015-09-24	-17	-33	88	16/35	0
Average	-14	-31	89	19/44	-
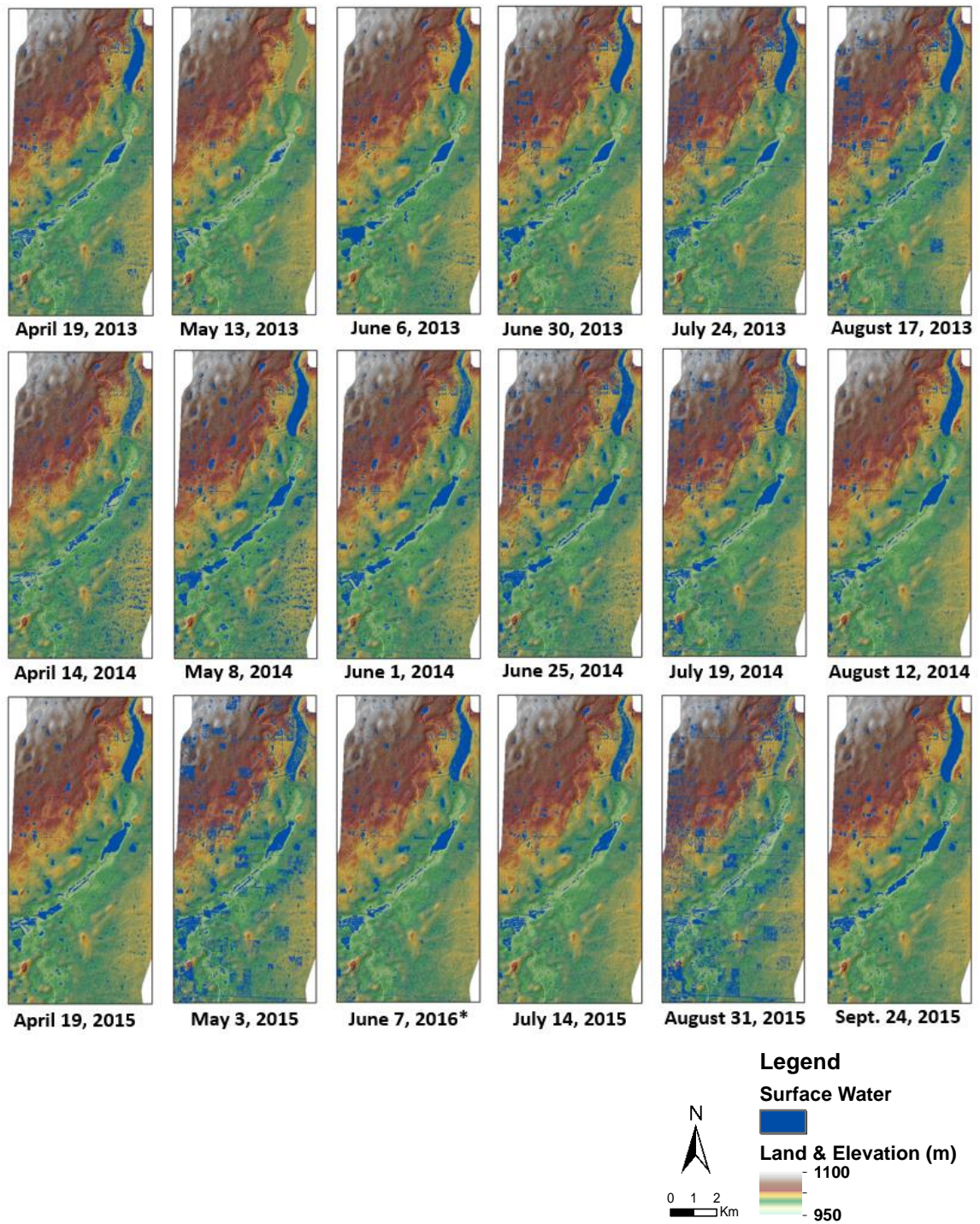
Figure 3.6. SAR derived surface water masks using an intensity (dB) thresholding approach for 2013 (top row), 2014 (middle), and 2015 (bottom). Images show the dynamic changes of wetland surface water over the growing season at Shepard Slough. Note quality issues with May 13, 2013, August 31, 2015, and that June 7, 2016 is substituted for June 2015.
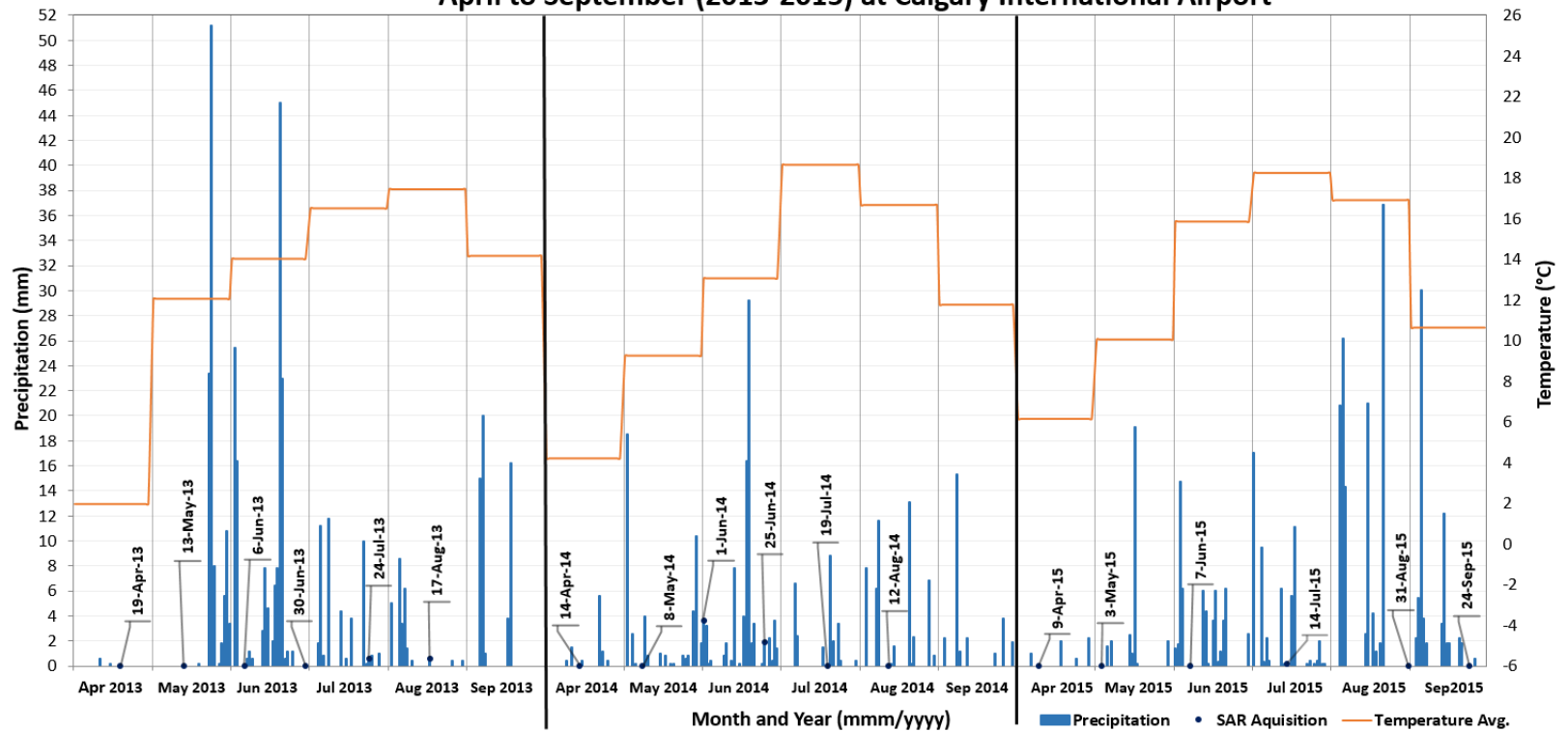
Figure 3.7. Metrological data with monthly average temperature and daily precipitation for Shepard Slough recorded at the Calgary International Airport. Note: total precipitation for June 7, 2016 was the same as June 7, 2015 at 0mm.

SAR water mask results reflect the spring and summer growing season. Two images

(May 13, 2013, and August 31, 2015) were found to be of poor quality for surface water

extraction. Areas of known surface water in these images illustrated high backscatter with

similar intensity (dB) ranges as surrounding areas of known land. It is likely these poor-

quality images were a result of surface waves associated with high winds during the days

of acquisition (gusts up to 67 and 57 kph, respectively, table 3.3). A noticeable change in

surface water extent of larger wetland areas is seen in these images, compared to smaller

wetlands.

3.3.2 Comparison of SAR and Optical Water Masks

Ten optical mask classifications of RapidEye (RE) and SPOT images were tested

for classification accuracy based on training areas for SAR water mask comparison

purposes, with overall optical classification accuracies ranging from 87-95%, and Kappa

values ranging 0.72-0.87. With the 24-day repeat visit of RADARSAT-2 and atmospheric

issues associated with RE and SPOT data (clouds, shadows and haze), few temporally

close images were ideal for comparative analysis. Water masks from three sets of near-

coincident (within four days) SAR and Optical images were compared to assess the

similarity of the SAR derived threshold masks (Figure 3.8). Confusion matrix data

produced positive correlation of > 76% when compared to the SAR data (Table 3.4). True

positive reflects the correlation between pixels classified as water in both SAR and

optical images.

Table 3.4. Confusion matrix results of near-coincident SAR and optical (RapidEye and SPOT) data from 2014 and 2015. Note: results do not represent absolute accuracies, as the optical water masks contain some uncertainty and the two weaker comparison results represent acquisitions from different days.

SAR Date	Optical Date	True Positive	False Positive	Misclassification Rate	Overall (%)
2014/05/08	2014/05/08	92.1	0.5	0.3	95.2
2015/07/15	2015/07/14	76.5	1.2	4.7	88.7
2015/09/24	2015/09/20	84.8	2.9	1.4	96.1

Red = RSat 2 only 4%
Blue = RapidEye only 4%
Purple = Both 92%
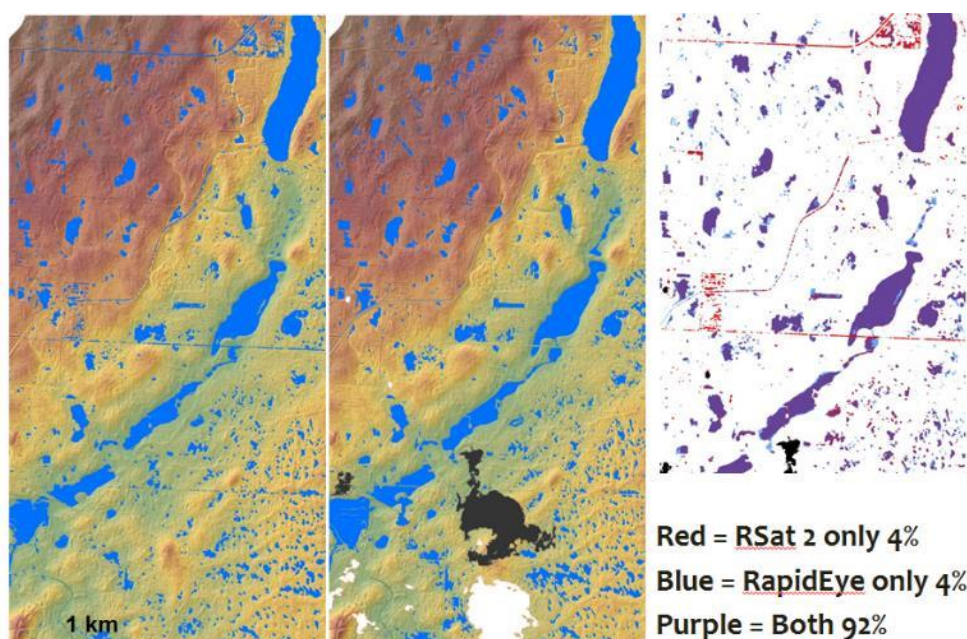
Figure 3.8. Comparison of binary water masks for temporally coincident SAR (left), and RapidEye (middle) on May 8, 2014. Cloud (white) and shadow (black) effects are shown in the RapidEye image. Correlation (right) shows areas of agreement in purple, SAR only as red, and RapidEye only as blue.

3.3.3 SAR Water Extent Field Validation and Wetland Vegetation

Pumpjack and West Chestermere are wetlands that have minimal agricultural disturbance from activities such as tilling, allowing for riparian vegetation growth; validated from riparian vegetation composition and abundance during field data collection (Figure 3.9a-b), (Tables 3.5 and 3.6). The RMSE of the riparian transects and water extent observed in field validation data and optical data used for hydroperiod classification of wetland water extent was between 0.2m and 0.7m, less than 10% error between field and model, or approximately 0.5 meters based on the limited number of transects.
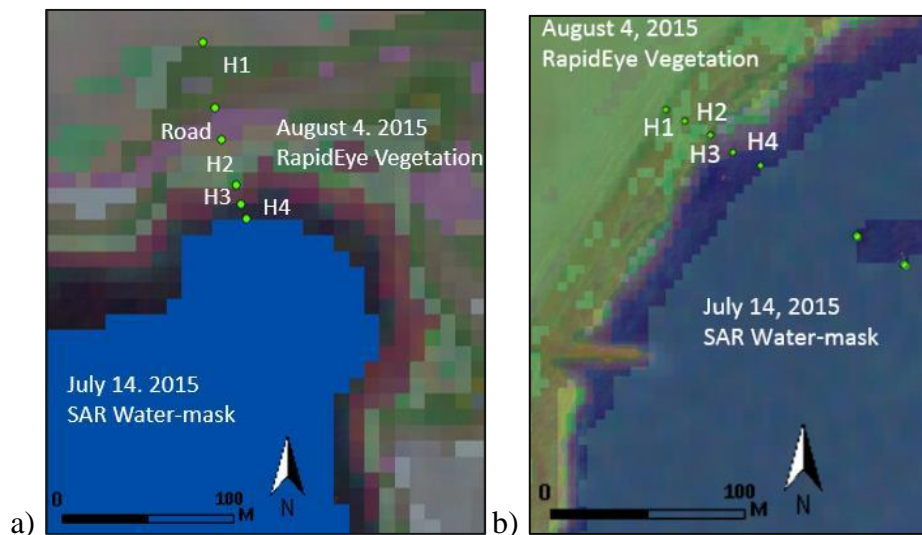
Figure 3.9. Wetland vegetation and water extent field transects collected in July 2015 near-coincident with SAR acquisition over: a) Pumpjack (Transect 3 in Table 3.5); and b) West Chestermere (Transect 2 in Table 3.6). Note: green points indicate field validation points. RapidEye vegetation zone colours have not been re-classified to represent any particular zone, therefore just indicate where general zones transition along transects.

Table 3.5. Riparian vegetation species transects for Pumpjack and West Chestermere. Refer to Figure 2 for transect locations. Transect 3 is seen in Figure 3.9a.

Wetland & Transect	Habitat zone	Plants sequenced by decreasing abundance
Pumpjack		
1	H1	Foxtail, sowthistle, goosefoot, mannagrass, cattail
	H2	Goosefoot, cattail
	H3	Cattail, buttercup
2	H1	Foxtail, cattail
	H2	Foxtail, goosefoot, sloughgrass, cattail, mannagrass
	H3	Goosefoot, bur-reed, dandelion
	H4/5	Duckweed
	H4/5	Duckweed
3	H1	Foxtail
	H2	Foxtail, sloughgrass, sedges
	H3	Buttercup, goosefoot, cattail, bulrush
	H4	Lamb's quarter, dandelion, goosefoot, ranunculus
West Chestermere		
1	1	Brome, rush, dandelion, sowthistle
	2	Sedges, foxtail, quackgrass, rush
	3	Mannagrass, foxtail
	4	Foxtail, goosefoot, manna grass
2	1	Brome, reed, wheatgrass, wildrye
	2	Foxtail, manna grass, sedges
	3	Manna grass, spikerush, sedges
	4	Sedges
3	1	Brome, reed canary grass, wheatgrass, wildrye
	2	Foxtail, manna grass, sedges
	3	Mannagrass, spikerush, sedges
	4	Sedges

Table 3.6. Most common plant species around the Pumpjack and West Chestermere wetlands, sequenced by decreasing occurrence across transect habitat zones.

Rank Occurrence	Common Name*	Scientific Name	Native/ Intro.	Growth	Wetland Status	Comment
1 (48%)	foxtail barley	*Hordeum jubatum* L.	N (hybrid)	graminoid	facultative	generalist – weed hybrid
2 (35%)	sedges, inc. beaked sedge	*Carex sp.*, including *C. rostrata* Stokes	N	graminoid	obligate wetland	specialists, hydrophytic
3 (30%)	mapleleaf goosefoot	*Chenopodium simplex* (Torr.)R	N	forb	upland	disturbance promoted
4 (30%)	American mannagrass	*Glyceria grandis* S. Watson	N	graminoid	obligate wetland	short/tall to 1.5 m
5 (26%)	broadleaf cattail	*Typha latifolia* L.	N	forb	obligate wetland	often emergent
6 (17%)	tall buttercup	*Ranunculus acris* L.	I	forb	facultative wetland	prolific weed
7 (13%)	common dandelion	*Taraxacum officinale* F.H. Wigg.	I	forb	facultative upland	widespread weed
8 (13)	smooth brome	*Bromus inermis.* Leyss	I	graminoid	obligate upland	weedy or invasive
9 (9%)	common sowthistle	*Sonchus oleraceus* L.	I	forb	facultative upland	noxious weed in Alberta
10 (9%)	reed canary grass	*Phalaris arundinacea*	N (hybrid)	graminoid	facultative wetland	concern for riparian zone
11 (9%)	sloughgrass	*Beckmannia syzigachne* Stued.	N	graminoid	obligate wetland	specialists, hydrophytic
12 (9%)	western wheatgrass	*Agropyron smithii* (Rydb.)	N	graminoid	facultative upland	upland regions
13 (9%)	Canada wildrye gras	*Elymus* sp.	N/I	graminoid	facultative upland	upland regions
14 (9%)	wire rush	*Juncus arcticus* Willd.	N	graminoid	facultative wetland	specialists, hydrophytic
15 (9%)	common duckweed	*Lemna minor* L.	N	forb/herb	obligate wetland	hydrophytic
16 (4%)	bur-reed	*Sparganium* L.	N	Forb/herd	obligate wetland	often emergent
17 (4%)	bulrush	*Schoenoplectus tabernaemontani* (Gmel.)	N	graminoid	obligate wetland	often emergent
18 (4%)	lamb's quarter	*Chenopodium album L.*	I	forb	facultative	disturbance promoted
19 (4%)	quackgrass	*Elymus repens* (l.) G.	I	graminoid	facultative	weedy or invasive
20 (4%)	common spikerush	*Eleocharis palustris* (L) R&S	N	graminoid	obligate	seasonally flooded areas

A mixture of native species and extensive occurrence of introduced plants was observed at all sites, generally associated with the prairie agricultural regions, with some weedy and invasive species (Table 3.6). Indicator plant species include duckweed, cattail, sedges, mannagrass, reed canary grass, which characterize inundation patterns and summer positions above the groundwater table, vegetation zones and hydroperiod. Based on the vegetation species composition and zones observed at both wetlands the habitat zones are classified as follows:

H5 - aquatic – open water

H4 - deep marsh zone

H3 - shallow marsh zone emergent plants and obligate wetland species – shallow wetland

H2 - wet meadow zone – facultative wetland species

H1 - low prairie zone – facultative upland plants

These habitat zones correspond to those found in a class IV or V marsh wetland described by Stewart and Kantrud (1971) (Figure 3.10), with wetland vegetation indicator ratings described by Lichvar et al. (2012). Five indicator ratings designate the preference of a plant species' occurrence in a wetland environment, ranging from 'obligate wetland', being the highest preference for wetland environments, to 'obligate upland', being the lowest preference in wetlands (Table 3.7). The entire range of indicator species are represented in the vegetation zones observed at Pumpjack and West Chestermere (Tables 3.5 and 3.6).
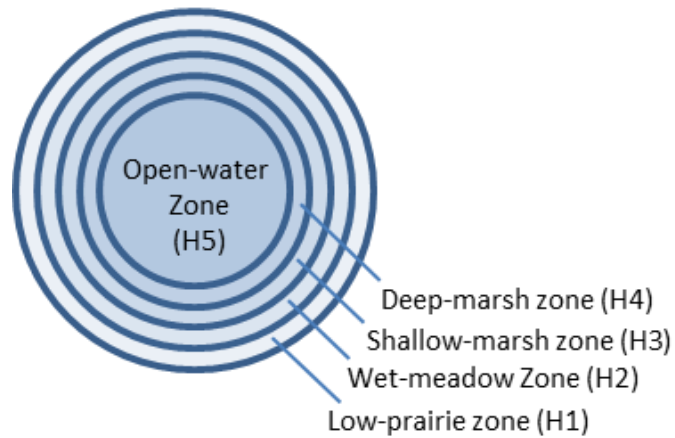
Figure 3.10. Vegetation habitat zones found in a semi-permanent (IV)/permanent (V) marsh wetland corresponding to zones found at Shepard Slough wetlands.

Table 3.7. Wetland indicator statuses used to designate plant species preference for occurrence in wetland or upland. (Lichvar 2012)

Indicator Species	Comment
Obligate Wetland	Always occur in wetlands
Facultative Wetland	Usually occur in wetlands, but may occur in non-wetlands
Facultative	Occur in wetlands and non-wetlands
Facultative Upland	Usually occur in non-wetlands, but may occur in wetland
Obligate Upland	Almost never occur in wetlands

Some apparent unique vegetation banding was observed (duckweed communities at Pumpjack, transect two), but overlap of species was observed across the sequential vegetation zones at each wetland (foxtail barley, and smooth brome). Reasonable consistency for multiple transects within sites was observed, with some consistency of indicator species across the two wetland sites (mannagrass, sedges).

3.3.4 Wetland Hydroperiod Frequency Analysis

Wetland hydroperiod classification results for each year (2013-2015) at the four study sites are presented in Figure 3.11. Hydroperiod (temporary, seasonal, and semi-permanent / permanent) are shown, as well as associated area of each hydroperiod class in hectares. SAR acquisition date, daily precipitation and temperature information from the Calgary International Airport weather station, the closest weather station to the study

area, is detailed in (Figure 3.7). Precipitation over the study period (April-September) for

each year is as follows; 2013=384mm, 2014=289mm, 2015=310mm (118mm in late

August), compared to an average of 346mm over the same months from 2007-2016.

Notable rainfall events are seen in May and June of 2013, as well as August and

September or 2015. For both well-defined basin wetlands (Pumpjack and West

Chestermere), less open water is observed in 2013, which was the year with the most

precipitation (West Chestermere was 11.5ha in 2013, compared to 13.9ha in 2014, and

14.7ha in 2015; Pumpjack was 16.3ha in 2013, 20.0ha in 2014, 17.8ha in 2015). Whereas

pothole area wetlands (Algae and Pothole), somewhat counter-intuitively, do not follow

the same trend, potentially due to differences in riparian vegetation growth, and wetland

shape and size (Figure 9).
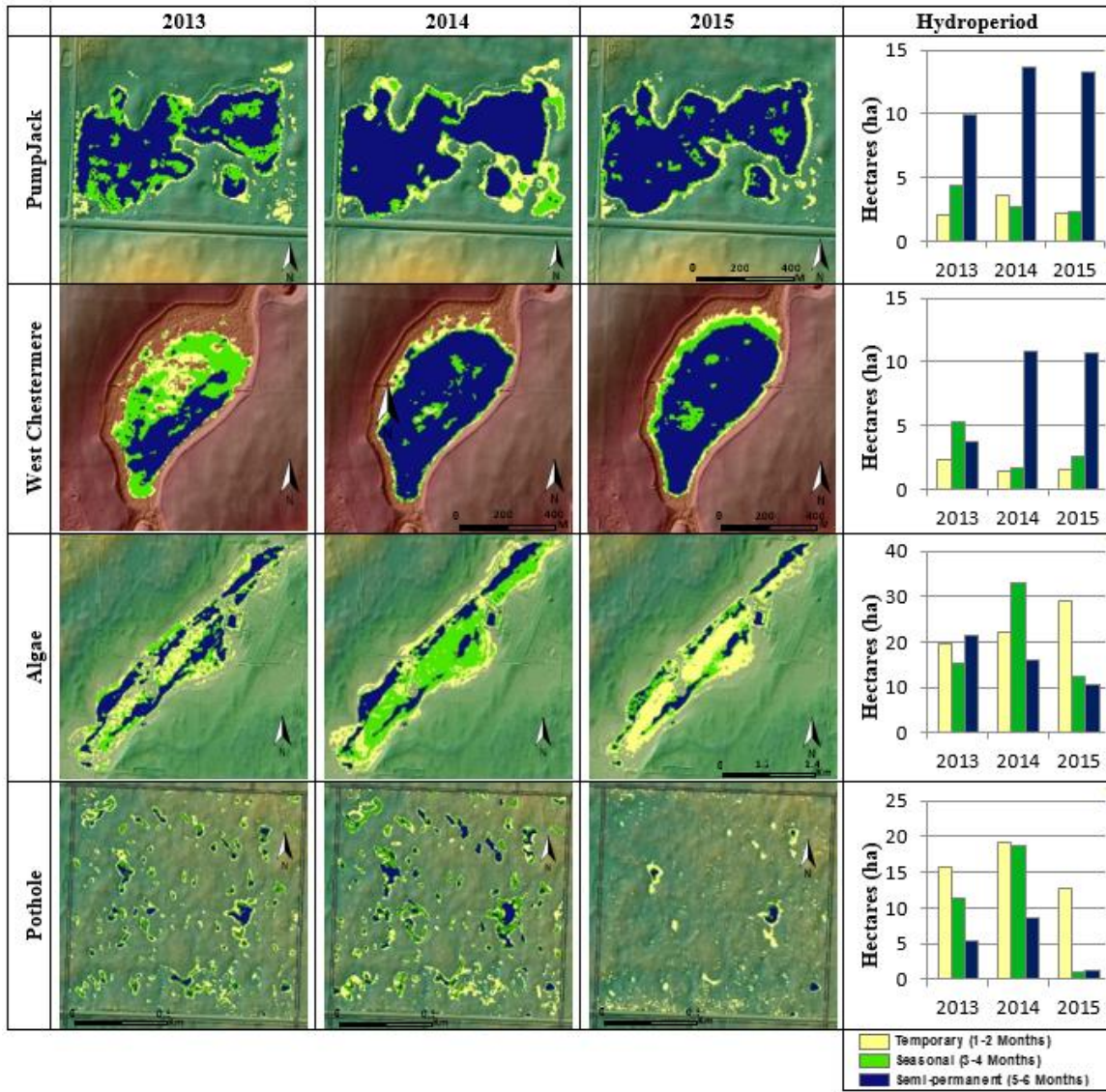
Figure 3.11. Hydroperiod results for Pumpjack, West Chestermere, Algae and Pothole study areas with associated area in hectares of each hydroperiod. Hydroperiods are shown as yellow for temporary (1-2 months), green for seasonal (3-4months), and blue for semi-permanent / permanent (5-6 months). Lidar DEM is used as the background to illustrate surrounding terrain.

Seasonal hydroperiod class fluctuations are identified in hydroperiod histograms detailing hydroperiod classes by year (Figure 3.12). The seasonal hydroperiod is found to be more variable than temporary and semi-permanent in both 'Algae' and 'Pothole', whereas, the semi-permanent/permanent hydroperiod is most variable in the defined basin wetlands of Pumpjack and West Chestermere. This indicates isolated pothole wetland hydroperiods

78

are more spatially variable than deeper wetlands in defined basins with surface

hydrological connectivity or downstream flow obstruction.
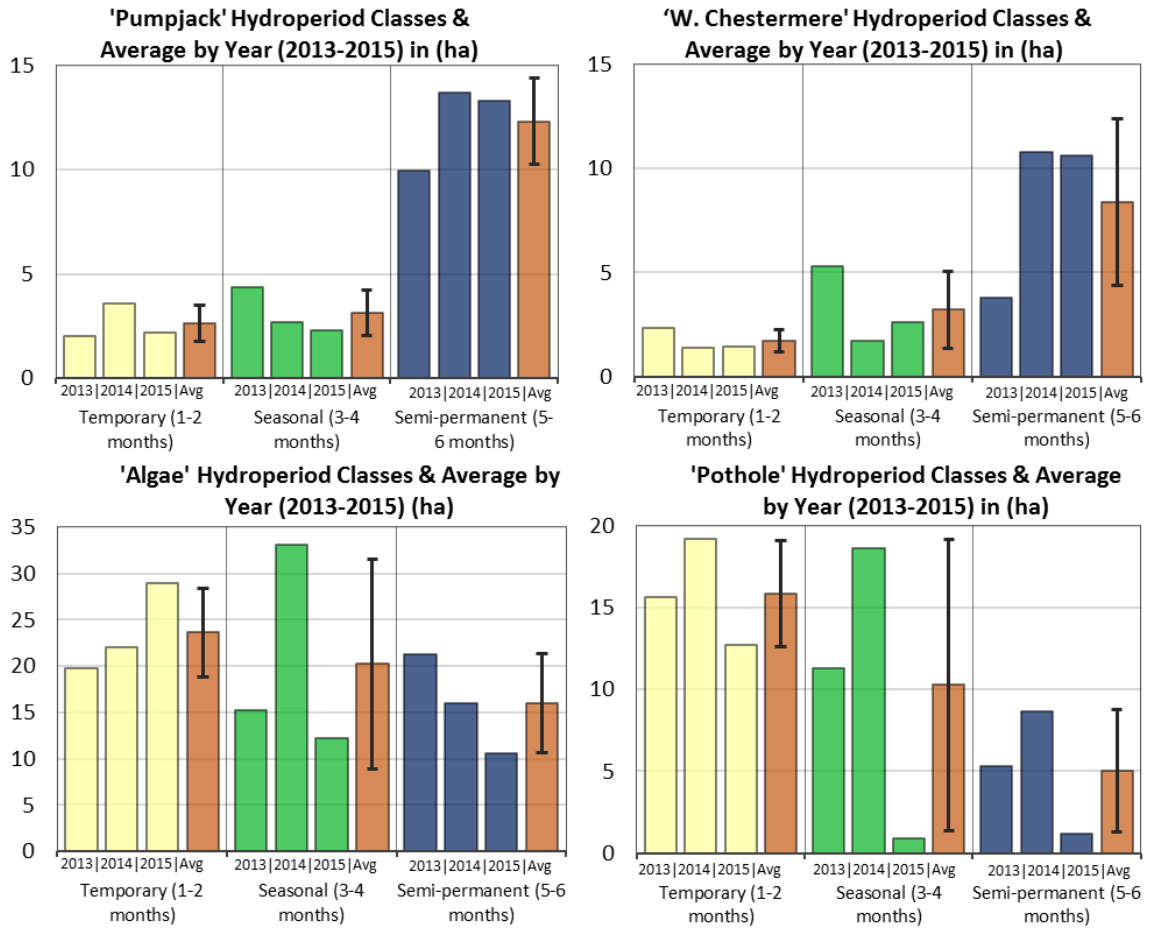
Figure 3.12. Hydroperiod classes grouped by year for each study wetland, showing average and variation of hydroperiod from the mean (orange) for each wetland study site.

West Chestermere is like Pumpjack in that it is contained in a well-defined

moderate-sized catch basin and has similar hydroperiod patterns as Pumpjack. One

difference is the spike in seasonal hydroperiod in 2013 resulting in more seasonal than

semi-permanent hydroperiod at over 5 ha, compared to 2-3 ha observed in 2014 and 2015.

Higher variation from the mean is seen in the semi-permanent class at Pumpjack

and west Chestermere. Lower variation from the mean is seen in the seasonal class at

Algae and Pothole (Figure 3.11). Hydroperiod fluctuations occur frequently and of inconsistent duration in 'Algae' and ''Pothole' study areas where a single rain event (Figure 3.7) contributes a disproportionate temporary hydroperiod (Figure 3.12), even in a drought year (2015) where many temporary hydroperiod pixels are found in areas along roadways (ditches) and shallow depressions on the landscape (Figure 3.11). This variability in per-pixel hydroperiod class is moderated in Pumpjack and West Chestermere, presumably as a result of increased surrounding hydrological connectivity (West Chestermere) or diminished opportunity for surface drainage (Pumpjack).

3.4 Discussion

3.4.1 Riparian Vegetation and Hydroperiod Variation

Wetlands with predominantly semi-permanent hydroperiods may contain fewer riparian vegetation species because of more consistent surface water extents (Figure 3.11 and Figure 3.12), which reflected in deep wetland and aquatic habitat zones (Figure 3.9, Table 3.5) due to overall reduced variation from the semi-permanent hydroperiod. Chernozemic soils of Southern Alberta are excellent for agriculture and vegetation growth in general (specifically in areas with temporary water) due to the natural accumulation, decomposition and transformation of the soil organic matter, where most of the carbon stored in a wetland is found below the surface (Soil Classification Working Group 1998). In the climatically sub-humid and low relief characteristics of Shepard Slough, wetlands with more semi-permanent or permanent pond areas surrounded by wetlands that are characterised by temporary hydroperiods promote periodic saturation of chernozemic soils, which supports greater ecological diversity described in Stewart and Kantrud (1971). Consistently similar ratios between the three hydroperiod classes each year and presence of each hydroperiod observed at Pumpjack, indicate low hydroperiod

80

variability and stable conditions from year to year (2013-2015), where hydroperiod

surface area ranges are as follows: temporary = 3ha to 4ha, seasonal = 3ha to 4.5ha, and

semi-permanent = 10ha -13ha. It is important to also discuss the implication of using the

September 2015 SAR acquisition in only 2015 as well, especially following the

significant late summer rain events (Figure 3.7). The most noticeable difference in surface

water extent is seen in the northeast corner of the 'Pumpjack' wetland that is dominated

by common cattail (*Typha latifolia*), which is a tall hydrophytic plant densely populated

in this region of the wetland. In 2013 and 2014 this band of cattail can be easily

identified, appearing as elevated topography (1-2m height) adjacent to the surface water

(Figure 3.11). In 2015 however, this area was inundated by temporary hydroperiod

surface water, suggesting conditions in 2015 prohibited growth density of these cattails,

or greater surface water was detected instead of vegetation due to seasonal dye-off

occurring in September, which would be consistent with vegetation succession observed

by Brisco et al. (2017) in similar vegetated wetland environments.

It is also important to note that at certain times of the year open water can be

covered by varying extents of emergent and floating aquatic vegetation (Brisco et al.

2015, Brisco et al. 2017). While field validation data is not available for 2013, a possible

explanation is that the large rain events on May 23-24, 2013 (74mm) and June 2-3 in

2013 (42mm) encouraged riparian and emergent vegetation growth earlier in the growing

season than normal. These precipitation events could result in less open water being

identified by the threshold routine which does not recognize flooded vegetation as a clear

unobstructed open water surface (White et al. 2014, Brisco et al. 2015, and Brisco et al.

2017). Wetland surface water extent was found to change dynamically corresponding to

rainfall occurring seasonally or annually. This effect is seen in both 'Algae' and 'Pothole'

where precipitation events (May/June 2013, and August/September 2015) was related to an increase in temporary hydroperiod compared to seasonal or semi-permanent. It should also be noted in the year with the closest to 'normal' (2014) rainfall magnitude and frequency (2014), a sharp increase in seasonal hydroperiod of pothole wetlands (algae (2013=15ha, 2014=32ha, 2015=12ha), and pothole (2013=12ha, 2014=18ha, 2015=2ha) is observed, suggesting these wetlands experience a sharp increase in not only overall water area, but also transition to a seasonal hydroperiod classification from either temporary or semi-permanent in comparatively dry or wet years, respectively.

Most notable is the variation from the mean of hydroperiod classes in the 'Algae' semi-permanent hydroperiod (Figure 3.13). In the 2013 wet year, there is 33% more semi-permanent water compared to the three-year mean, whereas in the dry 2015 year there is 34% less semi-permanent water compared to the mean. In the relatively steady (no extreme rainfall events) precipitation year of 2014 there is only a 0.5% change from the mean over the three-year study period, suggesting an increase or decrease in overall precipitation in the early growing season (April-June) with inversely related effects on the semi-permanent hydroperiod when comparing each year of this broad area/shallow wetland. This trend comparison is useful because it has the potential to be more widely applicable tool for monitoring, moving away from detailed measurements of local regions and time periods, into a more general measure of variation, providing and index of wetland ecosystem state and function.
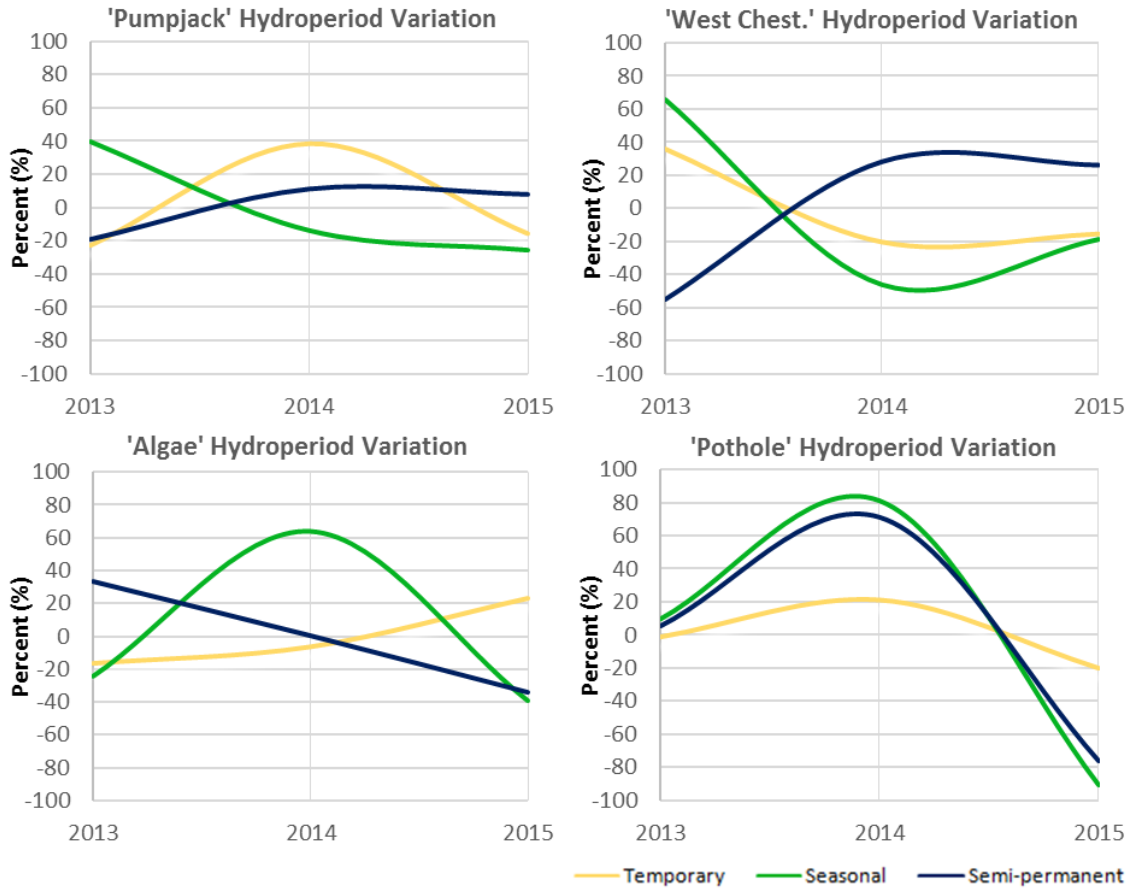
Figure 3.13. Inter-annual variation (%) of each wetland hydroperiod class from the mean ('0' representing the mean) of each hydroperiod class for each wetland study area from 2013 to 2015.

3.4.2 Data Limitations, Uncertainties and Future Directions

The major limitation of the study, specifically in sampling actual surface water conditions, relates to temporal image frequency. Since these prairie wetlands are hydrologically dynamic (Figure 3.13) and greatly influenced by precipitation events (Figure 7), there is a need for increased temporal resolution to better represent short term variations in hydroperiod. The C-Band RADARSAT Constellation Mission (RCM) planned for launch in 2018 will offer advanced capabilities for monitoring surface water with high spatial resolution modes such as Spotlight, providing enhanced monitoring of smaller wetlands. RCM is comprised of three satellites, providing daily coverage for 90%

of the world with larger swath width for some beam modes (at 50 x 50m resolution 350km swath width for RCM, compared to 300km for RS2), (Canadian Space Agency 2016). This is similar to RADARSAT-2, but the revisit time of RCM is 4 days (compared to 24 days for RADARSAT-2), allowing for more frequent monitoring and over larger areas. Increased temporal resolution has several implications for wetland hydroperiod classification; 1) precipitation events and subsequent local surface water changes will be better represented; 2) weekly hydroperiod comparisons can be made instead of monthly; and 3) increased acquisition frequency will make it easier to find coincident date optical data for comparative validation and data product improvement. This is important for understanding water resources and hydrological variations, especially in ungauged basins.

When a SAR image is acquired in conditions with little wind or surface water roughness, HH has been shown to be the best suited to mapping surface water (White et al. 2014). While the majority of HH polarisation images were found to be of adequate quality for the analysis (Table 3.3, and Figure 3.6), some of the images did show significant surface roughness from wind, and were therefore unusable for surface water extraction. Dual-polarized SAR data is recommended when mapping surface water over windy areas, as it is scene dependent, and HV is less affected by wind effects, described by Manore et al. (2001), Scheuchl et al. (2004), and White et al. (2014). This allows for the user to choose appropriately between HH or HV polarization depending on whether conditions are calm or windy at the time of image acquisition. While dual polarization data was not used, or tested in this study, we see the influence of wind effects in some images (May 3, 2013, October 31, 2015). This could be reduced by selecting a more condition-appropriate polarization. While the use of the PCI SAR Polarimetry tool and a consistent sample area polygon reduces the amount of error introduced in the thresholding

approach through user selection, uncertainty can still be introduced to the routine when choosing the threshold range from the output dB histogram.

3.4.3 Implications of Wetland Hydroperiod Time Series

The SAR derived binary water mask hydroperiod classification described in this study differs from other classification routines as it combines a series of images into a dynamic surface water hydroperiod product over the growing season of wetlands, rather than evaluating hydroperiod based on single snapshots in time. The performance and results of the hydroperiod classification may require further evaluation with the greater temporal resolution attained from RCM, in order to perform more rigorous validation. However, the hydroperiod analysis and methodology presented in this study provides a framework for long-term, high resolution water resource monitoring describing more than just water extent of wetlands, allowing for enhanced characterization and classification of wetlands in accordance with Alberta's provincial wetland classification criteria. It should be noted that the frequency routine could be carried out on any type of data that can produce binary water mask rasters (i.e. optical, Lidar). The strength of SAR extracted water masks lies in the ability of radar to collect images any time of day or night and under poor weather or atmospheric conditions.

3.5 Conclusion

SAR is an effective method of water extent mapping. The methodology developed in this study details a framework for a new time-series-based classification approach based on hydroperiod and hydro-climatic conditions that can be largely automated. The frequency analysis and classification based on Stewart and Kantrud (1971) provides a novel method of classifying dynamic marsh environments using temporal SAR data. The

results of this study suggest water mask frequency analysis can be used to determine hydroperiod and permanency of wetlands in a heterogenous prairie pothole area and can potentially be adapted to other end-member environments. Once the surface water extraction model has been constructed, the derived hydroperiod product can be quickly and easily produced. Frequency analysis is not a time intensive routine and can be developed into a batch script process capable of adding new or successive input rasters. It is recommended that users perform a post-classification review and edit of errors of commission and omission. Therefore, having recent landcover, digital elevation models and knowledge of the study site is recommended (White et al. 2014).

Hydroperiod, variation from the mean and surface water extent of the wetlands was found to be heavily influenced by short-term rainfall events observed in both abnormally wet and dry years, whereas staggered and persistent rainfall yielded the highest water surface area. Furthermore, the seasonal hydroperiod in many wetlands was found to be highly variable at sites when there is a decrease in either the temporary or semi-permanent class. Temporary hydroperiod class was observed in higher ratios at times following extreme rain events compared to both seasonal and semi-permanent.

Future research on the use of SAR for wetland hydroperiod classification would benefit from higher temporal resolution data to increase class reliability. The strength of the study is the ability to construct and examine meaningful hydroperiods of wetlands on large temporal and spatial scales that provide defining characteristics relevant to the current Alberta Wetland Classification System criteria, and better understanding the response of ungauged wetlands to precipitation events evapotranspiration. This is of relevance to decision or policy makers requiring accurate and temporally representative analysis of wetlands being impacted by infrastructure, agriculture or climate change.

Perceived temporary wetlands and associated classification and analysis are traditionally difficult to characterise or quantify.

With the existing SAR satellites and inventory, such as RADARSAT-2, Sentinel, TerraSAR X, and the upcoming RCM, temporal resolution of many environmental monitoring studies involving the stacking of data can be greatly enhanced and applied to the hydroperiod methodology presented in this paper for monitoring wetlands.

Indeed, the work presented is well-suited to a systematic monitoring regime as with the addition of new SAR data, the hydroperiod classification increases in accuracy and can be constantly updated. With the fusion of optical and/or Lidar data describing riparian vegetation communities, the hydroperiod analysis could be the basis for a more comprehensive wetland classification and monitoring framework. Such a framework would provide a valuable platform for land use permitting and regulation in heavily disturbed prairie or agri/urban landscapes in North America similar to the Shepard Slough study area in Alberta.

classification and wetland ecosystem monitoring from Government of Alberta (Economic

Development and Trade, Environment and Parks), Alberta Sustainable Resource

Development (now Alberta Environment and Parks); Discovery Grant funding from the

Natural Sciences and Engineering Research Council.

4.0 A Synthetic Aperture Radar, Optical, and Lidar, Data Fusion Approach to Wetland Classification Using Multi-temporal SAR.

Joshua Montgomery[1], Chris Hopkinson[1], Laura Chasmer[1], Brian Brisco[2], Kevin Devito[3]
1. *Department of Geography, University of Lethbridge, 4401 University Dr. W, Lethbridge AB, T1K6T5*
2. *Natural Resources Canada, Government of Canada, 560 Rochester St., Ottawa, Ontario, K1A 0E4*
3. *Department of Biological Sciences, University of Alberta,1-001, CCIS, University of Alberta, Edmonton, Alberta, Canada T6G 2E9*
Keywords: *SAR, Lidar, boreal wetland classification, data fusion*

*Corresponding Author: joshua.montgomery@uleth.ca
Author contributions are as follows: **Joshua Montgomery** – principal author and writer, performed all field data collection, developed methodology, conducted analysis and interpretation of results. **Christopher Hopkinson** – supervised development of work, helped in data interpretation and evaluation, and manuscript editing. **Laura Chasmer** – assisted with lidar topography interpretation, manuscript evaluation. **Brian Brisco** – data provider of SAR data, and helped evaluate the manuscript. **Kevin Devito** – site principal investigator at the Utikuma Regional Study Area.

Abstract

The objective of this study is to develop a decision-tree (DT) methodology focused on data fusion for wetland classification based on surface water hydroperiod and associated riparian vegetation community attributes. Multi-temporal, multi-mode data was examined from Lidar (Optech Titan), Synthetic Aperture Radar (Radarsat-2, single & quad polarisation), and optical (SPOT) sensors with similar acquisition dates. Model results are compared with 31 field measurement points for six wetlands at riparian transition zones and surface water extents in the URSA region producing high accuracies ($R^2 = 0.9$).

The results suggest the methodology offers an innovative time-series-based boreal wetland classification approach using data fusion of multiple remote sensing data source. Water mask frequency analysis showed accuracies of 93% to 97.2%, and kappa values of

0.8-0.9% when compared to optical data. Confusion matrix results comparing semi-permanent/permanent hydroperiod between 2015 and 2016 was found to be 98.3% correlated, suggesting very little change in wetland surface water extent. The decision tree methodology and data fusion could be applied to a wide range of wetland types and is not geographically limited, providing a platform for land use permitting, reclamation monitoring, and wetland regulation.

4.1 Introduction

Wetlands come in many sizes and forms, generally developing where the water table is at or near the surface allowing water to settle on the land surface promoting development of soil conditions for hydrophytic vegetation (National Wetlands Working Group 1998). Canada has over 150 million hectares of wetlands, occupying approximately 14% of the land area of Canada, which is estimated to be 24% of the wetlands in the world (Government of Canada 1991, Pole Star Geomatics Inc. 1996, Environment Canada 2016). Most Canada's wetlands are found in the boreal regions, where rates of boreal forest disturbance in 2008 were found to be approximately 78%, and among the highest in the world (Komers and Stanojevic 2013). Boreal wetlands are especially sensitive to disturbance and changes to hydrology, which are predominantly comprised of shallow ponds, treed fens and bogs on poorly drained organic soils. Natural resources extraction, agricultural land cover change, and drying because of warmer climate conditions are all contributing to some of the greatest boreal zone changes, especially in central Alberta. With increasing disturbance and changing hydrological patterns, accurate, high resolution classification of these boreal wetlands is required for understanding rates of boreal wetland change, many of which have yet to be accurately

identified or mapped, therefore, there is a need to characterize baseline wetland areas for the boreal region. The methodology presented attempts to conform to wetland classification criteria of the Alberta Wetland Classification (2015) and the Canadian Wetland Classification (1997) documents, which both require analysis of multiple wetland attributes. While both documents outline classification criteria, the accuracies and resolution required have yet to be firmly established but must meet a certain percentage of accuracy and resolution in the future, stated in the Alberta Wetland Mapping Standards Workshop Synopsis (AWMSWS) from March 23, 2017. Criteria and associated required/desired accuracies are as follows:

1. High accuracy of separation of upland and wetland: 90-95%

2. High confidence Treed/Not Treed: 85% - 95%

3. Accuracy requirement for all 5 Major Classes (fen, bog, swamp, marsh, shallow open water): 50-60%

4. Optional seasonality of marsh wetlands – seasonal, lumping type (I, II, III), Semi-Permanent (IV, V) (as outlined by Stewart and Kantrud 1971): 60% - 80%

Drying trends in many northern regions of Canada and the USA have been observed in the last decades, where changes in ground and surface water hydrology have been observed, thereby increasing vegetation succession in some years and altering the carbon balance of wetlands (Stow et al. 2004, Riordano et al. 2006, Kettridge 2013). Synthetic Aperture Radar (SAR) has proven to be a promising sensor for surface water and flooded vegetation mapping due to the contrast and reflectivity between land and water (eg. Brisco et al. 2009, Santoro and Wegmuller, 2014, White et al. 2014, 2015).

High spatial resolution data fusion methods using remote sensing data (lidar, SAR, optical) provides increased accuracy for wetland extent mapping and wetland type

classification (Millard and Richardson 2013, Irwin et al. 2017). Near coincident *in situ* field data collected within days of remote sensing data acquisition provides spatial validation for riparian vegetation species, composition, and open water extent over time, or pond/lake 'hydroperiod'. A combination of statistical analyses and ground validation of the output classes is used to evaluate the data fusion approach for mapping the riparian ecology and surface water extent of wetlands.

4.1.1 Objective

The objective of this study is to provide a new classification methodology for wetlands based on hydroperiod and associated riparian vegetation community attributes used in wetland classification according to the Alberta Wetland Classification System (2015), and the Canadian Wetland Classification System, using multi-temporal, multi-mode data from Lidar (Optech Titan), Synthetic Aperture Radar (RADARSAT-2, single and quad polarisation), and optical (SPOT) sensors with similar acquisition dates. The result of this data fusion methodology is to create a mapping product that is useful for wetland policy development and long-term wetland monitoring.

4.1.2 Study Area

The Utikuma Regional Study Area (URSA) is a boreal forest region located approximately 100 km north of Slave Lake in the Central Mixedwood Natural Subregion (Pettapiece and Downing 2006). The URSA series of study sites covers an area of 1,062 km^2 surrounding Utikuma Lake described by Ferone and Devito (2004); Devito et al. (2005); Petrone et al. (2007). It was established in 1998 as a long-term monitoring site, primarily to quantify key hydrological processes associated with disturbance and regeneration, nutrient cycles and hydro-ecological changes over time (Ferone and Devito

2004; Devito et al. 2005; Petrone et al. 2007). An approximately 10 x 20 km (200 km^2)

subset of the URSA region is investigated in this study (Figure 4.1).
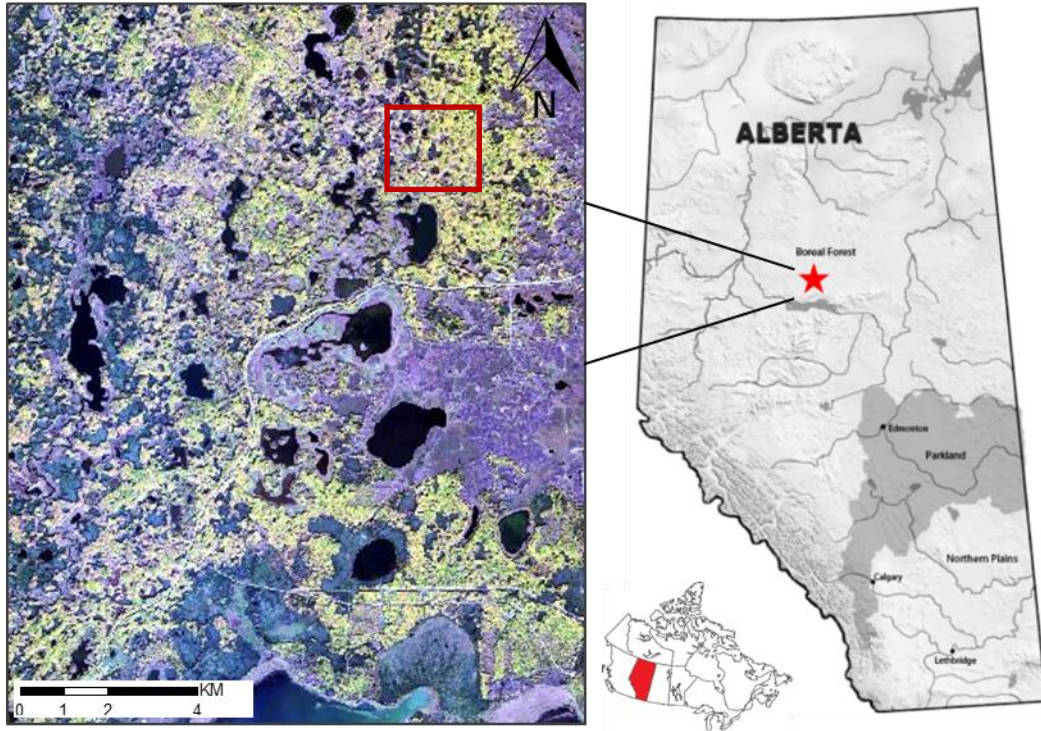
Figure 4.1. SPOT image from September 21, 2016 of the regional location of the ~10 x
20km area of interest subset of the Utikuma Regional Study Area (URSA) in the boreal
region of the province of Alberta, Canada. The north shore of Utikuma Lake is pictured at
the bottom of the image. Study ponds 45 and 43 are located within the red box.

Vegetation is characterized by a mix of aspen-dominant deciduous stands

(*Populus tremuloides*), with aspen-spruce mixedwood forests including white spruce

(*Picea glauca*), and jack pine (*Pinus banksiana*) found within the upland regions.

Wetland ecosystems are predominantly comprised of shallow ponds with submergent

macrophyte vegetation that may float on open water during summer. Treed fens and bogs

are found on poorly drained organic rich soils (Natural Regions Committee 2006; Petrone

et al. 2007). Treed wetlands are comprised of mainly black spruce (*Picea mariana*) and

are commonly underlain with *Sphagnum* spp. mosses, fibric peat, grasses up to 0.5m

height, and gyttja hummocks and hollows.

4.2 Data & Methods

4.2.1 SAR Data

RADARSAT-2 images were acquired during the 2015 and 2016 growing season

in single polarisation (HH) Wide Ultra-Fine (U24W2 descending orbit and U13W2

ascending orbit), and quad polarisation (HH, HV, VH, VV) Wide Fine-Quad (FQ10/5W)

beam modes (Table 4.1). Wide Ultra Fine has a nominal resolution of 1.6m x 2.8m, and

Wide-Fine Quad has a nominal resolution of 5.2m x 7.6m. Wide Ultra Fine data were

resampled using cubic convolution to 3m resolution for consistent resolution across all

images.

Table 4.1. SAR acquisition dates of Wide Ultra-Fine (U13W2 and U24W2) and Wide
Fine-Quad (FQ10/5W) beam modes over URSA for 2015 and 2016.

2015	2016
July 20 (U24W2)	May 3 (U24W2)
August 13 (U24W2)	May 24 (U13W2)
September 3 (U13W2)	May 27 (U24W2)
September 6 (U24W2)	June 17 (U13W2)
September 27 (U13W2)	June 20 (U24W2)
October 21 (U13W2)	July 11 (U13W2)
August 13 (U24W2)	July 14 (U24W2)
-	July 27 (FQ10/5W)
-	August 4 (U13W2)
-	August 8 (FQ10/5W)
-	August 28 (U13W2)
-	August 31 (U24W2)
-	September 21 (U13W2)
-	September 24 (U24W2)

4.2.2 Surface Water Extraction

SAR derived surface water masks were created using Geomatica 2016 (PCI Geomatics), which includes image filtering, predominantly to preserve edges. A model developed by White et al. (2014) using Geomatica v10.3.2, was updated to current module versions to extract surface water using input threshold intensity/decibel (dB) range values (Montgomery et al. submitted) (Figure 3.3). Filters in the model include: FGAMMA adaptive filter used to preserve edges, which is important for surface water extent analysis (Toutin 2011, Zhang et al. 2012); FAV filter is used to reduce speckle (White et al. 2014), and FMO filter to further reduce noise and help with the ortho-rectification of the SAR images (White et al. 2014, 2015). See chapter 3, section 3.6 for surface water extraction methodology, and section 3.7 for frequency analysis and hydroperiod methodology.

4.2.3 SAR Polarimetric Decompositions for Flooded Vegetation

Vegetation canopy penetration of the microwaves in a SAR system allows for mapping and classification of flooded vegetation due to enhanced backscatter from a double-bounce scattering mechanism (Brisco 2015). This results in enhanced HH backscattering with less increase seen in VV, therefore dual (HH/VV) or quad (HH, HV, VH, VV) polarised data sets can be used to identify flooded vegetation using polarimetric decomposition techniques (Brisco et al. 2011, Brisco 2015). Decompositions are physically based models that can be decompressed from several channels in quad polarised SAR data into a single intensity channel that estimates the amount of different types of scattering contributing to the total backscatter from each pixel (Freeman and Durden 1998, White et al. 2015). The phase information in the SAR data allows for the

95

SAR decomposition to discriminate between different scattering mechanisms, and

between areas of double bounce scattering which is indicative of flooded vegetation

(Brisco 2015). Well documented decomposition techniques include: Van Zyl (Van Zyl,

1989), Cloude-Pottier (Cloude and Pottier 1997), Freeman- Durden (Freeman and Durden

1998), and Touzi (Touzi et al. 2007). Decomposition techniques are widely accepted and

validated, and have been developed and implemented in remote sensing software for SAR

processing. Freeman-Durden (FD) decomposition is a physically based model and is

effective for mapping changes between land cover classes in wetlands using fully

polarimetric (four channel) SAR data, specifically for flooded vegetation applications

(Touzi et al. 2004, White et al. 2015). The model estimates the contribution of surface,

double-bounce, and volume scattering response to the total backscatter from each pixel in

an image and outputs a three-channel composite raster of the scattering responses

(Freeman and Durden 1998). The long wavelength of SAR systems can penetrate through

the vegetation canopy, detecting emergent and woody wetland vegetation represented by

the double-bounce backscatter (Pope et al. 1997, Townsend 2002, White et al. 2014).

Freeman-Durden decomposition has been widely used in boreal environments for

extracting flooded vegetation. This produces three bands, which identify volume

scattering (taller vegetation and forest), double-bounce scattering (flooded vegetation)

and surface scattering (water or rough surface), (Freeman and Durden 1998, Brisco et al.

2013, White et al. 2014, 2015). Freeman-Durden decomposition of quad polarised images

was applied using Geomatica 2016. To remove speckle, a 5x5 boxcar filter was applied

based on local pixel averaging, which increases the effective number of looks (ENL).

4.2.4 Airborne Lidar Data

Ground surface elevation and feature heights above ground are important data sources to aid in classifying lowland and upland wetland zones and associated wetland species (Wettstein and Schmid 1999). Airborne Lidar data was collected by the Airborne Imaging (Calgary, Canada) in 2008 over URSA. Ground point filtering and processing of a 1m x 1m digital elevation model (DEM) with inverse distance weighting (IDW) interpolation and 10m search radius was completed using TerraScan (TerraSolid, Finland) and Surfer (Golden Software, Colorado, USA). SAR and Optical data used in the study were ortho-rectified to the lidar DEM.

Multispectral airborne Titan ALTM (Teledyne Optech) Lidar was flown by the authors on August 6, 2016 over the study area coincident with the SAR acquisitions and field validation work. Processing of the 2016 Titan (Teledyne Optech) Lidar point cloud was performed using LMS (Teledyne Optech, Ontario, Canada), Terrascan (Terrasolid, Finland) and LAStools (Isenburg, 2017). The raw data were initially tiled to a 1 km grid with a 20m buffer between neighbouring tiles to mitigate edge effects. Each tile was ground classified and the height of each remaining point above the identified ground surface was calculated. Vegetation classified points were interrogated (using a 1 m search radius) to determine the 99th percentile height (P99), where only points > 2 m were considered in the calculation to negate contributions of tree and shrub understorey vegetation; i.e. P99 is the height at which 99% of vegetation classified points > 2 m above the ground occur. These heights were then rasterised to a 1 m grid to represent the study site's canopy height model (CHM).

Topographic Position Index (TPI) is a measure of the difference between the elevation value of a cell and the average elevation of nearby (neighbouring) cells (Guisan

et al. 1999, Jones et al. 2000, Weiss 2001). A positive value indicates higher elevation than its surrounding whereas negative indicates it is lower. TPI results provide the means to suggest the probability of a wetland occurring in a certain area by separating high and low areas, where the probability or landscape suitability of a wetland occurring in a topographic high (upland) is very low, while a low TPI indicates high suitability for a wetland. TPI is scale dependent, therefore the user needs to select parameters appropriate for the study area. A search window of 200m was found to be suitable for this landscape based on the high resolution of the data, topography criteria outlined by Jenness (2006), and circular moving polynomial windows was based on the size of upland till moraines in the area by Chasmer et al. (2015). Isolated outlier wetland pixels from the hydroperiod analysis located on plateaus were flagged and masked out creating a corrected hydroperiod from the TPI.

4.2.5 Optical Data

SPOT (*Centre national d'études spatiales*) optical imagery was acquired on July 19, September 19, October 5, 2015, and July 1, September 21, and September 24, 2016 each with 5 x 5m pixel resolution. Data were acquired at near-coincident or coincident days to SAR data acquisitions and are used for validation purposes. All images were atmospherically corrected using PCI Geomatica Focus ATCOR atmospheric correction tools. Surface water was classified using K-means unsupervised classification in PCI Geomatica Focus 2016 (Burrough et al. 2000, 2001, Lane et al. 2014).

4.2.6 Ground Validation Data Collection

An accessible wetland area within the broader study region was surveyed in July and August 2015 and July 2016 to determine surface water extent and riparian habitat

boundaries along transects to centimeter accuracy (Table 4.2). Surveys were carried out

using a Topcon (Livermore, CA, USA) HiPer SR Global Navigation Satellite System

(GNSS) rover unit using kinematic 'stop and go' survey techniques. GNSS rover

positions were differentially corrected to a static base station of known location calculated

using Precise Point Positioning (PPP) techniques in Magnet Office (Topcon, California,

USA) and through Natural Resources Canada online tools.

A summary of the data used and its intended purpose is detailed in Table 4.2.

Table 4.2. Data layers used in the classification and associated information.

Data	Derived From	Purpose of Layer
SAR open water	HH-SAR	Mask of open surface water
SAR FD decomposition	Quad-Pol SAR	Identifies flooded vegetation
Topographic Position Index	Lidar DEM	Local terrain attributes
Optical open water	SPOT	Validation for SAR open water mask
Vegetation height layer	Lidar CHM	Vegetation height
Road Layer	SPOT/Manual	Quality control layer

4.2.7 Decision Tree Fusion Workflow

A decision-tree methodology is developed that expands upon an earlier method

developed by Chasmer et al. (2014 & 2015) who based a classification on topography and

vegetation canopy attributes from Lidar intensity and structure expanding at the same

study area. The methodology incorporates the variation in hydroperiod and impact on

wetland aquatic transitional vegetation using RADAR. The combination of the SAR,

Lidar and Optical image products used to identify wetlands and classify them based on

logic, probability and 'if' statements provide the means for an accurate and more

descriptive wetland classification from that developed in Chasmer et al. (2015) (Figure

4.2). Water permanence and presence of flooded vegetation integration in fusion with

Lidar follows findings by White et al. (2015), and Brisco et al. (2017) regarding the

spatial distribution of wetland attributes. The decision-tree methodology includes deriving

SAR (single pol) water masks, associated hydroperiod classified according to Stewart and

Kantrud (1971) and Government of Alberta (2015), flooded vegetation from SAR (quad

pol) Freeman-Durden decomposition, and lastly Lidar-derived topographic index and

canopy cover attributes.
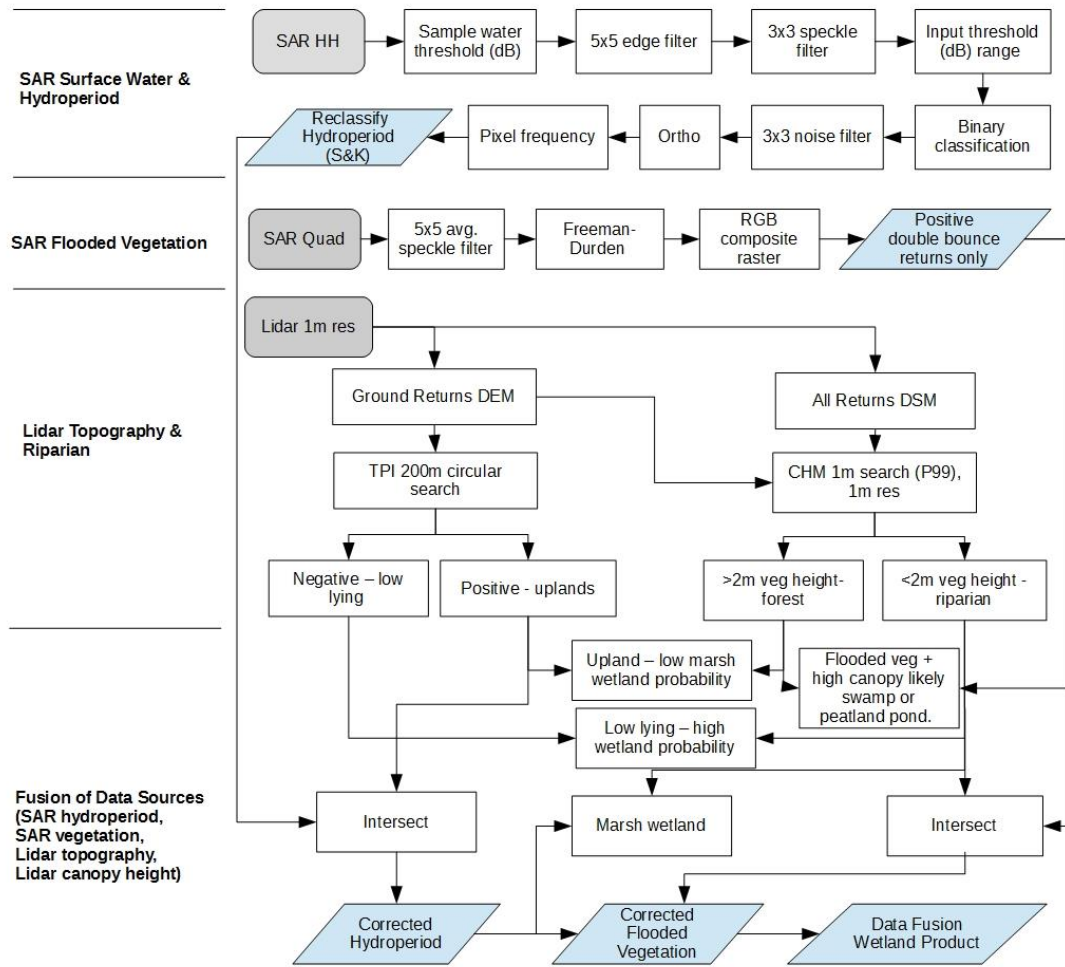
Figure 4.2. General data processing and decision-tree logic based data fusion workflow of the four primary products (SAR surface water masks, SAR flooded vegetation layer, topographic position index from DEM, and low riparian vegetation from CHM). The combination of each dataset acts as a quality control measure, high resolution wetland classification system, and creates an integrated, dynamic wetland product with potential monitoring implications.

Double bounce returns identified as flooded vegetation and utilized based on

scattering mechanisms from the Freeman Durden decomposition and studies in other

boreal environments (Freeman and Durden 1998, White et al. 2014, 2015, Brisco et al. 2015). The double bounce scattering returns were exported as a stand-alone raster from the composite Freeman-Durden decomposition image, then reclassified to represent positive scattering mechanisms, removing background values with very low double-bounce scattering, leaving only double-bounce scattering returns (Figure 4.3).
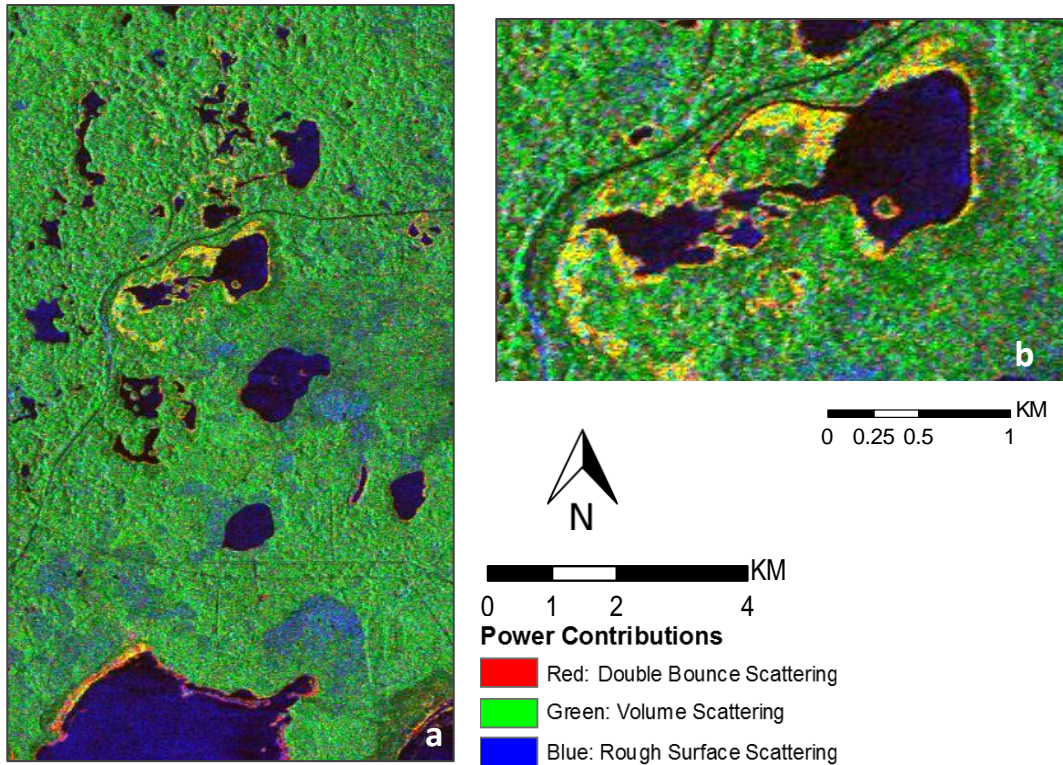
Figure 4.3a-b. a) Freeman Durden decomposition over the area of interest and part of Utikuma Lake (pictured at the bottom of the image), and b) enlarged area around a prominent wetland next to a roadway, showing the power contribution of each scattering mechanism (double bounce, volume, and rough scattering). Areas of red and red/orange/yellow indicate flooded vegetation.

The intersection of the riparian CHM and flooded vegetation double bounce returns removes commission errors from areas located in topographic uplands where positive values are found. This leaves only low areas where wetlands can form. Lastly the corrected flooded vegetation and corrected hydroperiod products are overlain as complimentary products creating a dynamic wetland attribute product.

4.3 Results

4.3.1 SAR Surface Water Masks

Results of the intensity threshold (dB) surface water masks developed by White et al. 2014 is visually compelling for extracting surface water of boreal wetlands at the URSA region in 2015 (Figure 4.4), and 2016 (Figure 4.5). The threshold range was found to be similar through all images, with the average upper limit found to be -18dB, and the lower limit -30dB. Similar consistency of decibel limits, although not the same limits, was observed in the Peace-Athabasca Delta (PAD) by White et al. (2014).
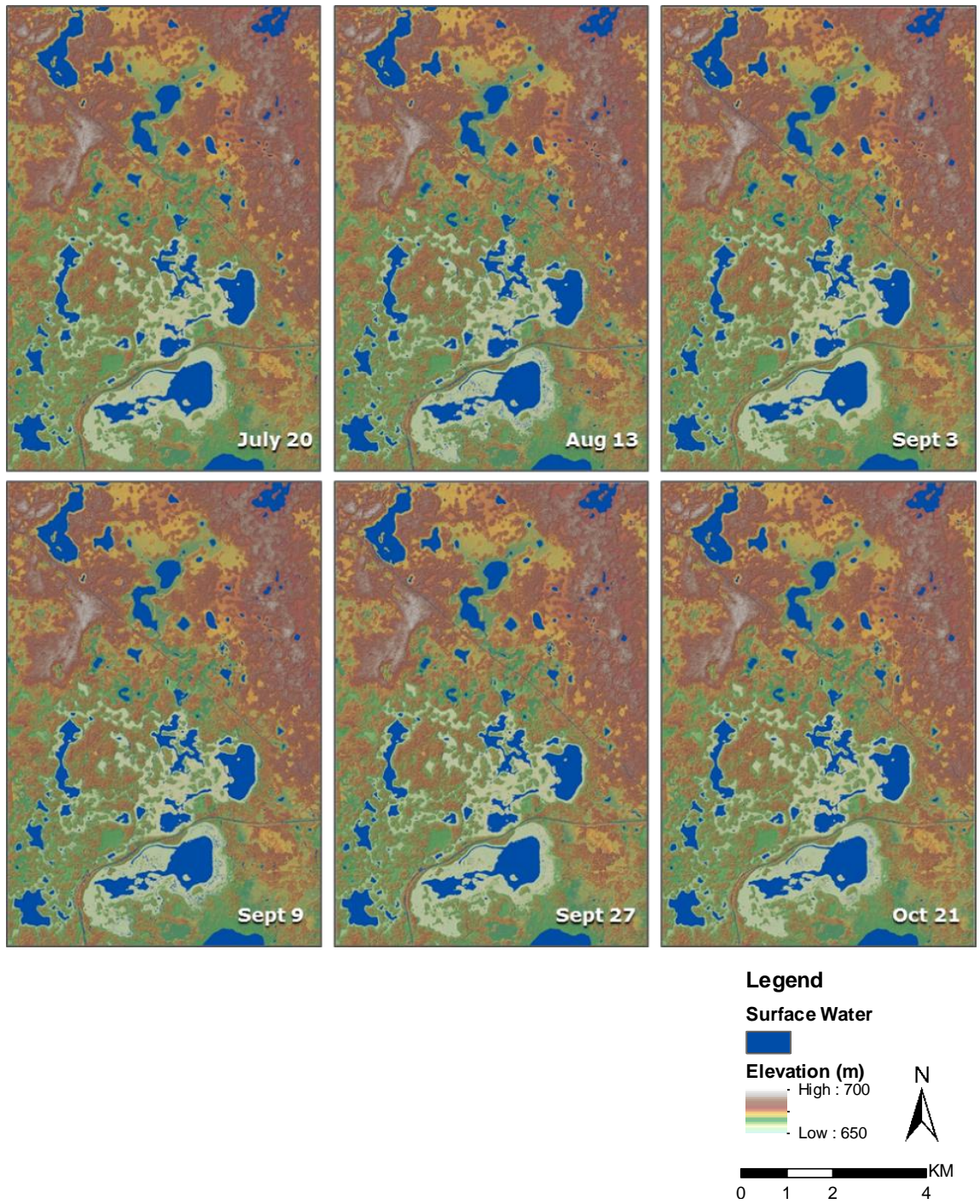
Figure 4.4. Intensity threshold (dB) SAR derived surface water masks over the URSA region in the growing season of 2015. Images show relatively consistent surface water extent.
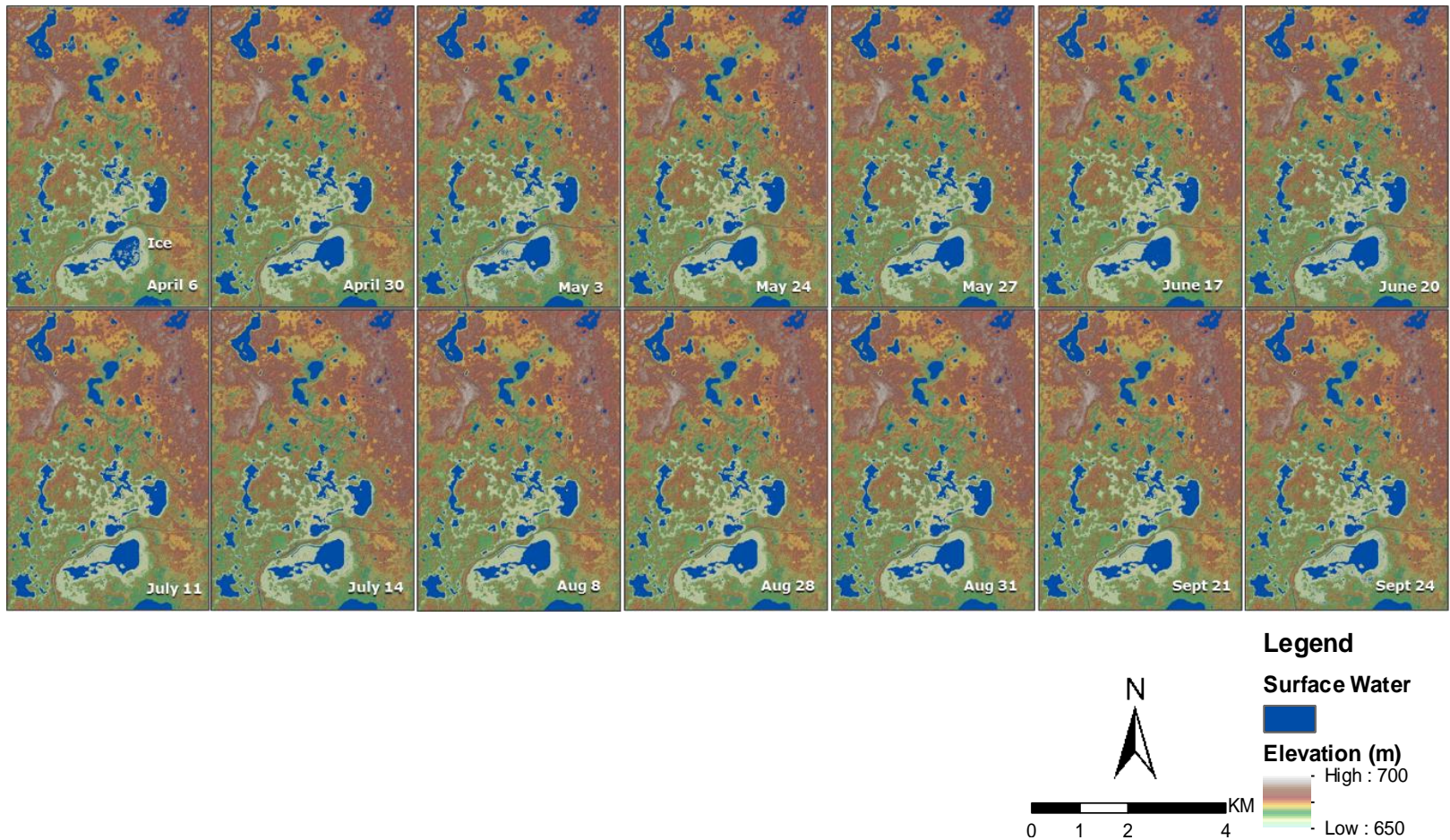
Figure 4.5. Intensity threshold (dB) SAR derived surface water masks over the URSA region in the growing season of 2016. Images show relatively consistent surface water extent.
Note: Some ice present in April 6 Image.

4.3.2 Optical Validation

Optical satellite open water classification is a well-established method for open surface water classification, and is therefore useful for validation with water masks derived from other sensors (Frazier and Page 2000, Sawaya et al. 2003). Peiman et al. (*Submitted*) compared both ascending and descending SAR texture and intensity thresholding with an optical SPOT mask from 05-10-2015 over the study area. Despite the temporal offset, overall accuracies were >90% (kappa = 0.8-0.9) (Table 4.3). Greater accuracy is expected without the temporal offset and with the removal of roadways and infrastructure.

Table 4.3. Confusion matrix results of near-coincident SAR intensity (dB) threshold derived surface water masks compared to a single clear sky optical SPOT scene from September 21, 2015. Note: results do not represent absolute accuracies, as the optical water masks contain some uncertainty and the comparison results represent acquisitions from different days.

SAR Acquisition	Overall Accuracy	Kappa (%)	C.ERR-O.ERR (%)
3-09-2015	95.8	0.9	-1.1
6-09-2015	97.1	0.8	5.5
27-09-2015	93.0	0.8	13.3
30-09-2015	97.2	0.8	0.9

4.3.3 Surface Water Hydroperiod

Surface water hydroperiod classes are presented for 2015 and 2016 in Figure 4.6. Temporary 1-2 months (yellow), seasonal 3-4 months (green), and semi-permanent/permanent 5+ months (blue) are represented in the hydroperiod analysis. Confusion matrix results comparing the 2015 and 2016 hydroperiods (Table 4.4), are as follows: for temporary 53% (43.6 ha), seasonal 49% (30.48 ha), semi-permanent/permanent 98% (744.7ha). Overall similarity of hydroperiods on pixel by pixel

basis is 79%, attributed to the low correlation of temporary and seasonal hydroperiod

compared to the very high correlation between semi-permanent/permanent.
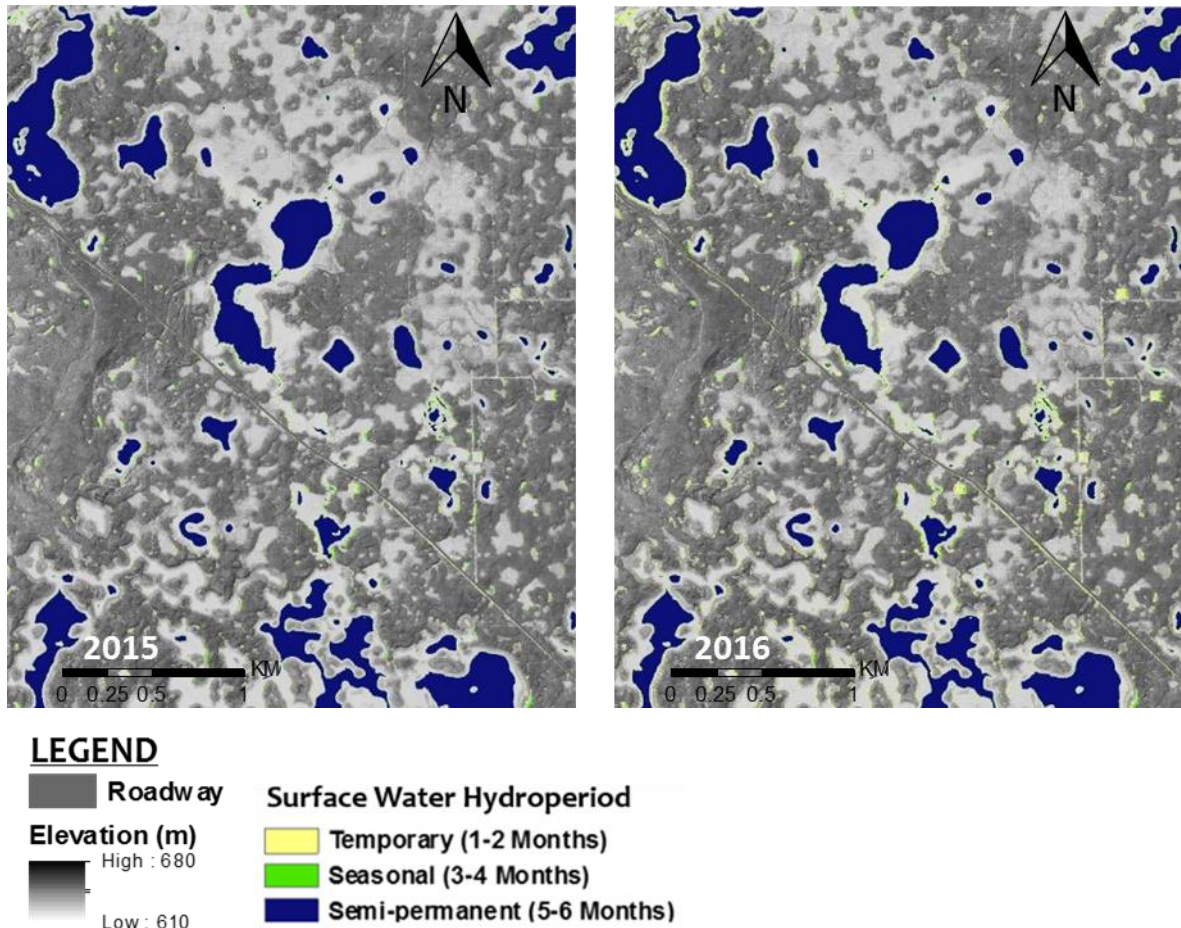
Figure 4.6. Hydroperiod results over the URSA subset AOI 2015 and 2016 SAR surface water hydroperiod. Hydroperiods are shown as yellow for temporary (1-2 months), green for seasonal (3-4months), and blue for semi-permanent / permanent (5-6 months). The 2016 Titan Lidar DSM is included to illustrate topography and canopy cover.

Note that 2015 includes only six image acquisitions, compared to 14 acquisitions

in 2016, where more scenes over the growing season increases the chance to capture

additional temporary or seasonal surface water hydroperiod events. It is expected that a

comparable number of acquisitions from each year would change the comparative

hydroperiod results.

Table 4.4. Comparison between 2015 and 2016 surface water hydroperiod classes and area in hectares (ha).

Hydroperiod (S&K)	True Positive	Hectares (ha)
Temporary I	53.0	43.6
Seasonal (II)	49.0	30.48
Semi-permanent (III)	98.3	744.7

4.3.4 Data Fusion Results

The results of the data fusion of both riparian vegetation and flooded vegetation from quad polarised SAR are shown in Figure 4.7. Flooded vegetation can be found in improbable areas such as roadways, and appear isolated from vegetation (<2m) normally associated with flooded vegetation (circled in Figure 4.7a), but this effect is mitigated by intersecting the vegetation height layer from the CHM and the flooded vegetation mask, creating a corrected mask of flooded vegetation around wetlands (Figure 4.7b). This methodology also prohibits commission errors from areas of flooded vegetation where no vegetation height is recorded (Hopkinson et al. 2005).
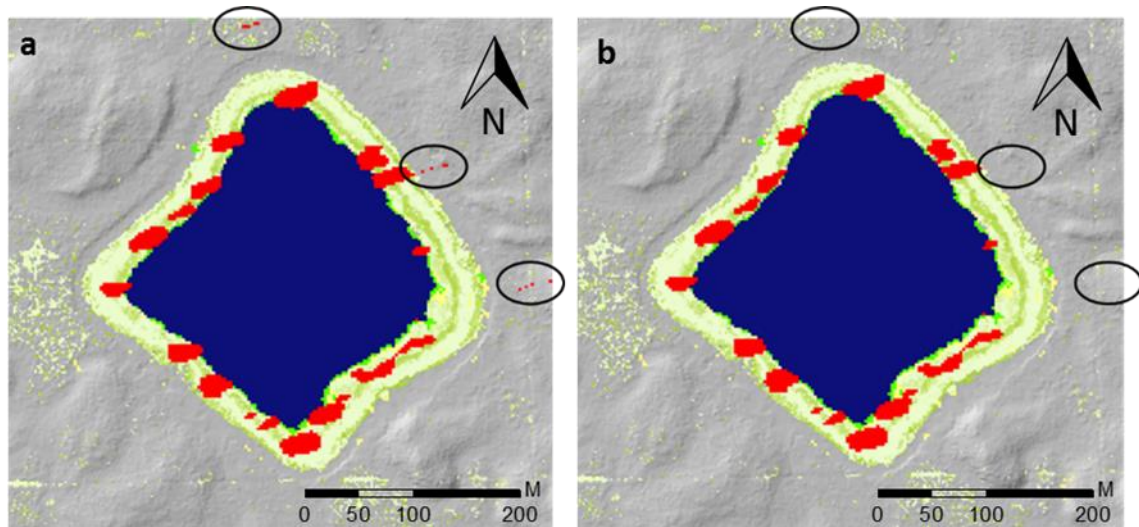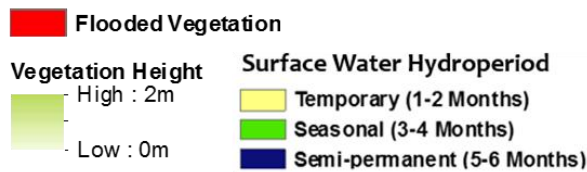
Figure 4.7a-b. a) Wetland with flooded vegetation comission errors outside of wetland riparian area and within surface water, b) corrected flooded vegetation raster mask.

The comphrensive wetland attribute product is shown in Figure 4.8. Attributes include: roadways derived from SPOT optical imagery, areas of high and low topography from the Lidar DEM topographic position index indicating where wetlands are most and least-likely to occur, vegetation height from Lidar CHM, flooded vegetation from quad polarised SAR Freeman Durden decomposition, and surface water hydroperiod from single polarisation SAR data extracted from dB thresholding and pixel frequency analysis in accordance with Stewart & Kantrud surface water classification.
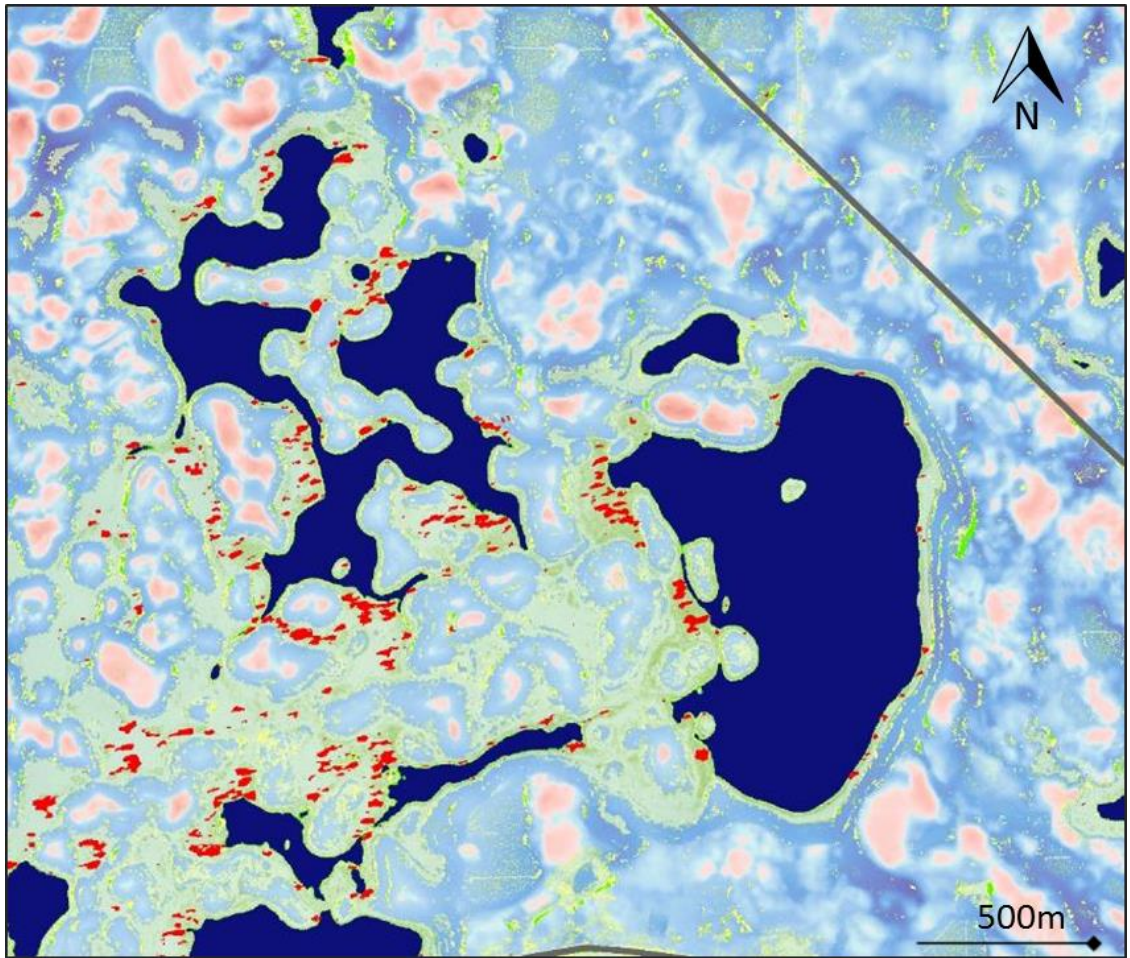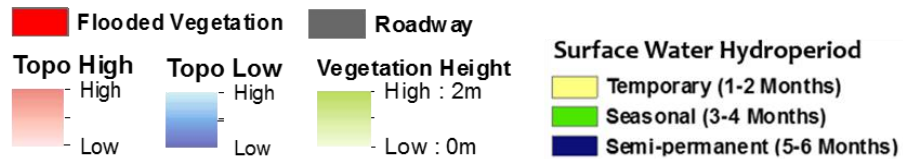
Figure 4.8. Complete data fusion product showing all wetland attributes and characteristics derived from the decision-tree, data fusion methodology.

Topographically corrected flooded vegetation and surface water hydroperiod is shown around a prominent wetland in the region with documented areas of dense cattail (Figure 4.9). Little open water is observed in these areas of flooded vegetation, but flooded vegetation and topographic attributes suggest there is a high probability these areas are inundated.

LEGEND

⬛ (grey)	Roadway
🟥 (red)	Flooded Vegetation

Surface Water Hydroperiod

⬜ (yellow)	Temporary (1-2 Months)
🟩 (green)	Seasonal (3-4 Months)
🟦 (navy)	Semi-permanent (5-6 Months)

Elevation (m)
High : 710
Low : 610
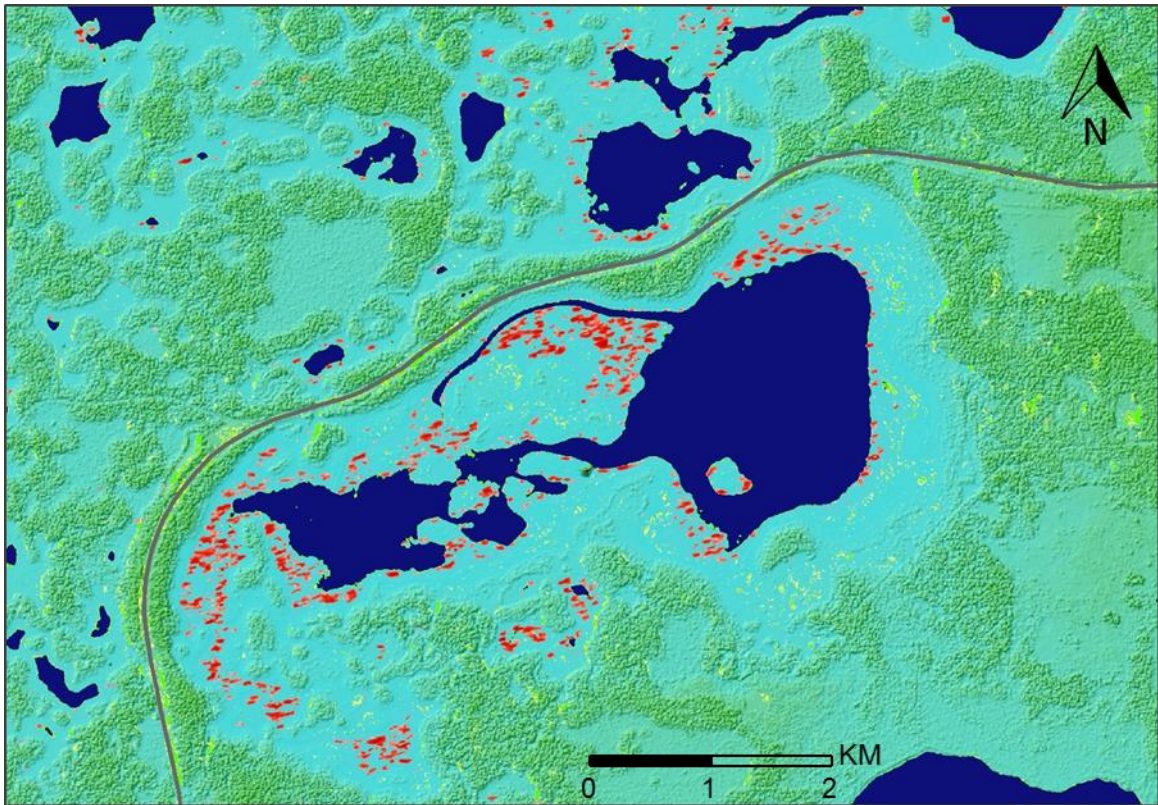
Figure 4.9. Data fusion product showing the presence of flooded vegetation around a large wetland with defined seasonal surface water extent.

4.3.5 Surface Water Extent and Riparian Vegetation Validation

For clarity and display purposes, two of the six ponds are compared with field validation (Pond 45 (Figure 10a) and Pond 43 (Figure 10b)), as they are the most rigorously field validated and have an appropriate spatial scale for display purposes. Distinct riparian and upland vegetation zones were observed during 2015 field data collection. Transition zones are notably abrupt (vegetation zones are distinct) in most transects (Figure 10a-b), except for areas where there is encroachment of woody vegetation such as willow, alder and birch from uplands into the grass and forb dominated

wetland riparian areas, where patches of young woody vegetation have largely replaced

tall grasses and sedge.
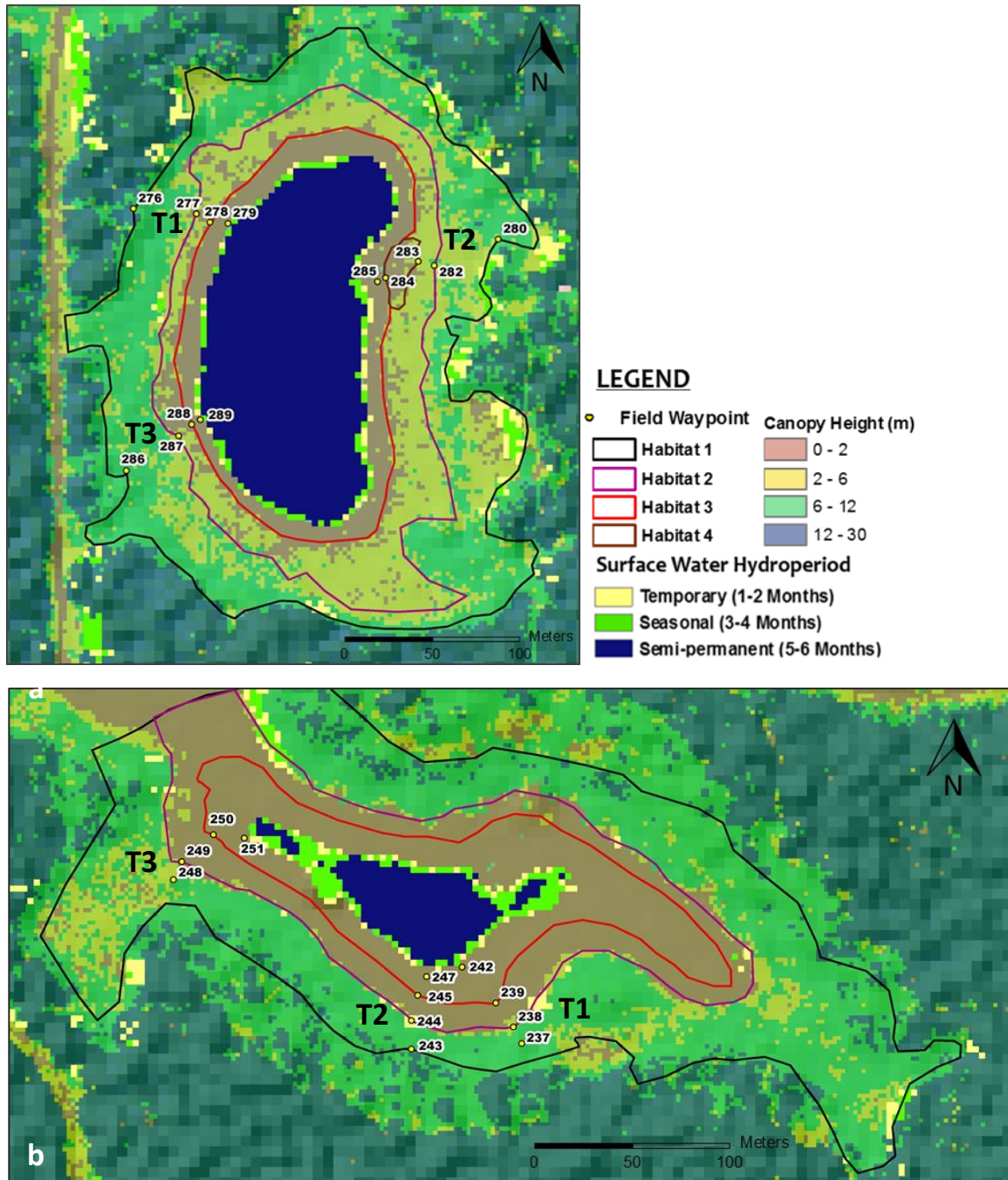
Figure 4.10a-b. Field validation of surface water extent and riparian boundaries for late July 2015. a) pond 45, b) pond 43. Riparian habitats are extrapolated from highly accurate field data points (Topcon Hiper SR GNSS), a series of SPOT optical imagery, and DEM data, then tested against canopy height cover. Field waypoints represent boundaries observed between riparian areas.

From the six wetlands surveyed the RMSE of the riparian transects and water extent observed in field validation data and those generated from the model was 4.6 m between field and model, with an R^2 value of 0.90 (Figure 4.11).
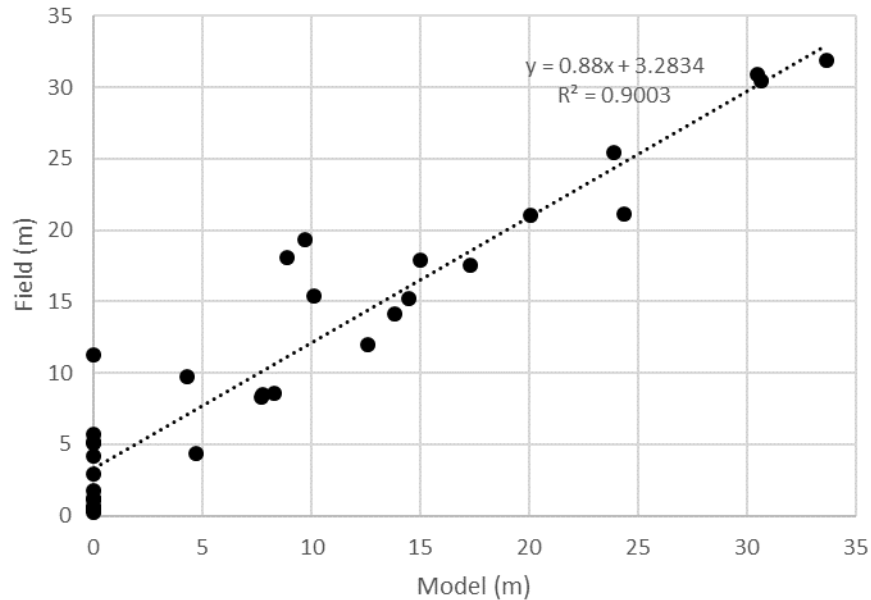
Figure 4.11. Regression of measured and model riparian and surface water extent accuracies (n=31) for six wetlands in the URSA region in 2015.

Most of the error is attributed to some notable surface water extent discrepancies within fen ponds with mud flats separating surface water and riparian vegetation. Vegetation species composition by transect for Pond 45 and Pond 43 are detailed in Table 4.6 (Pond 45), and Table 4.7 (Pond 43). Species composition was found to be relatively consistent at each transect for the wetlands, which can be divided into 3 distinct habitats, with occasional pockets of unique vegetation communities (habitat 4, Figure 4.1a).

Table 4.5. Riparian vegetation species composition for Pond 45 (refer to Figure 4.10a for transect and derived habitat locations).

Pond 45

T	Hab.	Vegetation Species
T1	H1	Paper birch/Alaska Birch (6-8m), young birch, rose, graminoids
	H2	Young birch (1-3m), buckbrush, snowberry, graminoids
	H3	Cattail, water sedge, buttercup sp., bur-reed, water parsnip
T2	H1	Paper birch (6-8m), green alder, young trembling aspen, rose, mosses
	H2	Tamarack, Labrador tea, willow, white spruce, young birch, graminoids
	H3	Cattail, water sedge, reed grass, buttercup sp.
	H4	Cattail, water cup sp. (float)., sedge sp., buttercup sp., goosefoot sp.
T3	H1	Paper/Alaska birch (6-8m). rose, black currant
	H2	Young birch (1-3m), buckbrush, snowberry, green alder, reed grass
	H3	Cattail, water sedge, goosefoot sp., water parsnip

Table 4.6. Riparian vegetation species composition for Pond 43 (refer to Figure 4.10b for transect and derived habitat locations).

Pond 43

T	Hab.	Vegetation Species
T1	H1	Paper birch (6-8m), raspberry, wheat grass sp., rye grass sp.
	H2	Young willow, young birch (<2m), water sedge, rice grass
	H3	Water parsnip, water sedge, bog birch, dock sp., mosses, cattail, bog birch
T2	H1	Paper birch (6-8m), raspberry
	H2	Willow, water sedge, rice grass
	H3	Sedge sp., young paper birch, water sedge
	H4	Common cattail, water sedge, goosefoot sp., mosses
T3	H1	Paper birch (6-8m), willows, bog birch, mosses
	H2	Green alder, willow, bog birch, graminoids, sedges
	H3	Cattail, water parsnip, sedges

Vegetation communities observed at Pond 45 and Pond 43 were diverse at the time of data collection, with many wetland indicator species present (cattail, sedges), showing minimal to no anthropogenic disturbance. Vegetation growth was only observed to be limited in areas where woody vegetation such as young willows and birch was encroaching into the riparian area (eg. Habitat 2 in all transects at Pond 43), potentially prohibiting succession of some riparian grasses.

4.4 Discussion

4.4.1 Subjectivity Associated with Manual Riparian Digitization

The results in Figure 4.10 and the associated accuracies in Figure 4.11 are accurate within ~10% of the area, but the manual classification shows some obvious discrepancies and associated subjectivity of the boundaries observed in the validation dataset and model (Figure 4.11). While optical data can be trained and classified to provide some measure of interpreted accuracy the process is still largely determined by delineation conducted by the operator. Boundaries of vegetation and water extent in some wetlands are also subjective. Crasto et al. (2015) discuss how criteria outlined by Jahn and Dunne (1997) influence remote sensing feature detection due to bias during digitization that is often influenced by experience and interpretations that are subjective (Goodchild, 2001). All validation data were collected by the same individua in the field, and areas were digitized by the same operator. Manual surveys of flooded vegetation boundaries were not conducted due to access and time limitations (Figure 4.8 and Figure 4.9), therefore these areas could not be validated to the same degree as less saturated riparian areas but the decomposition methodology has been well documented and studied for quality control in a variety of environments (Freeman and Durden 1998, Singh et al. 2012, Cui et al. 2012, Brisco et al. 2015). Any combination of uncertainties may contribute to discrepancies in the overall accuracy of the classification, and this highlights the importance of reliable ground validation data when working in logistically challenging regions.

4.4.2 Implications for Wetland Classification

While many studies focus on mapping known permanent waterbodies, this study differs by utilizing temporal and high spatial resolution information to create dynamic

surface water and associated riparian community thematic maps. Data availability is the

most important aspect when attempting to characterise non-permanent wetlands, requiring

increased temporal resolution and field measurements that represent the natural ranges in

hydrological conditions. The results of this high-resolution study suggest these criteria

can be met by products of the decision-tree methodology presented (Figures 4.8 and 4.9).

The methodology presented is also useful for the identification of marsh and

swamp wetlands with associated open water areas but there is also great potential to use

Lidar intensity following methods of Chasmer et al. (2015) to integrate more peatland

(treed fen/bog) environments. For example, simple 'if' statements can be implemented to

determine if an area is a swamp: eg 1) 'if trees are present and topography is low lying

(TPI) then high potential for a swamp'; 2) 'if the surface water level is above the DEM

then high potential for a swamp; 3) 'if no open water is present and flooded vegetation is

present then more likely a swamp or fen'. Absence of these statements in the

methodology are currently a limitation, but they should be explored and integrated in

further studies to provide a more complete classification system.

4.4.3 Data Limitations and Potential Sources of Error

The major limitation of the study relates to temporal image frequency of both

SAR and Lidar data. Increased temporal resolution will better represent short-term

variations. As mentioned in Chapter 3, the Canadian C-Band RADARSAT Constellation

Mission (RCM), expected to launch in 2018, will offer advanced capabilities for

monitoring surface water with high spatial resolution modes such as Spotlight, providing

enhanced monitoring of smaller wetlands (Canadian Space Agency 2016). As the

provincial Lidar database and coverage in Alberta expands and is updated, there is a

growing opportunity to integrate temporal Lidar datasets into wetland monitoring and enhance the understanding of precipitation variation influences on surface water and wetland vegetation change.

Working on such a large scale in the relatively remote URSA region makes it logistically difficult to collect ground validation across all wetland environments. Since classifiers or ranges for SAR-derived surface water masks are variable between images and acquisition, there is a need to calibrate the intensity threshold (dB) for each image in order to consistently extract all true open water returns from an image (eg. White et al. 2014), as well as instrument calibration and ground conditions (Hopkinson 2007).

A limitation of this approach is found in the fine resolution used in the large spatial area. Subtle changes in riparian vegetation on the order of <2m are difficult to extract with certainty due to homogeneity of many of the riparian vegetation communities. While it is easy to determine high and low topographical areas, and high, medium and low vegetation canopy, it is difficult to discriminate between species. For example, while it may be important to examine species encroachment, the difference between a patch of 2m tall willow trees and 2m tall birch trees is challenging due to similarities in structure, therefore it was found more convenient to group these similar canopy environments. This is detailed in Figures 4.9 and 4.10a-b, where both elevation and canopy height are somewhat ambiguous, likely as a result of the general flatness of topography and sporadic woody vegetation regeneration in clearings and meadows.

Shadow effects in the SAR ascending and descending images can cause classification errors along some forested boundaries but quality control data were not available within this study so the extent (if at all) of such shadow-induced errors in low-

lying riparian areas of the URSA study area is unknown. See Kropatsch (1990) for details

and potential methods to reduce error associated with shadowing.

When using SAR to derive surface water compared to other sensors, occasional

omission of surface water bodies that are narrow or have mixed pixels (such as

watercourses and fen pond boundaries), has been documented in shallow riparian areas

(Santoro and Wegmuller, 2014), which may be a potential source of error in many boreal

wetlands, where these boundary areas are mostly classified as land due to the unique

scattering properties. Surface water modeling would also be enhanced by delineating

water extent and elevation from Lidar, which can also provide further high-resolution

comparative data to both optical and SAR derived surface water masks, adding utility to

the wetland classification (eg. Hopkinson et al. 2011, Crasto et al. 2015).

4.5 Conclusion

The presented methodology offers a new time-series-based boreal wetland classification approach using data fusion of multiple remote sensing data sources, based on hydroperiod, topography and vegetation attributes. The results of this study indicate water mask frequency analysis can be used to determine hydroperiod and permanency in boreal environments similarly to prairie environments with overall accuracies of 93% to 97.2%, and kappa values of 0.8-0.9% when compared to optical data. Confusion matrix results comparing semi-permanent/permanent hydroperiod between 2015 and 2016 was found to be 98.3% correlated, suggesting there is very little change in open water extent in these wetlands between the two years. A longer time series would need to be used to determine if this is a consistent relationship. Regression analysis of field and model riparian and surface water extents from six wetlands also yielded high accuracies ($R^2 =$ 0.9), suggesting the decision tree methodology could be applied to similar open-water boreal wetlands with some certainty. The time-intensive and potential limiting factor of the methodology is the expertise required in data preparation for multiple types of data (Lidar, SAR, Optical). However, once the data preparation and foundation for data fusion has been conducted, additional data can readily be integrated and processed in the workflow. While there are limitations associated with data availability and frequency, the strength of the study is the ability to construct and examine meaningful comprehensive wetland characterization products conforming to provincial guidelines set forth by the AWCS and CWCS.

Future research using a logic-based decision-tree methodology would benefit from identifying additional topographic and vegetative attributes at a higher resolution to increase class reliability. SAR and Optical data to compliment Lidar data describing

riparian vegetation communities would further enhance the hydroperiod analysis for a more comprehensive wetland classification and monitoring framework. This framework could be largely automated through machine learning algorithms and would provide a platform for land use permitting, reclamation monitoring, and wetland regulation in remote boreal regions of Alberta.

5.0 Research Conclusion

5.1 Summary of Research Purpose

Research conducted in this thesis was motivated by the need for high resolution remote sensing monitoring of wetlands in Alberta of various endmember environments ranging from southern prairie regions to central and northern boreal forest regions. Wetland attributes and classes according to the Canadian Wetland Classification System, Alberta Wetland Classification System, and Stewart and Kantrud (1971), were targeted as a means to make the research innovative and relevant, potentially facilitating implementation of the methods and research findings into wetland policy. Remote sensing technology functions across many scales and is capable of imaging large, remote areas desired for wetland monitoring at high resolution, enhanced by using data from multiple types of sensors to extract different information and reduce uncertainty. While remote sensing provides an excellent means for wetland mapping, wetlands cannot be perceived or classified as static entities, which is a major limitation in how wetlands are currently classified, especially in-situ where a wetland is only documented at a certain time in a certain season – generally not indicative of the true dynamics of a wetland. Therefore, temporal resolution of remote sensing data is an equally important component for wetland monitoring. Thus, the research in this thesis examined temporal and spatial resolution by combining multiple data types in data fusion to model surface water extent and associated riparian areas to conform to and enhance wetland policy.

5.2 Research Findings and Future Research

It is acknowledged the logic-based approach used in this study differs to traditional approaches. Logic was used in this study using remote sensing observations as proxies for processes occurring in the environment. Statistical classification approaches

using sample data or machine learning algorithms, for example, can be robust and produce highly accurate classifications but they require extensive training data. The benefit of a logic-based approach that aims to represent the physical features and processes that characterise wetlands is that it not as reliant on extensive training data and model iterations in order to produce a comprehensive wetland classification product.

Synthetic Aperture Radar (SAR) was found to be an effective sensor for mapping open surface water extent in Alberta, at both prairie wetlands at Shepard Slough, and boreal wetlands at the Utikuma Regional Study Area (URSA). While water mask results at Shepard Slough were found to be less accurate, the intensity threshold (dB) approach was less influenced by environmental factors, specifically wind effects causing surface roughness. While the threshold range and limits were highly variable at Shepard Slough for most image acquisitions (ranging from -9 to -33 dB), it remained more consistent (-18 to -30 dB) at URSA, presumably due to increased canopy sheltering surrounding wetland areas.

Binary masking of surface water extent using SAR is well documented (White et al. 2014, 2015, Brisco 2015), but the innovative aspect of this research is the recognition that time-series SAR data enables wetlands to be explicitly classified as dynamic features. Wetland hydroperiod described by Stewart and Kantrud (1971) has long been used in prairie pothole and boreal wetland classification and continues to be used to predominantly describe prairie wetlands, and open surface water. Therefore, hydroperiod was determined based on the permanency classes described by Stewart and Kantrud (1971) through pixel frequency analysis of a stack of binary surface water masks, resulting in a product describing how long wetlands are present at seasonal and annual scales based on presence of open water. This hydroperiod classification provides the

means to accurately determine which wetlands fall under certain regulation and policy according to the Government of Alberta Wetland Policy (2014). While based on a regional policy, this methodology is not limited to jurisdictions or geographical regions and could be applied to wetlands across North America or in environments internationally, where it can also be applied to other applications such as floodplain inundation and flow regulation.

Fusion of Lidar, optical and several polarizations of SAR added topographical elements to the wetland classification, enhancing riparian vegetation transition zone identification and providing the means to conduct quality control of surface water products and flooded vegetation products. While overall accuracy was high compared to validation data (R^2=0.9), manual digitizing creates uncertainty and is highly subjective to the operator. Nonetheless, an interesting finding from the data fusion methodology is the presence of flooded vegetation found in low topographical areas, with low (<2m) riparian vegetation canopy height, was predominantly not associated with open surface water. This suggests wetlands are potentially greatly hydrologically influenced by sub-surface ground water interactions, rather than surface flow "fill and spill" mechanisms.

This thesis has contributed to the Geography and Remote Sensing literature in several ways: First, this is the first study attempting to characterize wetlands in Alberta using temporal data fusion to derive wetland characteristics conforming to provincial wetland classification requirements. The research also identifies, demonstrates and contrasts the limitations associated with data quality due to environmental factors when using SAR for surface water masking in the end-member environments examined. Lastly, the approach provides the means for high-resolution monitoring of wetlands with a focus

on wetlands in two important end-member environments of Alberta using data fusion, something not well documented.

It was not possible within this study to represent all end-member landscapes in Alberta but as there remain some distinct landscape types i.e. montane (e.g. Rockies and foothills regions), floodplain delta (e.g. the Peace Athabasca Delta) and parkland (e.g. Beaver Hills and Camrose areas) areas with distinct characteristics. Future research should evaluate whether the approaches tested here could be used in these landscapes or if hybrid approaches might work. While this research was presented in an Alberta prairie and boreal context, the basic logic could be applied to other parts of Canada and the United States, as it is only regionally constrained by data availability. One important variable if applied to other parts of Canada would be the consideration for differences in surficial geology, which could have a marked effect on the presence of a wetland and the type. For example, wetlands in the Canadian Shield with underlying bedrock and/or mineral soils will display distinct hydrological interactions compared to the deep organic soils found in peatland areas. Many soils and surface geology data layers have been created throughout Canadian territories and provinces that could be implemented into the logic based decision-tree methodology presented. Such extension of the current methodology and data use could be facilitated with a machine learning framework, such as random forest.

Future studies should also investigate the accuracies of using increased temporal resolution in this type of logic-based decision-tree methodology. As the Alberta provincial Lidar database grows, and with the advent of the Radarsat Constellation Mission (RCM) expected to launch of 2018, SAR and Lidar fusion based studies and

temporal change studies in general, will benefit from the increased Lidar coverage and 4-day repeat acquisition of RCM, compared to 24-day repeat acquisition with Radarsat-2.

References

Adam, S., Wiebe, J., Collins, M., Pietroniro, A. 1998. RADARSAT flood mapping in the Peace-Athabasca Delta, Canada. *Can. J. Remote Sens*. Vol. 24: pp. 69-79.

Alberta Environment & Sustainable Resource Development (ESRD). 2014. Alberta Wetland Classification System. Water Policy Branch, Policy Division. Edmonton. pp 38.

Alberta Environment and Sustainable Resource Development (ESRD). 2015. Alberta Wetland Classification System. Water Policy Branch, Policy and Planning Division, Edmonton, AB.

Alberta Wetland Mapping Standards Workshop. Alberta NAWMP Partnership. Leduc, Alberta. March 23, 2017.

Alsdorf D.E., Smith L.C., Melack J.M 2001. Amazon floodplain water level changes measured with interferometric SIR-C Radar. *IEEE transitions on geosciences and remote sensing*, Vol. 39, (No. 2): pp. 423-431.

Alsdorf DE. 2003. Water storage of the central Amazon floodplain measured with GIS and remote sensing imagery. *Annals of the Association of American Geographers*. Vol. 93. (No. 1): pp. 55–66.

Ameli A., Creed I. 2017. Quantifying hydrologic connectivity of wetlands to surface water systems. *Hydrology and Earth System Sciences*. Vol. 21(No. 1): pp. 1791-1808. DOI: 10.5194/hess-21-1791-2017

Amitrano D., Martino G., Iodice A., Ruello G. 2014. Sentinel-1 for Monitoring Reservoirs: A Performance Analysis. *Remote Sensing*. Vol. 6: pp. 10676-10693. DOI: 10.3390/rs61110676

Ardhuin, F., B. Chapron, F. Collard, M. Smith, J. Stopa, J. Thomson, M. Doble, P. Wadhams, B. Blomquist, O. Persson, and C. O. Collins, III, 2017. Measuring ocean waves in sea ice using sar imagery: A quasideterministic approach evaluated with sentinel-1 and in situ data. *Remote Sensing of Environment*, Vol. 189: pp. 211–222. doi:10.1016/j.rse.2016.11.024.

Barrette J., August P., Golet F. 2000. Accuracy assessment of wetland boundary delineation using aerial photography and digital orthophotography, *Photogrammetric Engineering & Remote Sensing*, Vol.66(No.4): pp.409-416

Beckingham, J. D. and J. H. Archibald. 1996. Field Guide to Ecosites of Northern Alberta. Vancouver, BC, UBC Press.

Beckingham, J. D., I. G. W. Corns and J. H. Archibald. 1996. Field Guide to Ecosites of West-Central Alberta. Vancouver, BC, UBC Press.

Boland J. and 16 co-aujthors. 2004. Chapter 8: Camerias and Sensing Systems. Mcglone, J.C. (Ed.). *Manual of Photogrammetry*, 5th edition, Bethesda: ASP&RS, pp. 629-636.

Bolanos S., Stuff D., Brisco B., Pietroniro A. 2016. Operational Surface Water Detection and Monitoring using Radarsat. *Remote Sensing*. Vol. 8: pp. 285. Doi:10.3390/rs8040285

Bourgeau-Chavez, L.L. Kasischke, E.S., Brunzell, S.M., Mudd, J.P., Smith, K.N., Frick, A.L. (2001) Analysis of space-bource SAT daa for wetland mapping in Virginia riparian ecosystems, *International Journal of remote Sensing,* Vol. 22(No.18): pp 3665-3687.

Bourgeau-Chavez, L.L.; Riordan, K.; Powell, R.B.; Miller, N.; Nowels, M. 2009. Improving wetland characterization with multi-sensor, multi-temporal SAR and optical/infrared data fusion. *In Advances in Geoscience and Remote Sensing*; INTECH: Rijeka, Croatia.

Brakenridge GR, Nghiem SV, Anderson E, Chien S. 2005. Spacebased measurement of river runoff. *Eos*, *Transactions*, *American Geophysical Union,* Vol. 86(No. 19): pp. 185, 188.

Brakenridge GR, Nghiem SV, Anderson E, Mic R. 2007. Orbital microwave measurement of river discharge and ice status. *Water Resources Research,* Vol. 43: W04405.

Brisco, B, Li, K., Tedford, B., Charbonneau, F, Yun, 2. Murnaghan K. 2013. Compact polarimetry assessment for rice and wetland mapping. *Int. J. Remote Sens.,* Vol. 34: pp. 1849-1964

Brisco, B. 2015. Remote Sensing of Wetlands: Applications and Advances, Chapter: Remote Sensing of Wetlands: Applications and Advances.

Brisco, B. Short, N, van der Sanden, J, Landry R, Raymond, D. 2009. A semi-automated tool for surface water mapping with Radarsat-1. *Can. J. Remote Sensing*. Vol. 35: pp. 336-344.

Brisco, B. Touzi, R., van der Sanden, J.J, Charbonneau, F., Pultz, T.J., D'Iorio, M. 2008. Water Resources applications with RADARSAT-2-A preview. *Int. J. Digital Earth*. Vol. 1: pp. 130-147.

Brisco, B., 2015. Mapping and monitoring surface water and wetlands with synthetic aperture radar. Remote Sensing of Wetlands, Applications and Advances, Edited by Tiner, R.W., Lang, M.W., and Klemas, V.V., CRC Press, Chapter 6, Pages 119–136.

Brisco, B., Ahren F., Murnaghan K., White L., Canisus F., Lancaster P. 2017. Seasonal Change in Wetland Coherence as an Aid to Wetland Monitoring. *Remote Sensing*. Vol. 9: pp 158; doi: 10.3390/rs9020158

Brisco, B., Kapfer, M., Hirose, T., Tedford, B., Liu J. 2011. Evaluation of C-band polarisation diversity and polarimetrey for wetland mapping. *Can. J. Remote Sens.* Vol. 37: pp. 82-92

Burrough, P.A., Gaans P.F.M., MacMillan R.A. 2000. High-resolution landform classification using fuzzy k-means. *Fuzzy Sets and Systems*. Vol. 113 (No. 1): pp. 37-52. doi.org/10.1016/S0165-0114(99)00011-1

Burrough, P.A., Wilson, J.P., van Gaans, P.F. 2001. Fuzzy K-means classification of topo-climatic data as an aid to forest mapping in the Greater Yellowstone Area, USA. *Landscape Ecology*, 16:523. Doi:10.1023/A:1013167712622

Brovelli, M., Cannata M., Longoni U. 2004. Lidar data filtering and DTM interpolation within GRASS. *Transactions in GIS*. Vol. 8(No.2): pp. 155-174.

Hopkinson, C., Crasto, H., Marsh P., Forbes D., Lesack, L. 2011. Investigating the spatial distribution of water levels in the Mackenzie Delta using airborne Lidar. *Hydrological Processes,* Vol. 25(No. 19): pp. 2995-3011

Canadian Space Agency. RADARSAT Constellation. Available Online: http://www.asc-csa.gc.ca/eng/satellites/radarsat

Chasmer, L., C. Hopkinson, J. Montgomery and Petrone R., 2016. A physically based terrain morphology and vegetation structural classification for wetlands of the boreal plains, Alberta, Canada. *Can. J. Remote Sens.,* Vol.00: pp. 1–20.

Chasmer, L., Hopkinson, C., Quinton, W., Veness, T., and Baltzer,J. 2014. A decision-tree classification for low-lying complex land cover types within the zone of discontinuous permafrost. *Remote Sensing of Environment*, Vol. 143: pp. 73–84.

Chetner, S. and the Agroclimatic Atlas Working Group, 2003. *Agroclimatic Atlas of Alberta, 1971 to 2000* . Alberta Agriculture, Food and Rural Development, Agdex 071-1. Edmonton, Alberta.

Cloude, S.R. and Pottier, E. 1997. An entropy based classification scheme for land applications of polarimetric SAR. *IEEE Transactions on Geoscience Remote Sensing.* Vol. 36: pp. 68-78.

Convention on Biological Diversity, 18th Meeting of the Subsidiary Body on Scientific, Technical and Technological Advice, June 23- 28, 2014, Opportunities and Challenges for Harmonization of Global Indicators for the Convention on Biological Diversity and the Ramsar Convention on Wetlands, UNEP/CBD/ SBSTTA/18/INF/18 (June 13, 2014)

Costanza, R., de Groot, R., Sutton, P., van der Ploeg, S., Anderson, S. J., Kubiszewski, I., Farber, S., & Turner, R. K. (2014). Changes in the global value of ecosystem services. *Global Environmental Change,* Vol. 26: pp.152-158.

Crasto N., Hopkinson C., Marsh P., Forbes D., Spooner I. 2012. Delineation of lakes and channels in the Mackenzie Delta, NWT, using airborne LiDAR. IAHS RedBook Publ. 352, 359-362.

Crasto, N., Hopkinson, C., Forbes, D.L., Lesack, L., Marsh, P., Spooner,I., Van Der Sanden, J.J. 2015. "A LiDAR-based decision-tree classification of open water surfaces in an Arctic delta." *Remote Sensing of Environment*, Vol. 164: pp. 90–102.

Crevier, y. Pultz, T.J. Analysis of C-band SIR-C radar backscatter over a flooded environment, Red River, Manitoba. In proceedings of the third international workshop (NHRI Symposium)- applications of remote sensing in hydrology, Greenbelt, MD, USA, 16-18 October 1996, pp47-60.

Cui Y., Yamaguchi Y., Yang J., Park S., Kobayashi H, Singh G. 2012. Three-component power decomposition for polarimetric SAR data based on adaptive volume scatter modeling. *Remote Sensing*, Vol.4: pp. 1559-1572; doi:10.3390/rs4061559

Curlander J.C. "Utilization of spaceborne SAR data for mapping," *IEEE Trans. Geosci. Remote Sens.*, Vol. GE-22(No. 2): pp. 106–112, Mar. 1984.

Dahl, T.E.; Watmough, M.D. Current approaches to wetland status and trends monitoring in prairie Canada and the continental United States of America. *Can. J. Remote Sens.* 2007, 33, S17–S27.

Daily, G.C.; Alexander, S.; Ehrlich, P.R.; Goulder, L.; Lubchenco, J.; Matson, P.A.; Mooney, H.A.; Postel, S.; Schneider, S.H.; Tilman, D. Ecosystem Services: Benefits Supplied to Human Societies by Natural Ecosystems; Ecological Society of America: Washington, DC, USA, 1997.

De Groot, W.J., Flannigan, M.D. and Cantin, A.S. 2013. Climate change impacts on future boreal fire regimes. *Forest Ecology and Management*, Vol. 294: pp. 35–44.

Devito K.J., Creed, I.F., and Fraser, C. 2005. Controls on runoff from a partially harvested aspen forested headwater catchment, Boreal Plain, Canada. *Hydrological Processes*, Vol. 19: pp. 3–25.

Di Baldassarre , G. Shucmann G., Brandimarte, L., Bates, P., 2011. Timely low resolution SAr imagery to support floodplain modelings: A case study review. *Surv Geophys*. Vol. 32: pp. 255-269.

Ewel, K. 1990. Swamps. In R. L. Myers and J. J. Ewel (eds.). Ecosystems of Florida. University of Central Florida Press, Orlando: 281-323.

Feyisa, G.L., Meilby, H., Fensholt, R. and Proud, S.R. (2014) Automated Water Extraction Index: A New Technique for Surface Water Mapping Using Landsat Imagery. *Remote Sensing of Environment*, Vol. 140: pp. 23-35.

Forgette T., Shuey J. 1997. A comparison of wetland mapping using SPOT satellite imagery and national wetland inventory data for a watershed in Northern Michigan. *Northern Forested Wetlands Ecology and Management.* Chapter 5: pp. 61-70.

Foster, Lisa D. 2007. Using Frequency Analysis to Determine Wetland Hydroperiod. Graduate Theses and Dissertations.http://scholarcommons.usf.edu/etd/3798

Frappart F, Do Minh K, L'Hermitte J, Cazenave A, Ramillien G,Le Toan T, Mognard-Campbell N. 2006. Water volume change in the lower Mekong from satellite altimetry and imagery data. *Geophysical Journal International,* Vol. 167(No.2): pp. 570–584

Frappart F, Seyler F, Martinez JM, Leon JG, Cazenave C. 2005.Floodplain water storage in the Negro River basin estimated from microwave remote sensing of inundation area and water levels. *Remote Sensing of Environment.* Vol. 99(No.4): pp. 387–399.

Frazier, P.S., & Page, K.J. (2000). Water body detection and delineation with Landsat TM data. *Photogrammetric Engineering and Remote Sensing*, Vol. 66(No. 12): pp. 1461–1468.

Freeman, A., Durden S.L. 1998. A three-component scattering model for polarimetric SAR data. *IEEE Trans. Geosci. Remote Sensing*, Vol. 36: pp. 963-973.

Frey, K.E. and Smith, L.C.,2007. How well do we know northern land cover? Comparison of four global vegetation and wetland products with a new ground-truth database for West Siberia. *Global Biogeochemical Cycles*, Vol. 21: pp. GB1016. doi:10.1029/2006GB002706.

Galatowitsch S., van der Valk A. 1996. The vegetation of restored and natural prairie wetalands. *Ecological Applications*, Vol.6 (No.1): pp. 102-112. doi:10.2307/2269557

Gan, T. Y., Zunic, F., Kuo, C-C., and Strobl, T. 2012. "Flood mapping of Danube River at Romania using single and multi-date ERS2-SAR images." *International Journal of Applied Earth Observation Geoinformation*, Vol.18: pp. 69–81.

Giardino, C.; Bresciani, M.; Cazzaniga, I.; Schenk, K.; Rieger, P.; Braga, F.; Matta, E.; Brando, V.E. 2014. Evaluation of Multi-Resolution Satellite Sensors for Assessing Water Quality and Bottom Depth of Lake Garda. *Sensors*, Vol. 14: pp. 24116-24131.

Goulden T., Hopkinson C. 2010. The forward propagation of integrated system components within airborne lidar data. *Photogrammetric Engineering and Remote Sensing.* Vol. 76(No.5): pp. 589.

Goodale R., Hopkinson C., Colville D., Amirault-Langlais D. 2007. Mapping piping plover (Charadrius melodus melodus) habitat in coastal areas using airborne Lidar data. *Can J. Remote Sens.* Vol.33(No.): pp. 519-533.

Goodchild, M.F. (2001). Metrics of scale in remote sensing and GIS. International Journal of Applied Earth Observation and Geoinformation, Vol.3(No. 2): pp. 114-110.

Government of Alberta (2014). Facts on Alberta: Living and Doing Business in Alberta

Government of Alberta. 2013. Alberta Wetland Policy. http://aep.alberta.ca/water/programs-and services/wetlands/documents/Alberta WetlandPolicy-Sep2013.pdf.

Government of Canada. 1991. The Federal Policy on Wetland Conservation. Environment Canada. Ottawa, Ontario. 14 p.

Goward, S. Terry A., Williams D,m Faundeen J., Irons J., Franks S. 2006. Historical record of Landsat global coverage. *Photogramm. Eng. Remote Sensing*. Vol.72(No.15): pp. 1155–1169

Guindon B. 1993. Development of a SAR data acquisition planning tool (SARPLAN) based on image simulation, *Int. J. Remote Sens.*, Vol. 14(No.2): pp. 333–344

Guisan, A., S. B. Weiss and A. D. Weiss. 1999. GLM versus CCA spatial modeling of plant species distribution. Kluwer Academic Publishers. *Plant Ecology*. Vol.143: pp. 107-122.

Haack B., Messina J. 1997. Space technology and applications international forum (STAIF - 97). AIP Conference Proceedings, Vol. 387: pp. 215-220

Halsey, L.A., Vitt, D.H., Beilman, D., Crow, S., Mehelcic, S., and Wells, R. 2004. Alberta Wetland Inventory Classification System, version 2.0. Pub # T/031. Edmonton, AB, Canada: Government of Alberta, Alberta Sustainable Resource Development.

Hamerly G., Elkan C. 2002. Alternatives to the k-means algorithm that find better clusterings. Proceedings of the eleventh international conference on information and knowledge management (CIKM).

Hartigan J., Wong M. 1979. Algorithm AS 136: K-Means Clustering Algorithm. *Journal of the Royal Statistical Society. Series C (Applied Statistics),* Vol. 28(No. 1): pp 100-108.

Hayashi, M., G. van der Kamp, and R. Schmidt. 2003. "Focused infiltration of snowmelt water in partially frozen soil under small depressions." *Journal of Hydrology*, Vol. 270: pp. 214-229.

Hess, L.L, Melack J.M, Simonett, D.S. 1990. Radar detection of flooding beneath the forest canopy. A review. *Int. J. Remote Sens.*, Vol. 11: pp. 1313-1325.

Hodgson, M.E., Jensen, J.R., Mackey, H.E. & Coulter M.C. (1987) Remote sensing of wetland habitat: A wood stork example, *Photogrammetric Engineering & Remote Sensing*, Vol.53: pp. 1075-1080.

Hong., Sang-Hoon., Wdowinski Shimon, Kim Sang-wan. 2009. Evaluation of TerraSAR-X Observations for Wetland InSAR Application. *IEEE Transactions of Geosciences and Remote Sensing*. Vol. 48(No.2). DOI:10.1109/TGRS.2009.2026895

Hopkinson, C., Chasmer, L.E., Zsigovics, G., Creed, I., Sitar, M., Kalbfleisch, W., Treitz,P. 2005. Vegetation class dependent errors in LiDAR ground elevation and canopy height estimates in a Boreal wetland environment. *Can. J. Remote Sens.*, Vol. 31(No.2): pp. 191-206

Hopkinson, C., Crasto, N., Marsh, P., Forbes, D.L., and Lesack, L.F.W. 2011. Investigating the spatial distribution of water levels in the Mackenzie Delta using airborne LiDAR. *Hydrological Processes*, Vol. 25: pp. 2995–3011.

Hopkinson, C., Pietroniro, A. and Pomeroy, J. (eds), 2008. HYDROSCAN: Airborne laser mapping of hydrological features and resources. Canadian Water Resources Association, Saskatoon.

Hostache, R., Matgen, P., Schumann, G., Puech, C., Hoffman, L., Phister, L. 2009. Water level estimation and reduction of hydraulic model calibration uncertainties using satellite SAR images of floods. *IEEE Transactions on Geoscience and Remote Sensing,* Vol. 47: pp. 431-441.

Irwin, K. Beaulne D., Braun A., Fotopoulos G., 2017. Fusion of SAR, Optical and Airborne Lidar for Surface Water Detection. *Remote Sensing.* Vol. 9: pp. 890, doi:10.3390/rs9090890

Isenburg M. 2017. LAStools - Efficient LiDAR Processing Software (version 141017, academic), obtained from http://rapidlasso.com/LAStools

Jahn, R.G., & Dunne, B.J. (1997). Science of the subjective. *Journal of Scientific Exploration*, Vol. 11(No. 2): pp. 201–224.

Jenness, J. 2006. Topographic Position Index (tpi_jen.avx) extension for ArcView 3.x, v. 1.2. Jenness Enterprises. http://www.jennessent.com/arcview/tpi.htm.

Jensen J.R. 2005. Introductory Digital Image Processing: A Remote Sensing Perspective, 3rd Ed., Upper Saddle River, Prentice-Hall, pp. 525.

Jensen J.R. 2007. Remote Sensing of the Environment: An Earth Resource Perspective (2nd Edition). Prentice Hall, Pearson Education Inc. pp. 592.

Johansen, K., Coops, N.C., Gergel, S.E. and Stange, Y., 2007. Application of high spatial resolution satellite imagery for riparian and forest ecosystem classification. *Remote Sensing of Environment*, Vol. 110: pp. 24 – 44

Jones K.B., D.T. Heggem, T.G. Wade, A.C. Neale, D.W. Ebert, M.S. Nash, M.H. Mehaffey, K.A. Hermann, A.R. Selle, S. Augustine, I.A. Goodman, J. Pedersen, D. Bolgrien, J.M. Viger, D. Chiang, C.J. Lin, Y. Zhong, J. Baker and R.D. Van Remortel. 2000. Assessing Landscape Conditions Relative to Water Resources in the Western United States: A Strategic Approach. Environmental Monitoring and Assessment 64: pp. 227 – 245.

Kantrud H.A., Millar J.B., Van Der Valk A.G. 1989. Northern prairie wetlands. Vegetation of wetlands of the prairie pothole region. Iowa State University Press, Ames, IA. pp. 132-187

Kanungo T., Mount D., Netanyahu N., Piatki C., Silverman R., Wu A., 2002. An efficient k-means clustering algorithm: Analysis and implementation. *IEEE Transactions* on Pattern Analysis and Machine Intelligence, Vol. 24(No.7).

Kasischke, E.S.; Bourgeau-Chavez, L.L. 1997. Monitoring South Florida wetlands using ERS-1 SAR imagery. *Photogram. Eng. Remote Sens.*, Vol. *63*: pp. 281– 291.

Kettridge N., Waddington J.M. 2013. Towards quantifying the negative feedback regulation of peatland evaporation to drought. *Hydrological Processes.* Vol, 28 (No.11). DOI: 10.1002/hyp.9898

Klein, E., Berg, E.E., and Dial, R. 2005. Wetland drying and succession across the Kenai Peninsula Lowlands, south-central Alaska. *Canadian Journal of Forest Research*, Vol. 35: pp. 1931–1941.

Klemas, V. 2011. Remote sensing of wetlands: Case studies comparing practical techniques. *J. Coast. Res.* Vol. *27*: pp. 418–427.

Komers, P.E., and Stanojevic, Z. 2013. Rates of disturbance vary by data resolution: implications for conservation schedules using the Alberta Boreal Forest as a case study. *Global Change Biology*, Vol. 19: pp. 2916–2928.

Kropatsch W.G., and Strobl D., 1990. The generation of SAR layover and shadow maps from digital elevation models, *IEEE Trans. Geosci. Remote Sens.*, Vol. 28(No.1): pp. 98–107

Kwok R., Curlander J.C. and Pang S.S. 1987. Rectification of terrain induced distortions in radar imagery, *Photogramm. Eng. Remote Sens.*, Vol. 53(No.5): pp. 507–513.

Lane, Charles R., Liu Hongxing, Autrey, B.C., Anenkhonov O., A. Chepinoga V., Wu Quisheng. 2014. Improved wetland classification using eight-band high resolution satellite imagery and a hybrid approach. *Remote Sensing.* Vol. 6: pp. 12187-12216; doi:10.3390/rs61212187

Leberl F. W., "Radargrammery," in Principles and Applications of Imaging Radar (Manual of Remote Sensing), 3rd ed, F. M. Henderson and A. J. Lewis, Eds. New York: Wiley, 1998, Vol. 2, Ch. 4: pp. 183–269.

Leberl F.W., Radargrammetric Image Processing. Norwood, MA: Artech House, 1990, Ch. 3: pp. 77–112.

Lee, J.-S., Jurkevich, I., Dewaele, P., Wambacq, P., and Oosterlinck, A. 1994. "Speckle Filtering of Synthetic Aperture Radar Images: A Review." *Remote Sensing Review*, Vol. 8: pp. 313–340.

Leprince S., Barbot S., Ayoub F., Avouac J.P. 2007. Automatic and precise orthorectification, coregistration, and subpixel correlation of satellite images, application to ground deformation measurements, IEEE Trans. *Geosci. Remote Sens.*, Vol. 45(No.6): pp. 1529–1558.

Lewis A.J. and MacDonald H.C. 1970. Interpretive and mosaicking problems of SLAR imagery, *Remote Sensing of Environment.*, Vol. 1(No.4): pp. 231–236.

Lichvar, R.W., N.C. Melvin, M.L. Butterwick, and W.N. Kirchner. 2012. *National Wetland Plant List indicator rating definitions.* U.S. Army Corps of Engineers, Engineer Research and Development Center, Cold Regions Research and Engineering Laboratory ERDC/CRREL TR-12-1.

Lindsey, J.B., Creed, I.F., Beall, F.D. 2004. Drainage basin morphometrics for depressional landscapes. Water Resources Research. Vol. 40: pp. W09307, doi:10.1029/2004WR003322

Lindsey, J., and Creed, I., 2005. Sensitivity of Digital Landscapes to Artifact Depressions in Remotely-Sensed DEMs. Photogrammetric Engineering and Remote Sensing Vol. 71(No. 9): pp. 1029-1036

Livingstone, C.E.; Sikaneta, I.; Gierull, C.; Chiu, S.; Beaulne, P. (2005) RADARSAT-2 System and Mode Description. In Integration of Space-Based Assets within Full Spectrum Operations (pp. 15-1 – 15-22). Meeting Proceedings RTO-MP-SCI-150, Paper 15. Neuilly-sur-Seine, France: RTO:http://www.rto.nato.int/abstracts.asp.

Long, S., Fatoyinbo, T. E., and Policelli, F. 2014. "Flood extent mapping for Nambia using change detection and thresholding with SAR." *Environmental Research Letters*, Vol. 9: doi:10.1088/17489326/9/3/035002.

Lopes A., Nezry E., Touzi R., H. Laur H. 1993. Structure detection and statistical adaptive speckle filtering in SAR images, *International Journal of Remote Sensing*, Vol. 14(No. 9): pp. 1735-1758,

Lopes A., Touzi R., Nezry E. 1990. Adaptive Speckle Filters and Scene Heterogeneity, *IEEE Transactions on Geoscience and Remote Sensing*, Vol 28(No. 4).

Lutz, A. F., Immerzeel, W. W., Shrestha, A. B. & Bierkens, M. F. P. 2014. Consistent increase in High Asia's runoff due to increasing glacier melt and precipitation. *Nat. Clim. Chang*. Vol. 4: pp. 587–592

Dixon, M.J.R., Loh, J., Davidson, N.C., Beltrame, C., Freeman, R., Walpole. M. 2016. Tracking global change in ecosystem area: The Wetland Extent Trends index. *Biological Conservation*, Vol. 193: pp. 27–35.

MacDonald, G. M. 2010. Water, climate change, and sustainability in the southwest. *Proc. Natl Acad. Sci*. USA 107, 21256–21262

Manore, M., Flett, D. G., Abreau, R. A. D., Ramsay, B. R., and van der Sanden, J. 2001. "Multi-polarization SAR data for operational ice monitoring." In *Proceedings of the IEEE International Geoscience and Remote Sensing Symposium*, Vol.3: pp. 1246–1248.

Marsetic A., Oštir K., Fras M. 2015. Automatic Orthorectification of High-Resolution Optical Satellite Images Using Vector Roads. *IEEE Transaction on Geoscience and Remote Sensing*, Vol. 53(No.11).

Marsh, P., Lesack, L., Hicks, F., Roberts, A., Hopkinson, C., Solomon, S. 2009. Hydrology of the Mackenzie Delta: Off-channel water storage and interactions between the Mackenzie Delta and Beaufort Sea. 17th International Northern Research Basins Symposium and Workshop Iqaluit-Pangnirtung-Kuujjuaq, Canada, August 12 to 18, 2009: pp. 217–226.

Martinis, S. and C. Rieke, 2015. Backscatter analysis using multi-temporal and multi-frequency SAR data in the context of flood mapping at river Saale, Germany. *Remote Sensing*, Vol. 7: pp. 7732-7752, doi:10.3390/rs70607732.

Martinis, S., C. Kuenzer, A. Wendleder and S. Dech, 2015. Comparing four operational SAR-based water and flood detection approaches. *International Journal of Remote Sensing,* Vol. 36(No. 13): pp. 3519–3543.

Martinis, S., Twele, A., and Voigt, S. 2009. Towards operational near real-time flood detection using a split-based automatic thresholding procedure on high resolution TerraSAR-X data. *Natural Hazards Earth System Sciences*, Vol. 9: pp. 303–314.

Maxa M., Bolstad P., 2009. Mapping Northern Wetlands with High Resolution Satellite Images and Lidar. *Wetlands.* Vol. 29(No.1): pp. 248-260. doi: http://dx.doi.org/10.1672/08-91.1

McFeeters, S.K. 1996. The Use of the Normalized Difference Water Index (NDWI) in the Delineation of Open Water Features. *International Journal of Remote Sensing*, Vol. 17: pp. 1425-1432. http://dx.doi.org/10.1080/01431169608948714

Mikhail E.M.,Bethel, J.S., McGlone J.C. 2001, Introduction to modern photogrammetry, NY: John Wiley: pp. 479.

Millard L., Richardson M. 2013. Wetland mapping with Lidar derivatives, SAR polarimentric decompositions, and Lidar/SAR fusion using a random forest classifier. *Can. J. Remote Sensing*. Vol. 39(No.4).

Mitsch, W. J., Gosselink J.G. 2000. Wetlands. John Wiley and Sons, Inc. New York, NY.

Mitsch, W. J. and J. G. Gosselink. 2007. Wetlands (4th Edition). John Wiley & Sons, Inc., Hoboken, NJ

Moffat K., Gorelick S. 2013. Distinguishing wetland vegetation and channel features with object-based image segmentation. *International Journal of Remote Sensing*, Vol. 34(No.4).

Mueller, N. Lewis A., Roberts D., Ring S., Melrose R., Sixsmith J., Lymbruner L., Mcintyre A., Tan P., Curnow S., Ip A. 2016. Water observations from space: mapping surface water from 25 years of Landsat imagery across Australia. *Remote Sensing of Environment*, Vol. 174: pp. 341–352

National Wetlands Working Group. 1988. *Wetlands of Canada*. Ecological Land Classification Series, No. 24. Environment Canada and Polyscience Publications Inc. Ottawa, Ontario. pp. 452.

National Wetlands Working Group. 1997. *The Canadian Wetland Classification System: A Revision of the Wetlands of Canada*, edited by B.G. Warner and C.D.A. Rubec. Ontario, Canada: Wetlands Research Centre, University of Waterloo.

Natural Regions Committee. 2006. *Natural Regions and Subregions of Alberta*. Pub # T/852. Compiled by D.J. Downing and W.W. Pettapiece. Government of Alberta. http://www.cd.gov.ab.ca/preserving/parks/anhic/Natural region report.asp.

Ozesmi, S.L.; Bauer, M.E. 2002. Satellite remote sensing of wetlands. *Wetl. Ecol. Manag.*, Vol. 10: pp. 381–402.

Peiman, R., Ali. H., Brisco, B., Hopkinson, C. An automated open-source Python-based processing engine for SAR water body extraction: SARWATPy. Submitted to *Can. J. Remote Sens.*

Pekel J., Cottam, A., Forelick, N., Belward A. 2016. High-resolution mapping of global surface water and its long-term changes. *Nature*, Vol. 540: pp. 418-422. doi:10.1038/nature20584

Petrone, R.M., Silins, U., and Devito, K.J.,2007. Dynamics of evapotranspiration from a riparian pond complex in the Western Boreal Forest, Alberta, Canada. *Hydrological Processes*, Vol. 21: pp.1391–1401.

Pierdicca, N., Chini, M., Pulvirenti, L., Macina, F. 2008. Integrating physical and topographical information into a fuzzy scheme to map flooded area by SAR. *Sensors* 8:4151-4164.

Pietroniro A, Prowse T, Peters DL. 1999. Hydrologic assessment of an inland freshwater delta using multi-temporal satellite remote sensing. *Hydrological Processes.* Vol. 13: pp. 2483–2498.

Pole Star Geomatics Inc. 1997. *Wetland Distribution of Canada*. Map and database. Geological Survey of Canada, Agriculture and Agri-Food Canada and Environment Canada. Ottawa, Ontario.

Pope, K.O., Rejmankova, E., Paris J.F., Woodruff R. 1997. Detecting seasonal flooding cycles in marshes of the Yucatan Peninsula with SIR-C polarimetric radar imagery. *Remote Sensing of Environment.*, Vol. 59: pp. 157-166.

Prigent, C., Papa F., Aires F., Jimenez C., Rossow W., Matthews E. 2012. Changes in land surface water dynamics since the 1990s and relation to population pressure, *Geophys. Res. Lett*., Vol. 39: pp. L08403, doi:10.1029/2012GL051276.

Ramsey E.W., Nelson G.A., Sapkota S.K. 1998. Classifying coastal resources by integrating optical and radar imagery and color infrared photography. *Mangroves and Salt Marshes.* Vol. 2: pp. 109-119.

Rio, J.N.R. & Lozano-Garcia, D.F. 2000. Spatial filtering of radar Data (RADARSAT) for wetlands (Brackish Marches) Classification, *Remote Sensing of Environment*, Vol. 73: pp. 143-151.

Riordan, B., Verbyla, D., McGuire, A.D. 2006. Shrinking ponds in subarctic Alaska based on 1950–2002 remotely sensed images. *Journal of Geophysical Research*, Vol. 111: pp. G04002.

Roulet, N.T. 2000. Peatlands, carbon storage, greenhouse gases, and the Kyoto protocol, prospects and significance for Canada. *Wetlands*, Vol. 20: pp. 605–615.

Rutchey, K., L. Vilchek. 1994. Development of an Everglades Vegetation Map Using a SPOT Image and the Global Positioning System. *Photogrammetric Engineering and Remote Sensing*, Vol. 60(No.6): pp. 767-775.

Rutchey, K., L. Vilchek. 1999. Air photo interpretation and satellite imagery analysis techniques for mapping cattail coverage in a norther Everglades impoundment. *Photogrammetric Engineering & Remote Sensing.* Vol. 65(No. 2): pp. 185-191

Santoro, M., & Wegmüller, U. 2014. Multi-temporal synthetic aperture radar metrics applied to map open water bodies. *IEEE Journal of Selected Topics in Applied Earth Observations and Remote Sensing*, Vol. 7(No.8): pp. 3225–3238.

Sawaya, K.E., Olmanson, L.G., Heinert, N.J., Brezonik, P.L., and Bauer, M.E. 2003. Extending satellite remote sensing to local scales: Land and water resource monitoring using high-resolution imagery. *Remote Sensing of Environment*, Vol. 88(No. 1): pp. 144–156.

Scarpace, EL., B.K. Quirk, R.W. Kieffer, and S.L. Wynn. 1981. Wetland mapping from digitised aerial photography, *Photogrammetric Engineering & Remote Sensing*, Vol. 55(No. 9): pp.829-838.

Scheuchl, B., Flett, D., Caves, R., Cumming, I. 2004. Potential of RADARSAT-2 Data for operational sea ice monitoring. *Can. J. Remote Sens.*, Vol. 30(No.3): pp. 448–461.

Schlaffer S., Chini M., Dettmering D., Wagner W. 2016. Mapping Wetlands in Zambia Using Seasonal Backscatter Signatures Derived from ENVISAT ASAR Time Series. *Remote Sensi*ng. Vol. 8(No. 5): pp. 402; doi:10.3390/rs8050402

Schmitt A., Liechtle M., Roth H. 2012. On the use of dual-co-polarised terrasar-x data for wetland monitoring. *International Archives of the Photogrammetry, Remote Sensing and Spatial Information Sciences*, Volume XXXIX-B7, 2012 XXII ISPRS Congress

Schmitt, A., and Brisco, B. 2013. Wetland Monitoring Using the Curvelet-Based Change DetectionMethod on Polarimetric SAR Imagery. *Water*, Vol. 5: pp. 1036–1051.

Schreier, G. Geometrical properties of SAR images, in SAR Geocoding: Data and Systems, G. Schreier, Ed. Karlsruhe, Germany: Wichmann, 1993, pp. 103–134.

Schwarz, K.P., M.A. Chapman, M.W. Cannon, and P. Gong, 1993. An integrated INS/GPS approach to the georeferencing of remotely sensed data, *Photogrammetric Engineering & Remote Sensing*, Vol. 59(No. 11): pp. 1667–1674.

Sheng Y., Gong P., Biging G.S., 2003. True orthoimage production for forested areas from large-scale aerial photographs. *Photogramm. Eng. Remote Sens.,* Vol. 69(No. 3): pp. 259–266

Singh, G.; Yamaguchi, Y.; Park, S.-E. 4-Component Scattering Power Decomposition with Phase Rotation of Coherency Matrix. In Proceedings of 2011 IEEE International Geoscience and Remote Sensing Symposium, Vancouver, BC, Canada, 25–29 July 2011

Smith LC, Isacks BL, Bloom AL, Murray AB. 1996. Estimation of discharge from three braided rivers using synthetic aperture radar (SAR) satellite imagery: potential applications to ungaged basins. *Water Resources Research,* Vol. 32(No.7): pp. 2021–2034.

Smith, A.M.S., Kolden, C.A. Tinkham, W.T., Talhelm, A.F., Marshall, J.D., Hudak, A.T., Boschetti, L. 2014. Remote sensing the vulnerability of vegetation in natural terrestrial ecosystems. *Remote Sensing of Environment*, Vol. 154: pp. 322–337.

Smith, K. B., C. E. Smith, S.F. Forest and A. J. Richard. 2007. A Field Guide to the Wetlands of the Boreal Plains Ecozone of Canada. Ducks Unlimited Canada, Western Boreal Office, Edmonton, AB.

Soil Classification Working Group (SCWG), 1998. The Canadian System of Soil Classification, 3rd edition. Agriculture and Agri-Food Canada Publication No. 1646. NRC Research Press, Ottawa, ON.

Stewart, Robert E., and Harold A. Kantrud. 1971. Classification of natural ponds and lakes in the glaciated prairie region. Resource Publication 92, Bureau of Sport Fisheries and Wildlife, U.S. Fish and Wildlife Service, Washington, D.C. pp.57.

Stow,D.A., Hope,A.McGuire, D.Verbyla, D., Gamon, J.,Huemmrich, F., Houston, S., et al. 2004. Remote sensing of vegetation and land-cover change in Arctic tundra ecosystems. *Remote Sensing of Environment*, Vol. 89(No. 3): pp. 281–308.

Tapsall B., Milenov P., Tasdemir K., 2010. Analysis of Rapideye imagery for annual landcover mapping as an aid to the European Union (EU) common agricultural policy. Wagner W., Székely, B. (eds.): ISPRS TC VII Symposium – 100 Years ISPRS, Vienna, Austria, July 5–7, 2010, IAPRS, Vol. XXXVIII, Part 7B

Toutin, T. 2011. "Corrigendum to the paper State-of-the-art of geometric correction of remote sensing data: a data fusion perspective. *International Journal of Image and Data Fusion*, Vol. 2: pp. 283–286.

Touzi, R., Boerner, W.M., Lee J.S., Luenberg E. 2004. A review of polarimetry in the context of synthetic aperture radar: Concepts and information extraction. *Can J. Remote Sens.* Vol. 30: pp. 380-407.

Touzi, R., Deschamps, A., and Rother, G. 2007. Wetland characterization using Polarimetric RADARSAT-2 Capability. *Can. J. Remote Sens.*, Vol. 33: pp. 56–67.

Townsend P.A. 2002. Relationship between forest structure and the detection of flood inundation in forested wetlands using C-band SAR. *Int. J. Remote Sens.* Vol. 23: pp. 443-460.

Townsend, P.A.; Walsh, S.J. 1998. Modeling floodplain inundation using an integrated GIS with radar and optical remote sensing. *Geomorphology*, Vol. 21: pp. 295–312.

Toyra J., Pietroniro A., Martz L.W. 2001.Multisensor hydrologic assessment of a freshwater wetland. *Remote Sensing of Environment.* Vol. 75: pp. 162-173.

Toyra, J.A. Piettroniro, L., Martz W., Prowse T.D. 2002. A multi sensor approach to wetland flood monitoring. *Hydrological processes* Vol. 16: pp. 1569-1581.

Töyrä, J., A. Pietroniro, C. Hopkinson, andW. Kalbfleisch, 2003.Assessment of airborne scanning laser altimetry (LiDAR) in a deltaic wetland environment, *Can. J. of Remote Sens.*, Vol. 29: pp. 679–690.

Turetsky M., Wieder K., Halsey L., Vitt D. 2002. Current disturbance and the diminishing peatland carbon sink. *Geophysical Research Letters*. Vol. 29, Iss. 11.

Turetsky M., Kane E., Harden J., Ottmar R., Manies K., Hoy E., Kasischke E. 2011. Recent acceleration of biomass burning and carbon losses in Alaskan forests and peatlands. *Nature Geoscience.* Vol. 4, Iss. 1: pp. 21.

Vachon P., Wolfe J. C-Band Cross Polarization Wind Speed Retrieval. 2011. *IEEE Geoscience and Remote Sensing Letters*, Vol. 8, No.3: DOI: 10.1109/LGRS.2010.2085417

Van der Sanden, J.J.; Geldsetzer, T.; Short, N.; Brisco, B. 2012. *Advanced SAR Applications For Canada's Cryosphere (freshwater ice and permafrost)*; Final Technical Report for the Government Related Initiatives Program (GRIP). Natural Resources Canada: Ottawa, ON, Canada: pp 80.

van Zyl, J.J. 1989. Unsupervised classification of scattering mechanisms using radar polarimetry data. *IEEE Trans. Geosci. Remote Sensing*, Vol. 27(No. 1): pp. 36-45.

Verpoorter, C., Kutser, T., Seekell, D. A. and Tranvik, L. J. 2014. A global inventory of lakes based on high-resolution satellite imagery. *Geophys. Res. Lett*. Vol. 41: pp. 6396–6402

Vörösmarty, C. J., Green, P., Salisbury, J. and Lammers, R. B. 2000. Global water resources: vulnerability from climate change and population growth. *Science,* Vol. 289: pp. 284–288.

Wald, L. 2001. The present achievements of the EARSeL SIG" Data Fusion. In A Decade of Trans-European Remote Sensing Cooperation: *Proceedings of the 20th Earsel Symposium* (p. 263).

Wald, L. 2002. *Data fusion: definitions and architectures: fusion of images of different spatial resolutions*. Presses des MINES.

Wang J., Su X., 2011. An improved K-means clustering algorithm. Communication Software and Networks (ICCSN), 2011 IEEE 3rd International Conference on Communication and Software Networks. DOI: 10.1109/ICCSN.2011.6014384

Wehr, A., and U. Lohr, 1999. Airborne Laser Scanning – An introduction and overview, *ISPRS Journal of Photogrammetry and Remote Sensing,* Vol. 54: pp. 68–82.

Weiss, A. 2001. Topographic Position and Landforms Analysis. Poster presentation, ESRI User Conference, San Diego, CA.

Wettstein W., Schmid B. 1999. Conservation of arthropod diversity in montane wetlands. Effects of altitude, habitat quality and habitat fragmentation on butterflies and grasshoppers. *Journal of Applied Ecology*, Vol. 36(No.3): pp. 363-373.

White L, Brisco B., Pregitzer M., Tedford B., Boychuck L. 2014. RADARSAT-2 beam mode selection for surface water and flooded vegetation mapping. *Can. J. Remote Sens.* Vol. 40: pp. 135-151

White, L., Brisco, B. Dabboor, M. Schmitt A. and Pratt, A. 2015. A collection of SAR methodologies for monitoring wetlands. *Remote Sensing,* Vol. 7: pp. 7615-7645, doi:10.3390/rs70607615.

Wickham, J. Stehman, S. Smith, J. Yang, L. 2004. Thematic accuracy of the 1992 National Land-Cover Data for the western United States. *Remote Sensing of Environment*. Vol. 91: pp. 452–468.

Winter, T. C. 1989. Hydrologic studies of wetlands in the Northern Prairie. p. 16–54. Iowa State University Press, Ames, IA, USA.

Winter, T.C. and LaBaugh, J.W. 2003. *Wetlands* Vol. 23: pp. 532. doi:10.1672/02775212(2003)023[0532:HCIDIW]2.0.CO;2

Wright, C.; Gallant, A. 2007. Improved wetland remote sensing in Yellowstone national park using classification trees to combine TM imagery and ancillary environmental data. *Remote Sensing of Environment*. Vol. *107*: pp. 582–605.

Yamazaki, D., Trigg, M. A. and Ikeshima, D. 2015. Development of a global ~90m water body map using multi-temporal Landsat images. *Remote Sensing of Environment,* Vol. 171: pp. 337–351

Xu, H.Q. 2006. Modification of Normalised Difference Water Index (NDWI) to Enhance Open Water Features in Remotely Sensed Imagery. *International Journal of Remote Sensing,* Vol. 27: pp. 3025-3033.

Zhang, F., Xie, C., Li, K., Xu, M., Wang, X., and Xia, Z. 2012. Forest and deforestation identification based on multi-temporal polarimetric RADARSAT-2 images in Southwestern China. *Journal of Applied Remote Sensing*, Vol. 6, DOI:10.1117/1.JRS.6.063527

Zhang J, Xu K, Watanabe M, Yang Y, Chen X. 2004. Estimation of river discharge from non-trapezoidal open channel using QuickBird-2 satellite imagery. *Hydrological Science Journal- Journal des Sciences Hydrologiques* Vol. 49(No. 2): pp. 247–260.

Appendix A: Surface Water extraction executed using PCI Geomatics

1) Import the Data to include all channels desired for processing, it is recommended to carry through metadata from the import phase to export phase to provide a comprehensive file. The module for this is called **'Import'**.

2) The data must be converted from linear to decibel in order to retrieve the intensity data from the HH channel. If there is complex channels in the data (C32R) the **PSIQINTERP** module in Modeler can be used to convert the data from linear to decibels.

Otherwise:

If using EASI or Python:

If the data are in Amplitude: %2= 20*log10 (%1)

If the data are in Intensity: %2= 10*log10 (%1)

Where %2 is an empty channel you created that will receive the results

%1 the channel, in amplitude or intensity, to be converted to decibels

In Geomatica Modeler this has to be done manually for each channel you want to convert.

If using Modeler:

s Model

File=" D:\Data\workingfile.pix

Source="D:\Data\Linear_to_DB.eas

Undefval=0

s Model

r Model

Here Linear_to_DB.eas is a text file containing your model, for example:

%2= 20*log10 (%1)

3) **Split** the data from step 2 where the data was converted to decibel so that it can be put through two separate filters detailed in steps 4 and 5.

4) Execute the **'FAV'** filter.

FAV performs spatial filtering on individual pixels in an image using the gray-level values in a square or rectangular window that surrounds each pixel. The dimensions of the filter size must be odd and can be between 1x3 or 3x1 to 1001x1001. The filter size must not exceed the size of the image. Common resample pixel sizes are 3, 5 or 7. Higher than 7 will result in significantly altered and dissolved data which is not indicative of the SAR phase response in most cases.

Example script for FAV that smooths a channel (eg. channel 1) of the file 'test.pix' using a 3x3-square filter:

```
from pci.fav import *
file    =    r'$PCIHOME/demo/test.pix'
dbic    =    [1]    # use elevation data
dboc    =    [1]    # overwrite input data
flsz    =    [3,3]  # use a 21x21 filter
mask    =    []     # process entire image
bgrange    =    []     # no background values
failvalu    =    []     # no failure value
bgzero =    "                    # default, set background to 0
fav( file, dbic, dboc, flsz, mask, bgrange, failvalu, bgzero )
```

5) A second filter is called **'FGAMMA'**.

An example of the FGAMMA filter that uses a number of looks (NLOOK) of 1 and filter size of 3x3:

```
from pci.fgamma import*
file      =      'test.pix'
dbic      =      [1]
dboc      =      [1]      # filtered results (overwrite DBIC)
flsz      =      [3,3]    # filter size
mask      =      [1024,1024,2048,2048]      # area to filter
nlook     =      [1.0]    # number of looks
imagefmt        =        'AMP'  # amplitude image format
fgamma( file, dbic, dboc, flsz, mask, nlook, imagefmt )
```

6) After filtering, both of the images go through a model where the threshold value is entered manually to extract the waterbodies.
The module in PCI is simply called **'Model'** and has the following arithmetic where the '-12' value in both examples is the value which is changed based on desired threshold:
Where for the **FAV** filter (step 4):
if (%1 >= -50 and %1 <= -**12**) then
%1 = 8888
endif;
Where for the **FGAMMA** filter (step 5):
if (%1 >= -50 and %1 <= -**12**) then
%1 = 9999
endif;

7) Both of the filtered (steps 4 and 5) and threshold processed (step 6) images are then combined using an arithmetic module called **'ARI'** which simply adds the two images pixels together. ARI performs an arithmetic or a logical operation on image data stored in two database image channels (DBIC) and/or a constant (CNST). The result is saved on a specified output channel (DBOC). The output channel can be one of the input channels:
 Where DBOC = DBIC(1) + DBIC(2).
8) The data from the FGamma correction goes through another 'model' that parses unwanted thresholding data into water vs non-water.
if (%1 = 18887) then
%1 = 77777
endif;

9) Again an **'ARI'** module is used to add the data from the 'model' (step 6) as a result of the FGamma correction (step 5) and the 'model' output from the previous (step 8)
10) To create the final binary masks of water and land, all of the data then goes through another **'model'** module that makes the data values either a 0 (land) or 1 (water):
if (%1 = 87776) then
%1 = 1;
else
%1 = 0;
endif;

11) All of the data from step 10 is then scaled back to linear from decibel as an 8 bit unsigned raster. This module is called **'Scale'**, which performs linear or non-linear mapping of image gray levels to a desired output range. This function is typically used to scale data from high-resolution (32- and 16-bit) channels to low-resolution (8- and 16-bit) channels.

The algorithm is explained in the following example:

A 16-bit radar image (test.pix, channel 1) is mapped to an 8-bit output range using the automatic normalized quantization algorithm within the model:

from pci.scale import *

```
fili      =      "test.pix" # input file
filo      =      ""         # output file same as input
dbic      =      [1]        # 16-bit radar image
dboc      =      [8]        # 8-bit channel
dbiw      =      []         # process entire image
dbow      =      []         # output entire image
inrange=          []
trim      =      []
outrange          =      []       # default range [0,255]
sfunct  =      "NQ"   # automatic normalized quantization
scale (fili, filo, dbic, dboc, dbiw, dbow, inrange, trim, outrange, sfunct)
```

12) Lastly the data is filtered one more time through a mode filter called "FMO'.

The mode filter computes the mode of the gray-level values (the most frequently occurring gray-level value) in the filter window that surrounds each pixel. Mode filtering is ideal for cleaning thematic maps for presentation purposes because it replaces small 'island' themes with larger surrounding themes. The minimum filter size is 1x3; the maximum is 7x7. The filter window need not be square. The input channel (DBIC) can be the same as the output channel (DBOC).

The script is as follows which applies a 3x3 mode filter to a whole channel using test.pix.

from pci.fmo import *

```
file           =      "test.pix"
dbic           =      [7]                 # Filters channel 7
dboc           =      [8]
flsz           =      [3,3]    # Specifies a 3x3 filter size
mask           =      []                    # Processes the entire database
thinline       =      "OFF" # Does not preserve thin lines
keepvalu       =      []
bgzero         =      "YES"
fmo( file, dbic, dboc, flsz, mask, thinline, keepvalu, bgzero )
```

13) The data is then ready to be exported as a .pix file. Which is a GDB file that contains all of the metadata and processed data from the classification. The module is simply called **'Export'**. The raster file is in .tiff format within the .pix file, which can be exported directly from the .pix database file if desired.